Winter 1-31-2022

Flexural Strengthening of RC Slabs using Near Surface Mounted GFRP bars

Sama Taha
samatarek@aucegypt.edu

THE AMERICAN UNIVERSITY IN CAIRO

DEPARTMENT OF CONSTRUCTION ENGINEERING

FLEXURAL STRENGTHENING OF RC SLABS USING NEAR SURFACE MOUNTED GFRP BARS

A Thesis Submitted to
The Department of Construction Engineering

In partial fulfillment of the requirements for the degree of
Master of Science in Construction Engineering

By

Sama Tarek Taha Mahmoud
BSc. in Construction Engineering, 2018
The American University in Cairo

Under the supervision of

Dr. Ezzeldin Yazeed Sayed-Ahmed
Professor, Department of Construction Engineering

Dr. Mohamed Nagib AbouZeid
Professor, Department of Construction Engineering

September 2021

Dedication

This thesis is dedicated to my beloved family. To my Grandmother, Kamelia Abdelhalim, you are the reason I do everything I can to become the best version of myself and I hope I'm making you proud. To my Mother, Nevine Hedayat, thank you so much for the unconditional love and support, I wouldn't have become who I am if it wasn't for you. To my Father, Tarek Taha, thank you for the assistance, the encouragement and for always believing in me. To my Fiancé, Ahmed Romaih, thank you for the ongoing support and for going through this journey with me, I couldn't have done any of this without you being part of it.

Acknowledgements

First and foremost, I am thankful to my advisors Professor Ezzeldin Yazeed and Professor Mohamed AbouZeid, for their unconditional support and guidance throughout my masters' as well as bachelors' study. The encouragement they have given me in a time of a global pandemic was incomparable. I am thankful to their time, expertise and trust, for this thesis wouldn't have happened without their ongoing support.

Would like to thank Schöck Combar for their cooperation in providing the GFRP bars in kind and for the provided support.

I would like to acknowledge and thank Dr. Omar El Kady for his management in the AUC Structure Lab, he always supported me in my experimental work conducting it with the best quality and safety precautions. Additionally, I would like to thank Mr. Madbouly and all AUC laboratory personnel who provided all the needed assistance throughout this study.

I also would like to thank AUC Office of the Dean of Graduate Studies for the Research Support Grant and the financial support it provided to accomplish this thesis. As well as thanking the Construction Engineering Department.

Abstract

Glass Fiber reinforced polymers (GFRPs) have been recently successfully used to increase reinforced concrete elements' strength. In general, FRPs have many advantages such as resistance to corrosion, and high strength-to-weight ratio. On the other hand, debonding from concrete may constitute a limitation to using GFRP bars; hence the increase in strength of RC elements strengthened using GFRP bars may be limited by this premature debonding failure mechanism.

This study aims to investigate the strengthening effect of GFRP bars on the capacity of RC slabs when subject to flexure loading. The work studies the use of different bonding lengths, diameters and numbers of GFRP bars in strengthening RC slabs. The objective is to show the effect of debonding failure on the capacity of the GFRP strengthened slabs relative to the different variables used. The work presents the details of the adopted experimental investigation and the results of the flexural tests performed on twelve slabs with different variables. These results are adopted to validate the currently available design provisions of the ACI code of practice for using NSM GFRP to strengthen RC slabs.

The GFRP bars were added to the slabs using the near surface mounted technique, due to its better advantages over the externally bonded technique. The results of this work demonstrate that the GFRP NSM strengthened slabs experienced a 13% increase in strength with the use of 1 no.8 GFRP bar with 2 m length, a 27% increase in strength with the use of 1 no. 12 GFRP bar with 2 m length and a 48% increase in strength with the use of 1 no. 16 GFRP bar with 2 m length. This is a substantial increase and would be of great impact if used in the repair of projects. The mode of failure for the GFRP bar with 2 m length is mainly found to be due to Flexural failure. Moreover, when checking the slabs strengthened with 2 no.16 GFRP bars with 1.5 m length, even though the mode of failure was due to debonding, there was a 103% increase in strength. Finally, for the slabs strengthened with the use of 1 no. 16 GFRP with length 1 m, which is less than the minimum bonding length specified by the ACI Code, the mode of failure is found to be concrete crushing at the edge of the GFRP bar, and it showed a 38% increase in strength when compared to the control sample. The results unveiled the ability of the GFRP strengthened slabs to enhance the flexural strength using different diameters, number of bars, and bonding lengths.

It is recommended to expand on this work in future research work, to both validate the findings of this study as well as achieve better understanding of the use of Near Surface Mounted GFRP bars in structural applications.

Keywords: RC, One-Way Slabs, Near Surface Mounted, GFRP bars, Repair, Flexural Strengthening,

Table of Contents

List of Tables

List of Figures

List of Symbols

C_c = Concrete Cover

C = Compression Force

T = Tension Force

c = Depth of Neutral Axis

d = Depth of Slab

d_s = Depth to Steel Reinforcement

d_f = depth to GFRP bar

A_s = Area of Steel Reinforcement

A_f = Area of GFRP bars

D = Minimum dimension of Groove

d_b = Diameter of GFRP bar

E_c = Modulus of Elasticity of Concrete

E_s = Modulus of Elasticity of Steel Reinforcement

E = Tension Modulus of Elasticity of GFRP

$\tau_b = f_{bd}$ = Design Value Bond Strength

$f_{fu} = f_{fd}$ = GFRP Mean Strength Value

f_{cu} = Concrete Compressive Strength

ε_{cu} = Concrete Strain

ε_s = Steel Strain

ε_{fu} =ε_{fd} = GFRP Strain

ε_{fe} = Effective Strain in GFRP

ε_{bi} = Existing Strain

F_s= Steel Reinforcement Strength

f_y= Steel Reinforcement Yield Strength

l_{db} = Development Length of NSM GFRP bars

P = Failure Load

P_u = Ultimate Load

P_{cr} = Crack Load

M_r = Resistance Moment

M_n = Nominal Moment

M_{ns} = Steel Nominal Moment

M_{nf} = GFRP Nominal Moment

M_{cr} = Crack Moment

M_{ow} = Moment due to own weight

M_f = Failure Moment

W_s = Weight of slab

w_s = Uniform weight of slab per unit length

k_m = Bond-Dependent Coefficient

Chapter 1 – Introduction

This chapter provides an introduction about the topic and a background of the work. The properties and applications of the different FRP materials including the GFRP used are explained. Moreover, it includes the research problem statement which the study will be looking into, as well as the objectives and expected outcomes.

1.1 Background

Buildings are everywhere around us, with different materials and different designs. Concrete is the second most used material after water and is the most widely used construction material in the world because of its high compressive strength, relatively low cost, etc. However, increased challenges of recently designed structures require an improved method for strengthening.

Consequently, Glass Fiber reinforced polymers (GFRPs) have been recently successfully used to increase reinforced concrete elements' (Slabs, Beams, Columns, etc.) strength. In general, FRPs have many advantages such as resistance to corrosion, durability, lightweight and high strength-to-weight ratio. To improve the structural performance, FRP has been used widely in a lot of construction projects (Parvin et al., 2016).

The use of FRP in strengthening RC structures is shown in Figure 1.1, as Figure 1.1 (a) shows the flexural strengthening of a RC slab, where the FRP strips are being EB to the slab. Also, Figure 1.1 (b) shows the flexural strengthening of a RC beam, where the FRP strips are added to the bottom of the beam. Moreover, Figure 1.1 (c) shows the strengthening of an RC column, where the FRP strips confine the column and increase its strength. Lastly, Figure 1.1 (d) shows the wrapping of a RC tank. This

proves that FRP can be used in the strengthening of different RC elements (Gunaslan and Karasin, 2017).

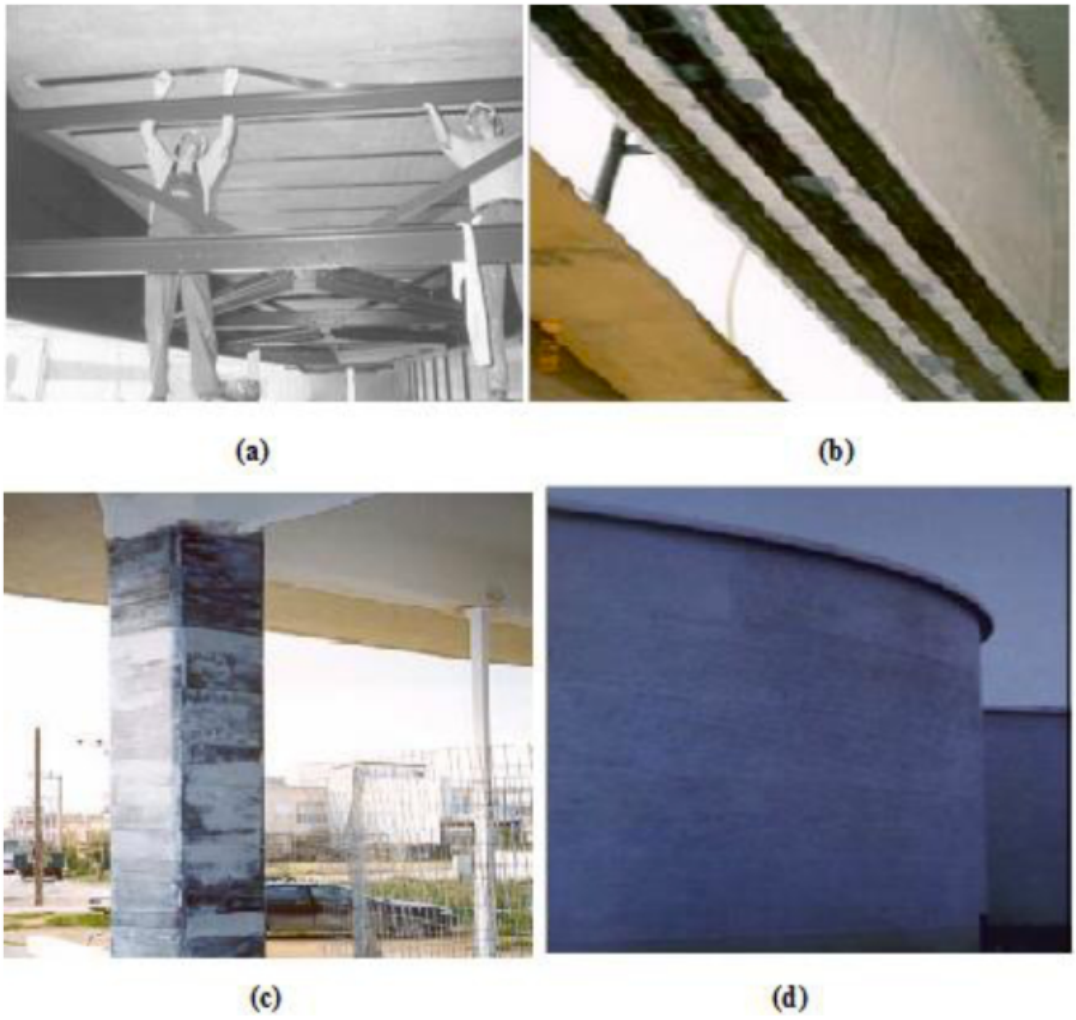

Figure 1.1 Applications of FRP in strengthening RC Structures (Gunaslan and Karasin, 2017)

An example of the use of GFRP in construction is the Flood Mitigation Channel in the new Jizan Economic City, Saudi Arabia, shown in Figure 1.2. It is currently under construction, but it is planned to be the biggest project being constructed using GFRP as the primary reinforcement, without the use of steel reinforcement. GFRP was chosen for the construction of the channel, as the channel will be exposed to materials that would lead to the corrosion of steel, like chemicals and salinity water (Pultron Composites, 2019).

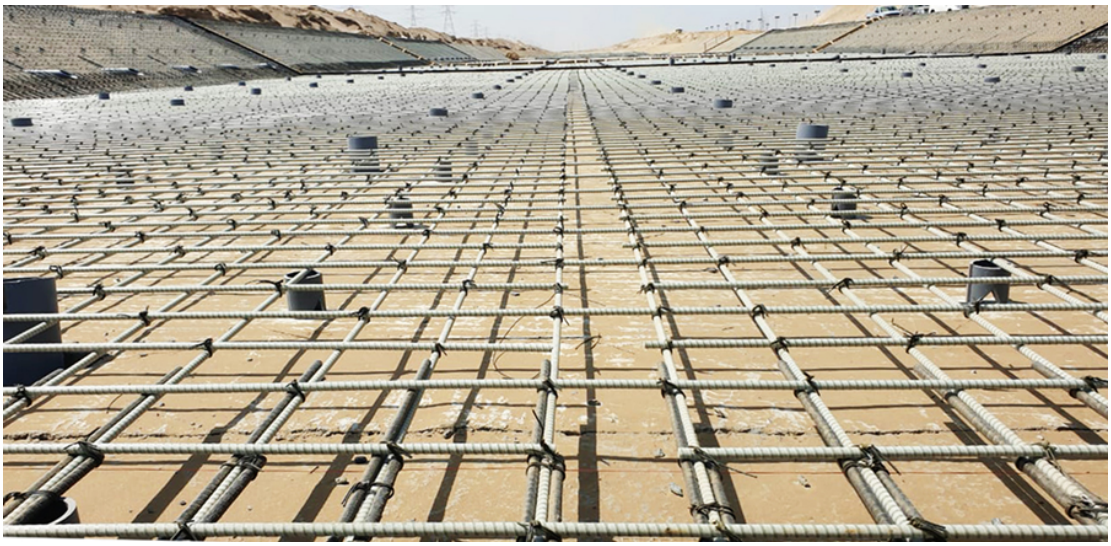

Figure 1.2 Flood Mitigation Channel in the new Jizan Economic City, Saudi Arabia (Pultron Composites, 2019)

There are multiple advantages for the use of FRP materials in strengthening, first advantage is its high strength relative to its weight, as to obtain such strength using steel reinforcement a significant weight of it will be needed. Second advantage is that it does not corrode, which is one of the major disadvantages of steel reinforcement. Other advantages are its high fatigue strength and its resistance to chemicals (Behzard et al., 2016).

There are different types of FRP: Carbon (CFRP), Glass (GFRP), Aramid (AFRP) and Basalt (BFRP) as shown in Figure 1.3. Even though CFRPs are more widely used in cases that requires high strength, GFRP is also promising and possesses good properties. Although GFRP does not have strength and stiffness as high as CFRP, their reduced cost and good mechanical properties make them promising (Xing et al., 2018).

Figure 1.3 Different types of FRP (Abbood et al., 2020)

There are different configurations to the FRP materials, as shown in Figure 1.4, (a) and (b) are BFRP sand-coated round bars with different diameters, (c) is GFRP spirally wound round bar and (d) is GFRP round bar, similar to the one used in this work. Continuingly, (e) is CFRP smooth round bar, (f) is CFRP smooth square bar and (g) and (h) are CFRP smooth strips with different length and thickness.

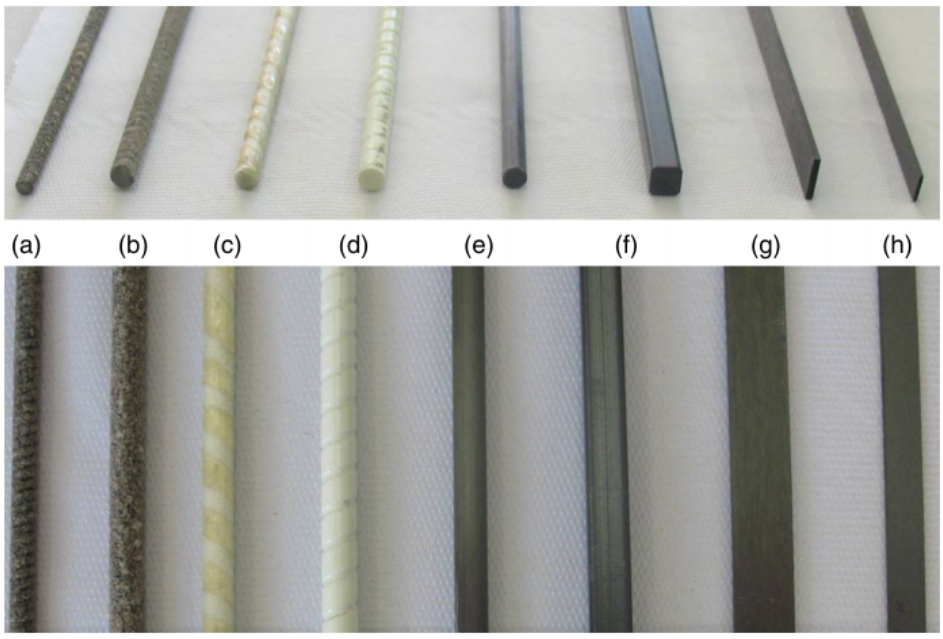

Figure 1.4 Different FRP configurations (Bilotta et al., 2015)

There are different techniques to strengthening RC elements with FRP materials, the most promising of which are the externally bonded (EB) technique and the near surface mounted (NSM) technique. In the EB technique the FRP is attached to the external surface of the RC element, as shown in Figure 1.5 on the left, the FRP sheet is EB to the RC slab. However, in the near surface mounted (NSM) technique, the FRP bar is attached inside the RC element near its surface, where we have a small groove in the RC element and the FRP is placed, as shown in Figure 1.5 on the right, the FRP bar is attached inside the RC slab.

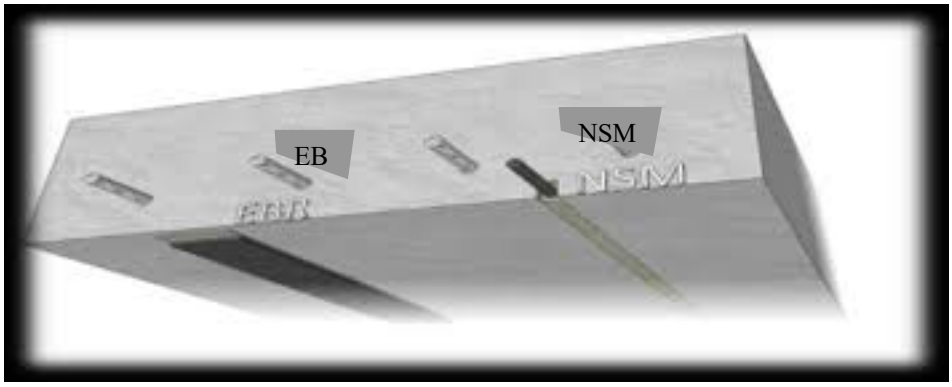

Figure 1.5 EB vs NSM technique (Soror et al., 2019)

The NSM technique has a couple of advantages over the EB technique, as since it is part of the element, the bonded area is larger, and it is less prone to premature debonding. In the NSM technique, the FRP bar is inside the element so it is protected against any external factors with the concrete or adhesive cover.

1.2 Problem Statement

GFRP is a material with great properties and low cost, it is no doubt that it will be used a lot in the future, especially in the strengthening of different RC elements. Apart from the various advantages of FRP materials mentioned above, debonding from concrete may constitute a limitation to using FRP in general and GFRP bars in particular. As even if the NSM technique is used instead of the EB technique, still FRP

bars do not reach the expected increase in strength due to the bars debonding from the RC element. Hence, the increase in strength of RC elements strengthened using GFRP bars may be limited by this premature debonding failure mechanism.

Lately, the necessity of studying the increase in strength and the different modes of failure when strengthening RC elements with FRP bars is increasing. As well as studying the different bonding lengths, to reach the maximum possible strength without debonding failure, to be able to benefit from the various advantages of using FRP materials.

Moreover, there is a significant amount of research experimenting and discussing strengthening of RC beams using NSM FRP, especially CFRP bars and strips. Therefore, several experiments and research should be done for strengthening of RC slabs, like that done for RC beams. Also, more experiments and research should be done for the use of GFRP like that done for CFRP.

1.3 Objectives and Expected Outcomes

This work aims at investigating the strengthening effect of GFRP bars on the capacity of RC slabs when subject to flexure. The main objective of this work is to study the effect of the premature debonding failure on the capacity of the NSM-GFRP strengthened slabs. The effect of the diameter and numbers of bars (i.e., GFRP reinforcement ratio) on the flexural strength of the slab is investigated. The failure modes of the NSM-GFRP are studied. Moreover, the limitation defined by ACI on the development length of NSM-GFRP bars and its effect on debonding failure is also investigated.

The study will present the details of the adopted experimental investigation and the results of the flexural tests. These results will be adopted to validate the currently

available design provisions of different codes of practice for NSM GFRP strengthen flexural element and the application of these provisions to slabs.

Meeting the objective of this work will involve the following:

1. Study the different modes of failure and limitations to strengthening RC slabs with NSM GFRP bars,
2. Determine the percentage increase in strength relative to the number of GFRP bars used,
3. Evaluate the percentage increase in strength relative to the GFRP bar diameter, and
4. Compare the ACI design equation that takes into consideration the debonding of GFRP bars and concrete, with the experimental results

This work has the potential of yielding the following expected outcomes:

1. Pinpointing means to increase the flexural strength in RC slabs through using GFRP
2. Achieving better understanding of the performance and interaction of Near Surface Mounted in reinforced concrete slabs
3. Encourage the use of composite structures to overcome the disadvantages of steel reinforcement, and
4. Finding means to optimize the bond strength between the concrete and the GFRP bars.

1.4 Methodology

An experimental investigation will be conducted at the AUC structural engineering lab to investigate strengthening of RC Slabs using NSM GFRP bars. 12 full scale slabs with dimensions 1 m × 2.5 m × 0.1 m will be tested in the experimental program. The first series composed of two control specimens with normal steel reinforcement of bars no. 10 @ 200 mm, and they will have no NSM-GFRP bars. The other 10 slabs will be tested while changing different parameters. The second series (2 slabs) will be tested using one no.12 GFRP bar with a bonding length of 2.0 m, this series will be used to know the increase in strength of the slab using NSM GFRP bars in comparison to the first series. The third series (2 slabs) will be tested using one no.8 GFRP bar with bonding length of 2.0 m and the fourth series (2 slabs) using no.16 GFRP with bonding length of 2.0 m.

Moreover, to be able to achieve the purpose of the thesis, and since the NSM technique has a disadvantage of debonding between the bars and the concrete, the fifth series (2 slabs) will experiment the bonding length of the GFRP bar with the concrete. The fifth series will be tested using one no.12 GFRP but with bonding length 1.0 m instead of 2.0 m, which is less than the minimum specified by the ACI Code.

The first four series showed the slab's performance when strengthened with GFRP bars with different diameters, and with different bonding lengths versus not being strengthened. Therefore, the sixth and last series (2 slabs) will be tested with a greater number of GFRP bars, where 2 no.12 bars will be used with bonding length 2.0 m. The purpose of this series is to be able to compare the increase in strength of the slab strengthened with NSM GFRP bars in respect of the number and the size of the bars, taking into consideration the bonding length and debonding failure. By testing the

six different series with good quality and skilled workmanship, a reliable design equation can be proposed to be used in the future.

1.5 Thesis Content

Chapter I - Introduction

Provides an introduction about the topic and the area of the work. It explains the properties and applications of the different FRP materials including the GFRP used. Moreover, it includes the problem statement that the work will be looking into, as well as the objectives and expected outcomes. It gives a brief introduction about the design and methods used throughout the study.

Chapter II – Literature Review

Goes through the available literature and the various similar topics that were carried out in previous research. The literature review discusses the FRP materials, starting with their history, the importance of their use, their different types and properties and their applications in Egypt. It then shows the different techniques used for strengthening of RC elements using FRP, with the gap available in literature that reflects the problem statement discussed in the introduction.

Chapter III – The Experimental Program

Illustrates the experimental work conducted in this study, stating the materials used and their properties. Also, stating the number of samples and the different series used, to explain the importance of each series and the comparison between them, that will reinforce the results. Furthermore, the design equations used in the calculations are explained and the calculations for the different series are done.

Chapter IV – Results and Discussion

Demonstrates the results of the flexural tests conducted for the twelve samples, as well as detailed analysis conducted for each sample, elaborating the mechanical properties of GFRP and comparing between the different series.

Chapter V – Conclusions

Summarizes the findings of the experimental work and presents the conclusions reached throughout the work. Followed by a set of recommendations for possible future work that would add to the thesis topic or that the studied topic would be of benefit to.

References

A full set of the references used throughout the paper, are listed herein

Chapter 2 – Literature Review

This chapter reviews the available literature and the various similar topics that were carried out in previous research. The literature review discusses the FRP materials, starting with their history, the importance of their use, their different types, properties and their applications in Egypt. It then shows the different techniques used for strengthening of RC elements using FRP, with confirming the available gap in literature, that verifies the problem statement discussed in the introduction.

2.1 Fiber Reinforced Polymers

FRPs have been recently widely used due to their advantages such as resistance to corrosion and high strength-to-weight ratio. In comparison to steel, FRP materials have diverse properties and characteristics that are of great benefit and encourage their use in the Civil Engineering Industry. They can substantially enhance the corrosion resistance for structures, which is one of the main disadvantages to steel reinforcement. Moreover, FRP have light weight and high strength with a much better strength to weight ratio than steel reinforcement, which would be very beneficial as it would reduce in the total dead load of the structure while increasing its carrying capacity.

FRPs' matrix is a combination of "organic, polyester, thermostable, vinylester, phenolic and epoxy resins". Such combination gives unique properties that cannot be achieved by either the fibers alone nor the matrix alone, with higher stiffness than aluminum, and quarter the specific gravity of steel (Sathishkumar et al., 2014). When comparing FRP composites to steel, it was noticed that they are unresponsive to the chloride-induce corrosion on account of its non-corrosive and non-metallic intrinsically" (Abbood et al., 2020).

However, as shown in Figure 2.1, whether Carbon Glass or Aramid, are linear elastic without a known or calculated yielding stage, which is a disadvantage as it results in brittle failure. Also, other than CFRP, FRPs have a lower modulus of elasticity than steel (Abbood et al., 2020)

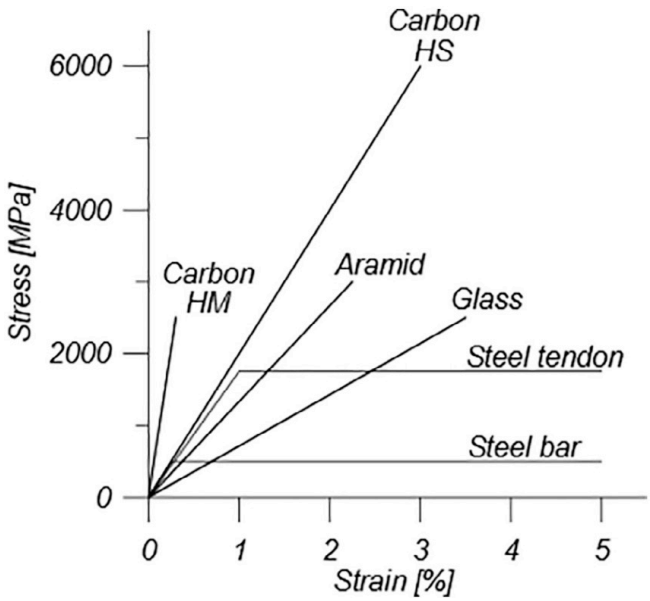

Figure 2.1 Steel vs FRP materials (Carolin, 2003)

2.2 Types and Properties of FRP

There are different FRP types with different properties; Carbon, Glass, Aramid and Basalt FRP are the most known and used types. As shown in Table 2.1, all FRP types have lower density than steel, higher tensile strength, more than twice that of steel and less elongation % than steel.

Table 2.1 Steel and FRP types' properties (Abbood et al., 2020)

Property/Material	CFRP	GFRP	AFRP	BFRP	Steel
Density (gm/cm^3)	1.50 - 2.10	1.25 - 2.50	1.25 - 1.45	1.90 - 2.10	7.85
Tensile Str. (MPa)	600 - 3920	483 - 4580	1720 – 3620	600 - 1500	483 - 690

Property/Material	CFRP	GFRP	AFRP	BFRP	Steel
Young's Modulus (GPa)	37 - 784	35 - 86	41 - 175	50 - 65	200
Elongation (%)	0.5 - 1.8	1.2 - 5.0	1.4 - 4.4	1.2 - 2.6	6.0 - 12.0

CFRP has a lot of advantages, some types of CFRP are the only FRPs with a higher modulus of elasticity than steel, it has low conductivity and is resistant to chemical effects. However, it is manufactured at 1300ºC which requires high energy to produce and therefore increases its cost relative to other FRP (Abbood et al., 2020).

Glass is isotropic in nature, which means that it has uniformity in all orientations, it has high strength. GFRP is well resistant to water which gives it a wide variety of applications and it has low-cost relative to other types of FRP. All the above-mentioned make GFRP the most used type of FRP in the Construction Industry. However, as shown in Figure 2.1, GFRP has a low modulus of elasticity compared to steel and to other types of FRP, stress rupture occurs leading to low long-term strength and it has low resistance to alkaline, which can be a drawback when using GFRP with concrete as cement is incredibly alkaline (Abbood et al., 2020).

AFRP has low density, higher modulus of elasticity than GFRP but less than CFRP, high stiffness and tensile strength and is very sufficient for the use of tension applications such as tendons and cables. However, they have low compressive strength and are highly costly compared to GFRP.

BFRP is mainly made of crushed Basalt rocks, which is type of igneous rock. It has tensile strength that can reach up to 1500 MPa, and since they are made from

rocks found in nature, they are extremely durable. Moreover, just like all other FRP types, they can resist corrosion (Abbood et al., 2020).

2.3 Use of FRP in Egypt

To know the importance of FRP in Egypt, one has to research its uses and applications. GRPs are widely used in pipes for water and sewage systems in Egypt. Also, GFRP does have an important role and can be a solution to many of the current design challenges. Due to Egypt's exceptional geographical location, having long coasts on the Mediterranean and the Red Sea, this leads to deterioration to structures due to corrosion of steel reinforcement. This promotes the use of FRP in Egypt which encouraged having a code approved by the Egyptian Authorities in December 2005, being the first formal design code for FRP in Egypt. "As a result, the use of FRP for repair, strengthening and retrofitting of structures have become a very well accepted practice in Egypt" (Mohamedien et al., 2013). Examples of Projects that were strengthened using FRP in Egypt are given below.

The Egyptian Museum is a historical building in Tahrir Square with a great value, it consists of reinforced concrete arches of 17 m span and 13 m clear height, supported on masonry walls. The concrete of the Egyptian Museum deteriorated due to corrosion of steel reinforcement and it was decided to strengthen it using CFRP strips added to the bottom and sides of the arches (Mohamedien et al., 2013).

Another example is the Dolphin Piles of Abu Qir Harbor in Alexandria. Piles experienced flexural damage with cracks, they were strengthened by applying one layer of GFRP sheets and one layer of CFRP sheets as well as CFRP anchors uniformly spaced around the circumference of the pile, then 4 more layers of CFRP sheets (Mohamedien et al., 2013).

2.4 Externally Bonded Technique vs. Near Surface Mounted Technique

There are different techniques for the use of FRP materials in strengthening concrete structures. However, the most promising techniques are the externally bonded and the near surface mounted FRPs techniques. As shown in Figure 2.2 (a), FRP plates or sheets are attached (externally bonded) to the concrete face with Epoxy.

However, Near Surface Mounting (NSM) technique is a recent technique relative to the externally bonded method with a purpose to replace or enhance as it has better advantages. As shown in Figure 2.2 (b) and (c), the FRP rods, bars or laminates are inserted into the concrete near the surface in the place of the concrete cover; it is surrounded by Epoxy to enhance the bonding between the FRP and the Concrete (Parvin et al., 2016).

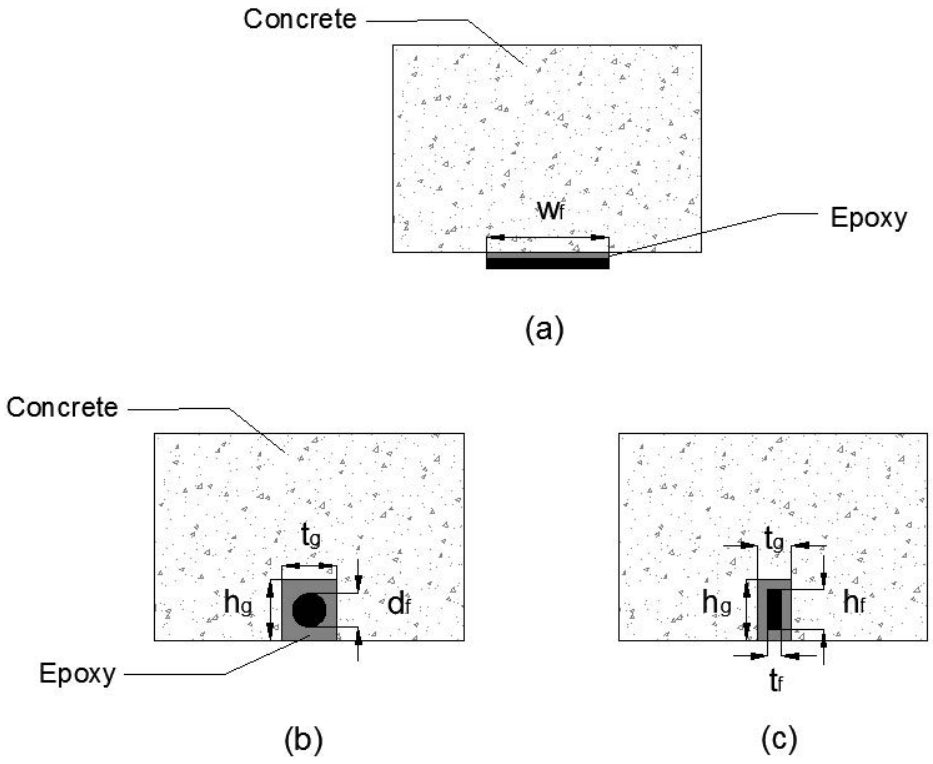

Figure 2.2 FRP strengthening (a) EBR FRP plate or sheet, (b) NSM FRP rod or bar, (c) NSM FRP laminate (Parvin et al., 2016).

The externally bonded technique has been the used method for retrofitting FRP with RC elements, it has been popular for years and has been effective. It is easily applied, as shown in Figure 2.3, where the surface of the RC element is roughened to ensure proper bonding, the adhesive is applied along with the FRP and then they are pressured to bond together. Even though this method has been widely used, it was proved that it fails at low strains due to interfacial debonding between the FRP and the RC surface. This failure reduces the efficiency of the system as it doesn't actually reach the strength FRP can actually reach, limiting its advantages (Soror et al., 2019).

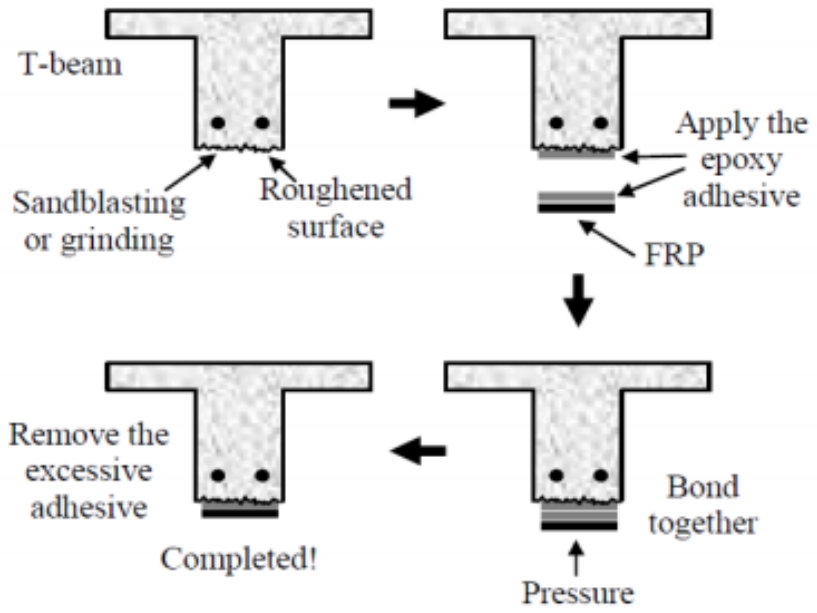

Figure 2.3 Detailed procedure of applying FRP using the EB technique (Soror et al., 2019)

Failure modes for the EB technique are divided into 2 categories, the first are the full composition action, where the failure happens after the element is strengthened and the ultimate flexural capacity is reached. Possible failures in the full composition action failure category are due to flexural failure. As shown in Figure 2.4, failure happens due to concrete crushing, where the concrete surface no longer handles the stress and crushes, or due to FRP rupture, where the FRP no longer is attached to the concrete surface and debonds, splitting from the concrete element (Soror et al., 2019).

The second category is the premature failure, where the failure happens initially without the element reaching its ultimate capacity. Possible failures in the premature failure category are usually due to shear failure or due to combined shear and flexural failure. As shown in Figure 2.4, failure happens due to end cover separation or end interfacial delamination, where the FRP takes the cover or the adhesive and separates from the concrete element, due to high shear and normal stresses. Failure can also happen due to flexural crack induced debonding or shear crack induced debonding, it happens due to combined shear and flexural stresses (Soror et al., 2019).

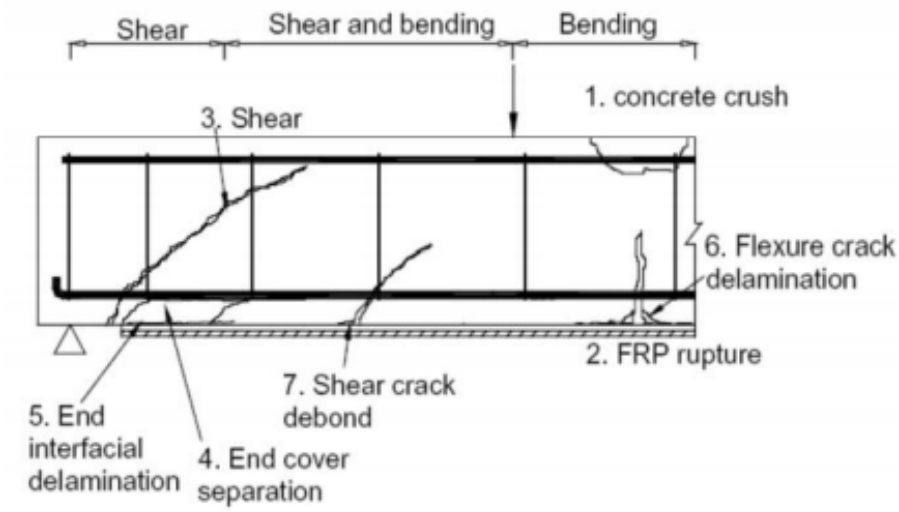

Figure 2.4 Failure Modes of RC Beam strengthened using EB technique (Soror et al., 2019)

The Near Surface Mounted technique has been recently used, as it has advantages over the EB technique. It is easily applied, even easier than the EB technique, as shown in Figure 2.5, where a groove is done in the concrete cover, the adhesive as well as the FRP are inserted in the groove and they are left to bond together.

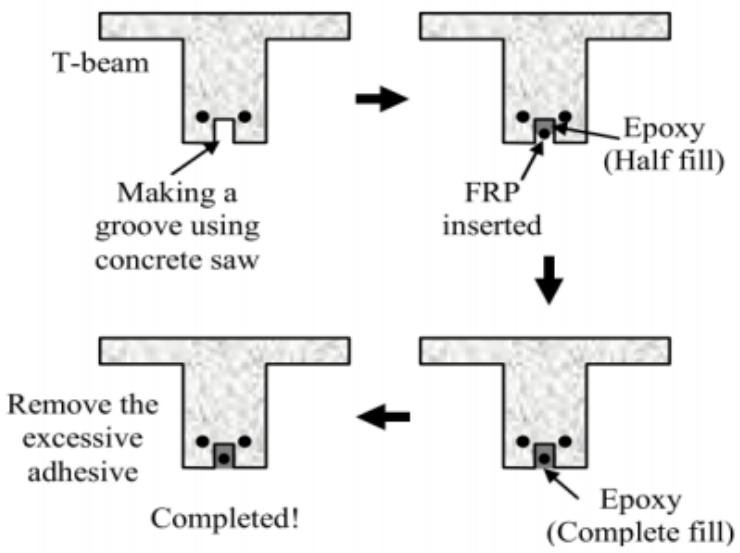

Figure 2.5 Detailed procedure of applying FRP using the NSM technique (Soror et al., 2019)

Advantages of NSM technique in comparison to the EB FRP Technique are (Coelho et al., 2015: the NSM technique requires less time and needed work for installation, as the application is easier. Moreover, it is less susceptible to premature debonding, since the FRP is inside the element and not externally bonded to it and is bonded with the element through multiples sides. This allows the sample to reach higher flexural strength and allows better use of the reinforcement. Another advantage is the fact that in the NSM technique the is protected by a cover and adhesive against aggressive factors.

2.5 Flexural Strengthening of RC Beams Using NSM FRP Bars

Many researchers investigated flexural strengthening of beams using CFRP bars, as it is showed to be efficient in increasing the stiffness and the flexural strength of RC beams (Soliman et al., 2010), especially with beams having low steel reinforcement ratio. However, the common mode of failure for the beams strengthened with NSM FRP laminates is debonding between the FRP and the concrete. It happens in the form that the concrete cover splits then the CFRP bar debonds coming out of the specimen. It was noticed that the smaller the groove size, the more time it takes for the

sample to fail, reaching higher flexural capacities (Soliman et al., 2010). This is mainly due to the fact that using a small groove size increases the spacing between the steel reinforcement and the FRP bar.

There is experimental work conducted for flexural strengthening of different RC elements using GFRP and/or CFRP, summarized by Parvin and Syed Shah (2016). One of which is a four-point bending test conducted on a simply supported RC T-beam with span 4.572 m, wed dimensions 0.152 × 0.305 m and flange dimensions 0.381 × 0.102 m, using GFRP and CFRP rods with diameters 9.5 and 12.7 mm. The observed failure mode was due to concrete crushing and FRP debonding, but there was a 26-44% increase in ultimate load. Another test is four-point bending test conducted on a simply supported RC beam with span 3.01 m, cross section dimensions 0.2 × 0.3 m, using CFRP and GFRP rods with diameters 9.5, 12.7, 11.3 and 15.9 mm. The observed failure mode was due to steel yielding and concrete cover splitting, and there was an increase in ultimate load up to 104% (Parvin and Sayed Shah, 2016).

There are several types of failure criteria to the beams strengthened with NSM FRP laminate, as listed below (Hsieh and Lin, 2016):

1. Failure at the reinforcement adhesive interface
2. Failure at the epoxy-concrete interface
3. Splitting of the cover
4. Splitting of the edge
5. FRP tensile rupture

The above-mentioned premature failure criteria delays and obstructs the FRP bars from reaching their strength and reduces the efficiency of the strengthening.

2.6 ACI Code/Design for Flexural Strengthening Using NSM FRP

American Concrete Institute Committee 440 (ACI 440-R-08 2008) presents a guideline for design and construction of strengthening RC elements using EB and NSM techniques using FRP.

2.7 Literature Gap

As shown from the above literature, GFRP is a good material that will be of added value when used for strengthening of RC structures. Also, its use is increasing in Egypt and in the World and will continue to increase due to the problems of using steel reinforcement like corrosion. However, all the available literature does not cover the use of NSM GFRP bars in strengthening RC slabs. The aim of this work is to study the effect of strengthening RC slabs using NSM GFRP bars, to overcome the disadvantages of steel reinforcement, as well as the disadvantages of using externally bonded GFRP bars.

Moreover, since all the available literature shows that the main disadvantage for using FRP for strengthening RC elements is the debonding of the FRP bar or sheet, this work will study the impact of changing the GFRP bonding length on the strength of the RC slab, as well as the impact of changing the diameter of the GFRP bar and the number of bars used in the samples.

Chapter 3 – The Experimental Program

This chapter illustrates the experimental work conducted in this study, stating the materials used and their properties. The chapter also lists the number of samples and different series used. It explains the importance of each series and a comparison between their behavior and strength. Furthermore, the design equations used in the calculations are explained and the calculations for the different series are presented.

3.1 The Experimental Series

Six series were chosen to compare the results of NSM strengthened slabs. Each series consists of testing 2 different samples to validate the results. The six series investigate the different variables, first objective is to test the bonded length and its impact on the slabs strengthening. The second is study the effect of the number of GFRP bars on the percentage increase in strengthening of the slab. Lastly, tested series check the impact of the different GFRP bars diameters on the strength of the slab. Table 3.1 shows the details of the series used in the experimental work.

Table 3.1 Test Series

#	# of slabs	Slabs dimensions (m)	Steel Reinf.	Groove dimensions (mm)	GFRP length (m)	# of GFRP bars	GFRP dia. (mm)
S1	2	1.0×2.4×0.1	no.10 @ 200 mm	-	-	-	-
S2	2	1.0×2.4×0.1	no.10 @ 200 mm	20 × 20	2.0	1	12
S3	2	1.0×2.4×0.1	no.10 @ 200 mm	20 × 20	2.0	1	8
S4	2	1.0×2.4×0.1	no.10 @ 200 mm	25 × 25	2.0	1	16
S5	2	1.0×2.4×0.1	no.10 @ 200 mm	25 × 25	1.0	1	16
S6	2	1.0×2.4×0.1	no.10 @ 200 mm	25 × 25	1.5	2	16

3.1.1 Series 1

Two samples are experimented in this series, they are considered the control samples that will be used for comparison with all other samples. Series 1 slabs have dimensions of 1.0 × 2.5 m and a 100 mm thickness, they are reinforced with no. 10 @ 200 mm. No GFRP bars are added to these samples, to have results for the flexural strength of the slab with the used type of concrete and steel only. Figure 3.1 shows Series 1 dimensions and details.

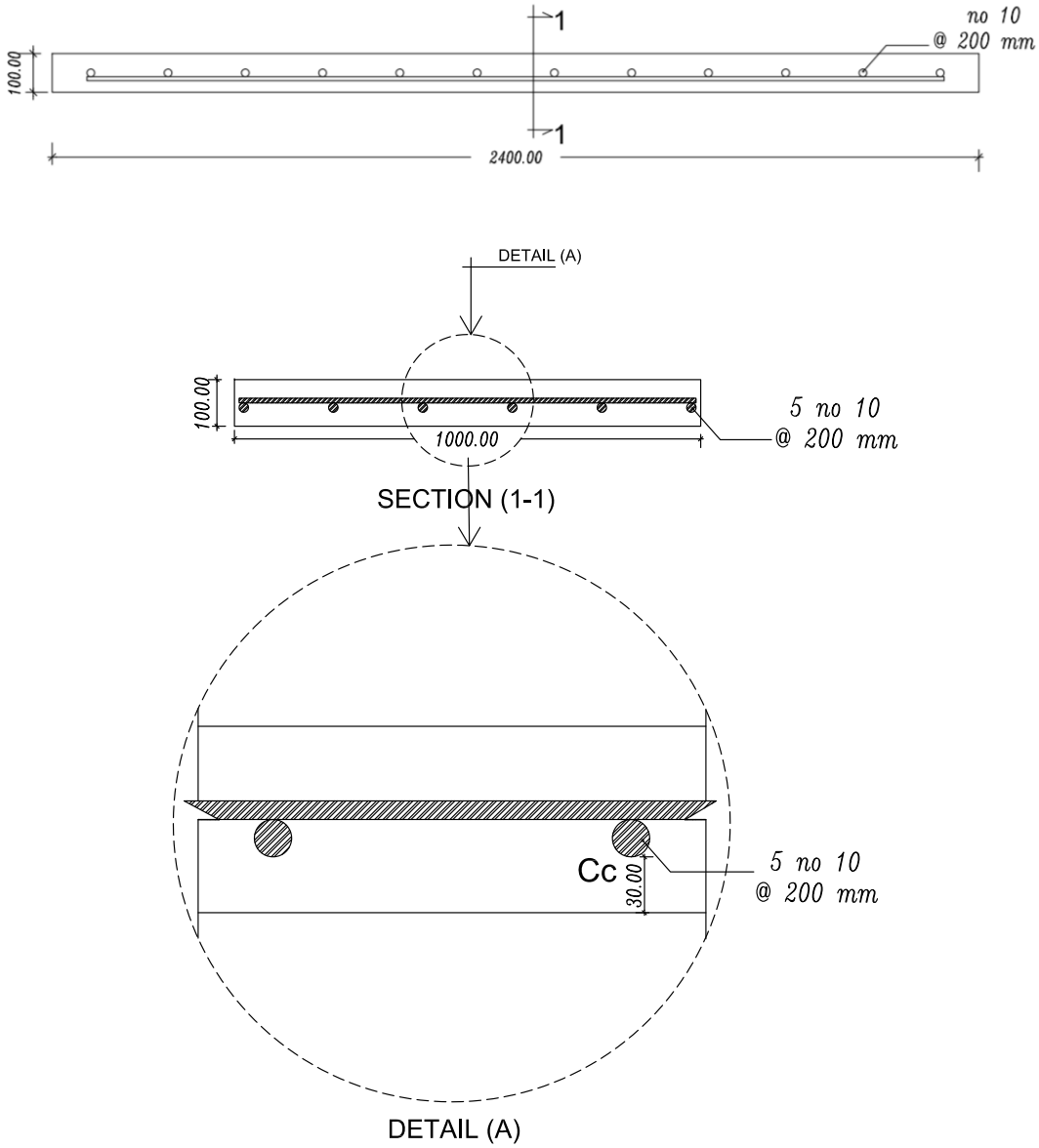

Figure 3.1 Series 1 Cross-section Drawings

3.1.2 Series 2

Two samples are experimented in this series. Series 2 slabs have dimensions of 1.0 x 2.5 m and a 100 mm thickness, they are reinforced with no. 10 @ 200 mm, similar to Series 1. The difference is that there is a groove with dimensions 20 × 20 mm and one GFRP bar 12 mm in diameter and 2 m long added to these samples, to have results for the flexural strength of the slab with the use of 1 GFRP bar with the 2 m length and diameter 12 mm. Figure 3.2 shows Series 2 dimensions and details.

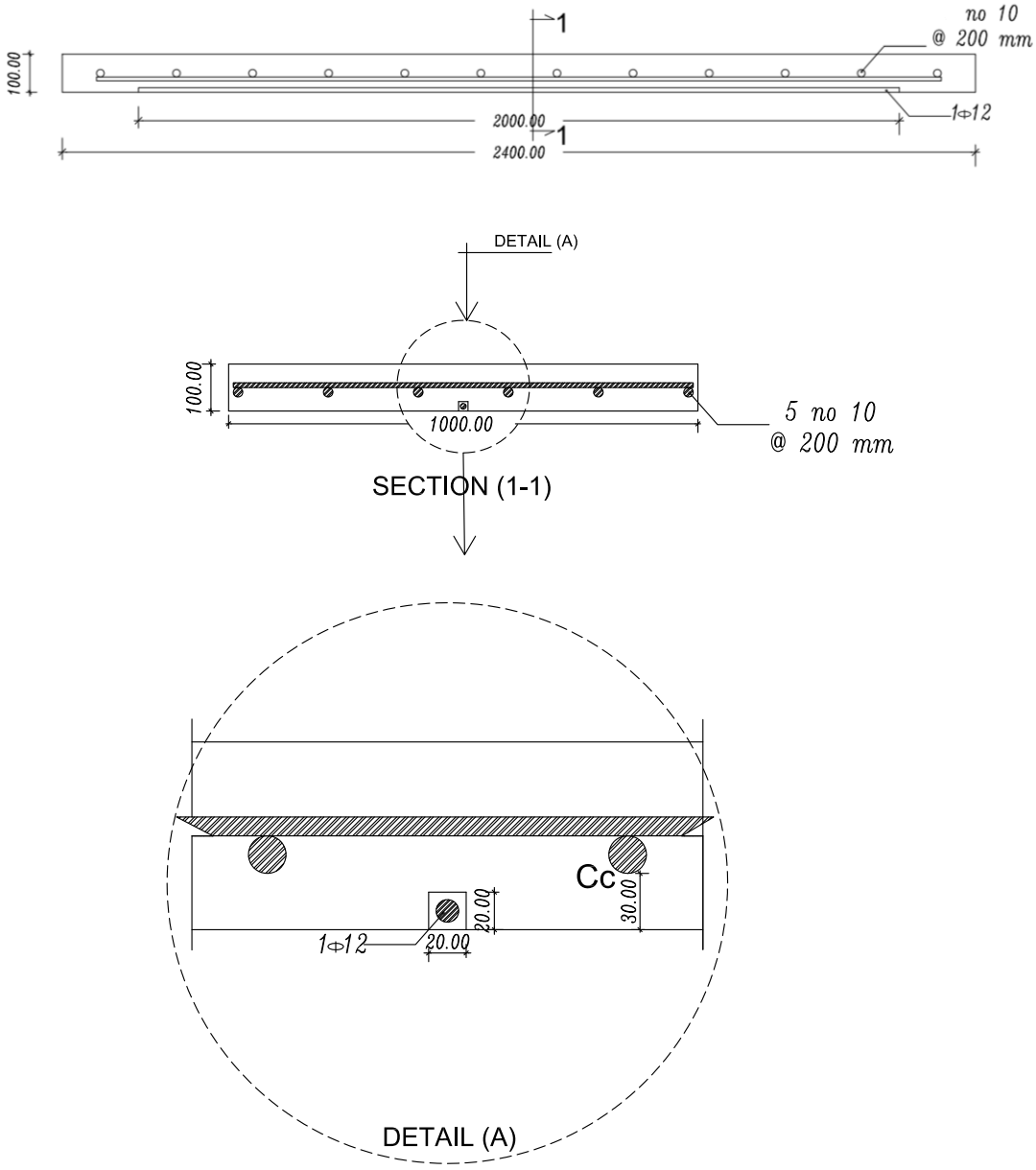

Figure 3.2 Series 2 Cross-section Drawings

3.1.3 Series 3

Two samples are experimented in this series. Series 3 slabs have dimensions of 1.0 x 2.5 m and a 100 mm thickness, they are reinforced with no. 10 @ 200 mm, similar to Series 1 and 2. There is groove with dimensions 20 × 20 mm similar to Series 2, but the difference is that one GFRP bar 8 mm in diameter and 2 m long is added to these samples, instead of diameter 12 mm, to have results for the flexural strength of the slab with the use of 1 GFRP bar with the 2 m length and diameter 8 mm. Figure 3.3 shows Series 3 dimensions and details.

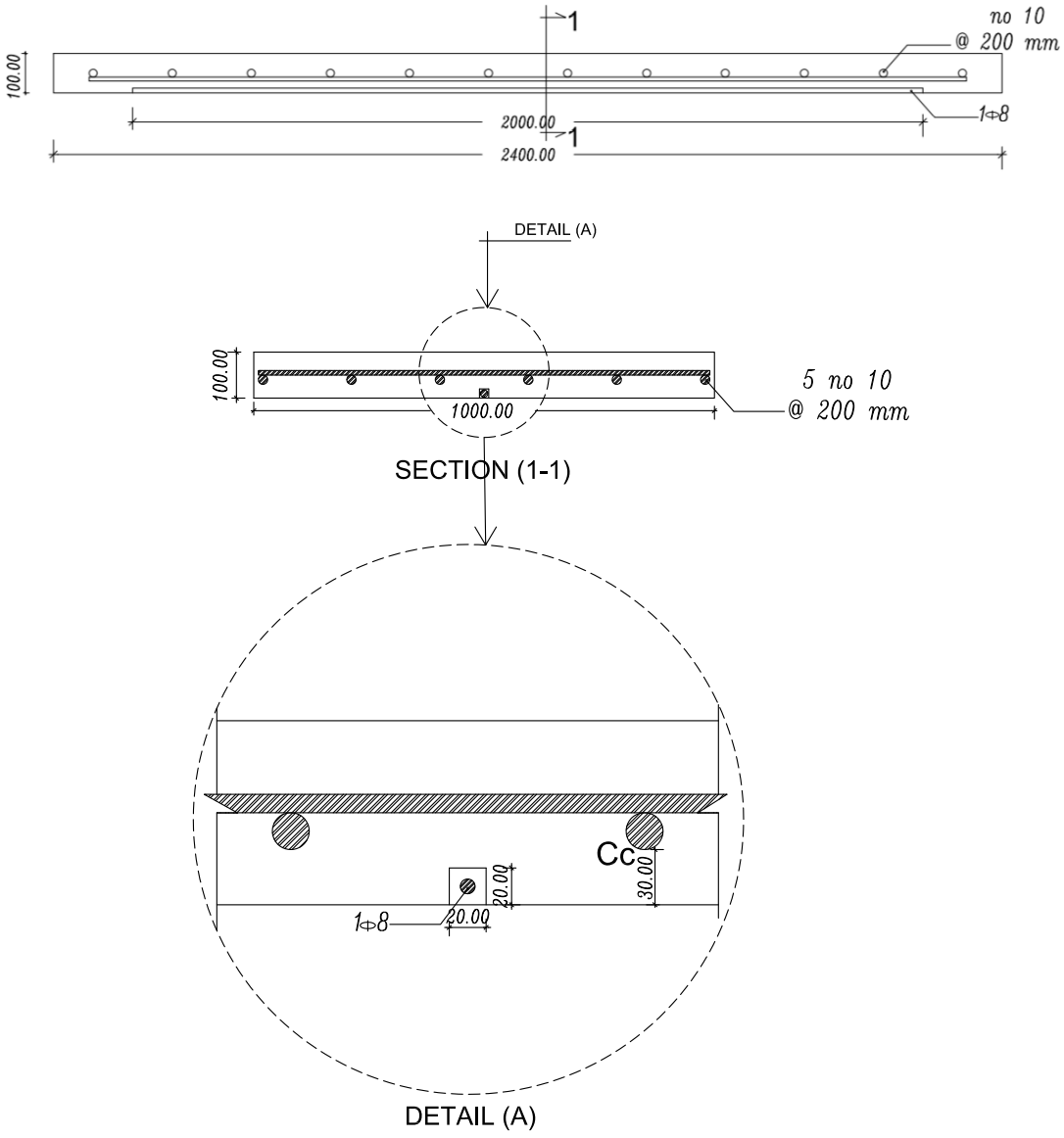

Figure 3.3 Series 3 Cross-section Drawings

3.1.4 Series 4

Two samples are experimented in this series. Series 4 slabs have dimensions of 1.0 x 2.5 m and a 100 mm thickness, they are reinforced with no. 10 @ 200 mm, similar to Series 1, 2 and 3. The difference is that there is groove with dimensions 25 × 25 mm and one GFRP bar 16 mm in diameter and 2 m long added to these samples, instead of diameters 12 and 8 mm, to have results for the flexural strength of the slab with the use of 1 GFRP bar with the 2 m length and diameter 16 mm. Figure 3.4 shows Series 4 dimensions and details.

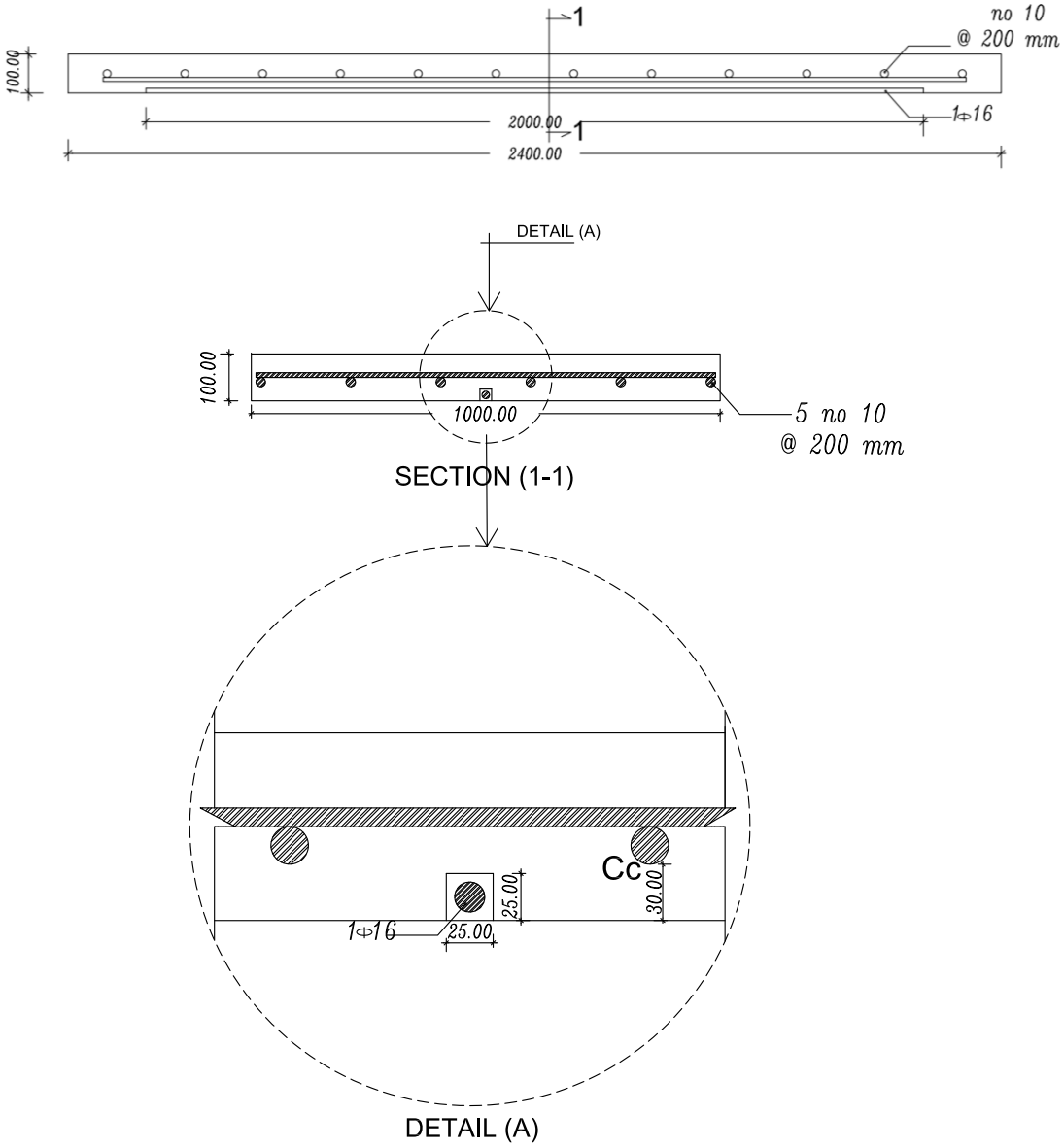

Figure 3.4 Series 4 Cross-section Drawings

3.1.5 Series 5

Two samples are experimented in this series. Series 5 slabs have dimensions of 1.0 x 2.5 m and a 10 cm thickness, they are reinforced with no. 10 @ 200 mm, similar to Series 1, 2, 3 and 4. There is groove with dimensions 25 × 25 mm and one GFRP bar 16 mm in diameter is added similar to Series 4, but the difference is that the GFRP bar is 1 m long, instead of 2 m long, to have results for the flexural strength of the slab with the use of 1 GFRP bar with the 1 m length and diameter 16 mm. Figure 3.5 shows Series 5 dimensions and details.

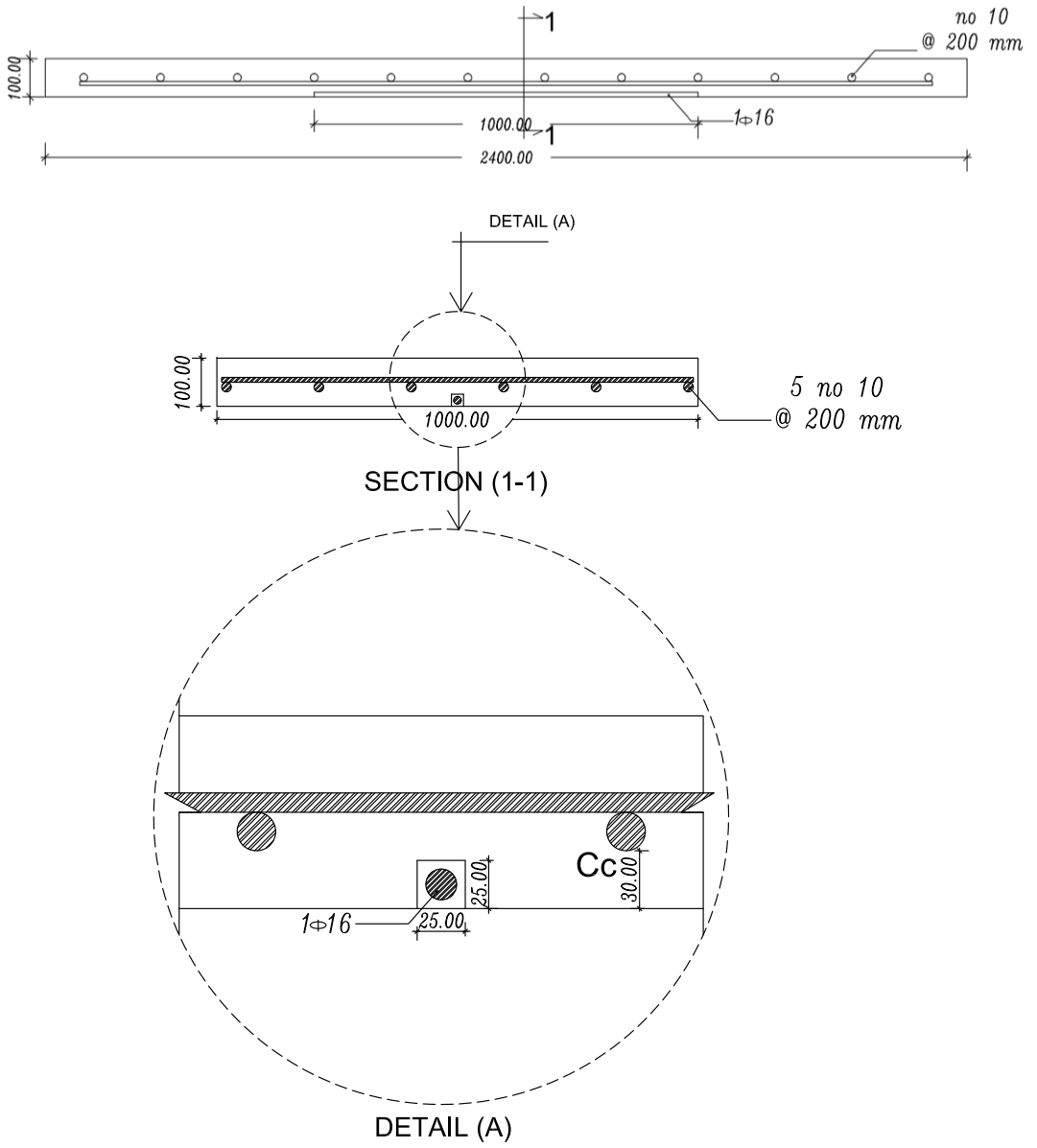

Figure 3.5 Series 5 Cross-section Drawings

3.1.6 Series 6

Two samples are experimented in this series. Series 6 slabs have dimensions of 1.0 x 2.5 m and a 100 mm thickness, they are reinforced with no. 10 @ 200 mm, similar to Series 1, 2, 3, 4 and 5. The difference is that there are 2 grooves with dimensions 25 × 25 mm and two GFRP bars 16 mm in diameter and 1.5 m long added, to have results for the flexural strength of the slab with the use of 2 GFRP bars with the 1.5 m length and diameter 16 mm. Figure 3.6 shows Series 6 dimensions and details.

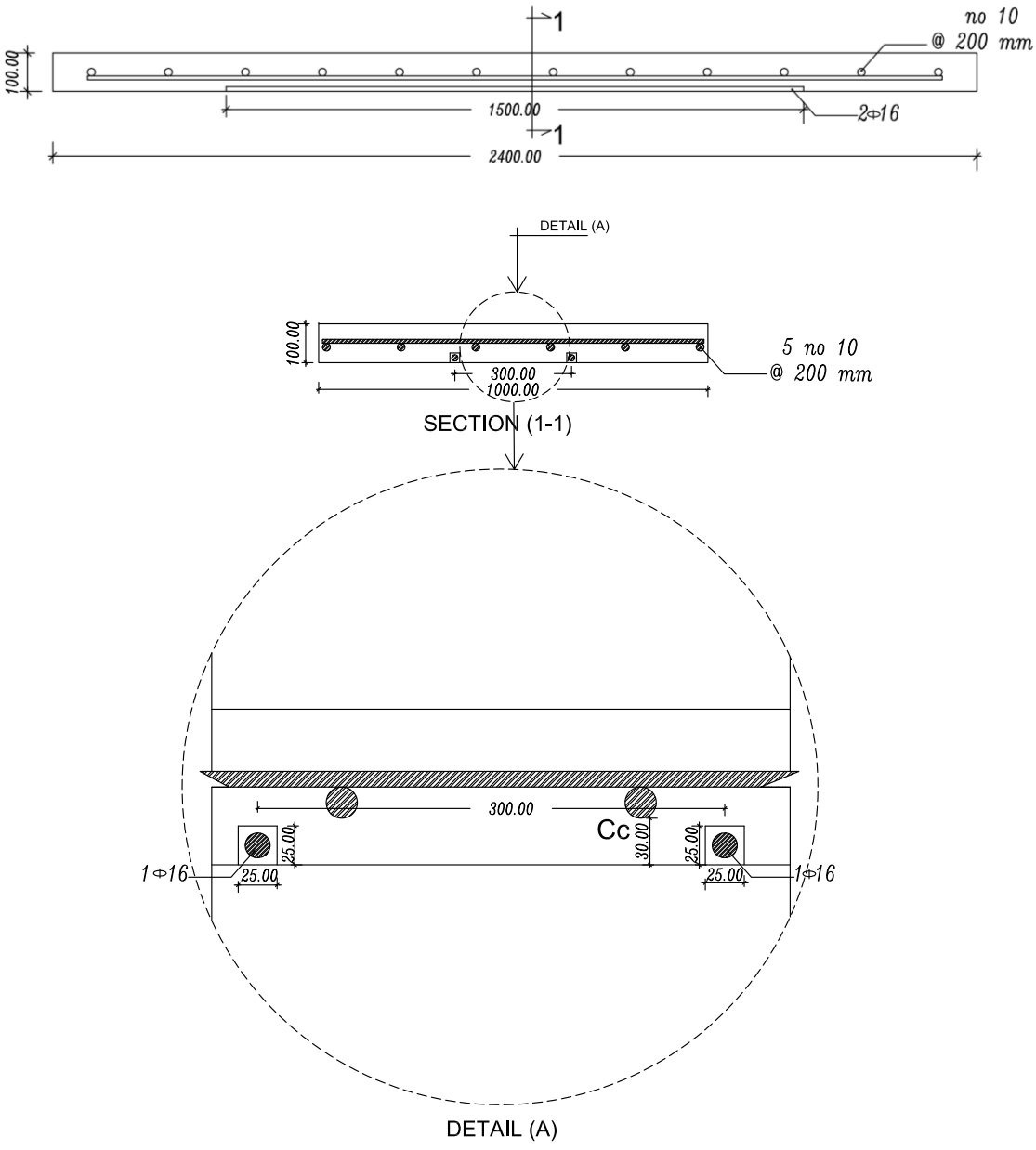

Figure 3.6 Series 6 Cross-section Drawings

3.1.7 Series Comparison

Series 1 will be compared to Series 2,3 and 4, with the variable being the use of GFRP bars. The objective is to compare the use of conventional reinforced concrete versus the use of 1 GFRP bar with 12 mm, 8 mm or 16 mm diameters. Series 2, 3 and 4 will be compared together, with the variable being the GFRP bar diameter (8 mm, 12 mm and 16 mm)

Series 4 and 5 will be compared to each other, with the variable being the GFRP bar length. The objective is to compare the use of 1 GFRP bar with a 16 mm diameter and a length of 2 m with the use of 1 GFRP bar with 16 mm diameter and a length of 1 m.

Series 4 and 6 will be compared together, with the variable being the GFRP bar length as well as the number of bars. The objective is to compare the use of 1 GFRP bar with a 16 mm diameter and a length of 1 m with the use of 2 GFRP bars with 16 mm diameter and a length of 1.5 m.

Series 5 and 6 will be compared together, with the variable being the GFRP bar length as well as the number of bars. The objective is to compare the use of 1 GFRP bar with a 16 mm diameter and a length of 2 m with the use of 2 GFRP bars with a 16 mm diameter and a length of 1.5 m.

3.2 Material Properties

3.2.1 GFRP

The GFRP bars were obtained (in-kind) from Schöck Bauteile GmbH (Germany). Straight ComBAR GFRP bars are certified worldwide and are in compliance with ACI 440.R2 (Schoeck, 2018); below is a comparison of reinforcing steel and Schoeck ComBAR GFRP. As shown in Figure 3.7, the stress for Schoeck ComBAR GFRP bars is almost twice of steel reinforcement, reaching up to 1000 MPa for the same 2% strain. However, it has a much lower tension modulus of Elasticity, as shown in Table 3.2.

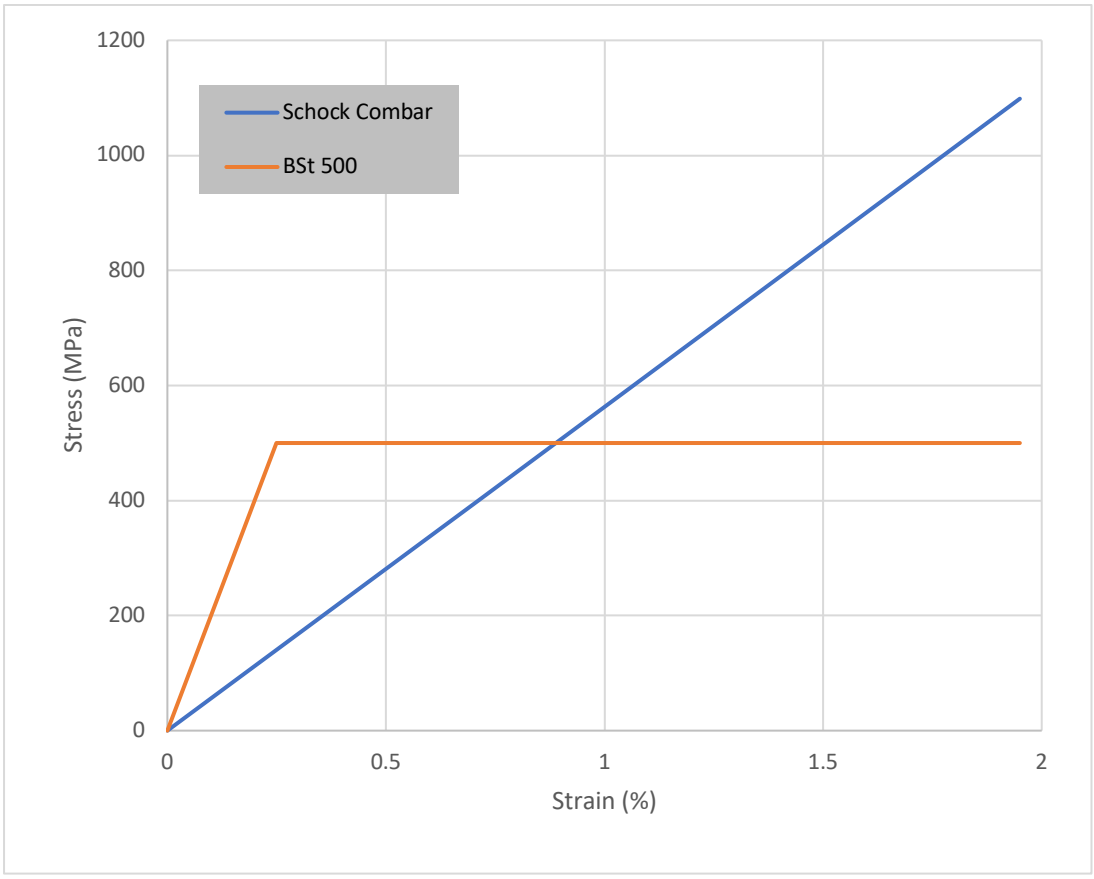

Figure 3.7 Stress-Strain Graph of Schoeck ComBAR GFRP (Schoeck, 2018)

Table 3.2 Properties comparison Schoeck ComBAR GFRP vs. steel reinforcement (Schoeck, 2018)

Material Properties	Reinforcing Steel	Schock Combar acc. to EC 2
Characteristic Yield Strength f_{yk} (MPa)	500	≥ 10,000
Design Value Yield Strength f_{yd} (MPa)	435	≥ 445
Tension Modulus of elasticity E (MPa)	200,000	60,000
Design Value Bond Strength f_{bd} (MPa)	acc. to EC-2	≤ C40/50 – acc. to EC-2 > C40/50 – f_{bd} = 3.7
Concrete Cover C_c (mm)	acc. to EC-2	d_s + 10

According to Schock Combar material manual, the compressive modulus of elasticity is approximately 80% for GFRP, 85% for CFRP, and 100% for AFRP of the tensile modulus of elasticity for the same product (2008). The diameters used for GFRP bars will be equal to 8 mm, 12 mm and 16 mm, weight of each diameter can be obtained from.

Table 3.4. The tension modulus of elasticity from Table 3.2, is equal to 60,000 MPa, the compressive modulus of elasticity is 80% of E so E_c is equal to 48,000 MPa. The design value bond strength as obtained from Table 3.2 is equal to 3.7 MPa and the tensile strength from Table 3.3 depends on the bar diameter ranging from 1200 to 1500 MPa.

Table 3.3 GFRP Short Term Tensile Stress Mean Values (Schoeck, 2018)

Bar diameter (mm)	Mean value f_{fk} (MPa)
8	1,500
12	1,350
16	> 1,200

Table 3.4 GFRP bars diameter and weight (Schoeck, 2018)

Combar diameter (mm)	Designated diameter (ACI/CSA)	Core diameter (mm)	Exterior diameter (mm)	Cross-sectional diameter (mm^2)	Weight per meter (kg/m)
8	M8	8	9	50.3	0.13
12	M13	12	13.5	113	0.29
16	M15	16	18	201	0.52

3.2.2 Reinforced Concrete

A ready-mix design concrete from Elsewedy Ready Mix was used with a 28-days compressive strength f_{cu} of 35 MPa, ultimate strain ε_{cu} of 0.003 and Young's modulus E_c of 27,806 MPa. Each slab will have no. 10 @ 200 mm steel bars with Yield strength F_{ys} of 360 MPa, strain ε_s of 0.03 and Young's modulus E_s of 200,000 MPa. Figure 3.8 shows the slabs' samples right after pouring the concrete.

Figure 3.8 Reinforced Concrete

3.2.3 Formwork

Plywood sheets with dimensions 120 × 240 × 16 mm were used at the bottom of the slabs, and timber wood strips were used as supports on the sides of the slabs as shown in Figure 3.9, they act as the formwork for the slabs.

Figure 3.9 Slab Formwork and Reinforcement

3.2.4 Strain Gauges

3 types of strain gauges were used during testing, 10 mm Kyowa Gages to measure the deflection on steel reinforcement and on the GFRP bars. Moreover, 30 mm – Tokyo Measuring Instruments Laboratory Co. Ltd. were used to measure the

deflection at the top surface of the concrete section in compression and on the epoxy surface. Finally, 60 mm – Tokyo Measuring Instruments Laboratory Co. Ltd. were used to measure the deflection at the bottom surface of the concrete section in tension.

3.2.5 Epoxy Adhesive

A 2-part non-shrink epoxy adhesive mortar, Kemapoxy 165 was used from CMD, to act as an adhesive and enhance the bonding between concrete and GFRP bars. It complies with ASTM C881, has a density of 1.95 ± 0.02 kg/l and has an adhesive strength on concrete of 103 kg/cm.

3.2.6 Loading Beam, Rubber Pads and Rod Support

A loading I-beam with length 1 m was used for applying the load on the slabs, the load is uniformly distributed on the slab in the short direction. Also, since the concrete surface is rough and uneven, 4 rubber pads were added between the loading beam and the slab to ensure proper distribution of the load on the surface. Moreover, a circular steel rod was added under the slab as a support, to make sure it allocates with the slabs' deformation

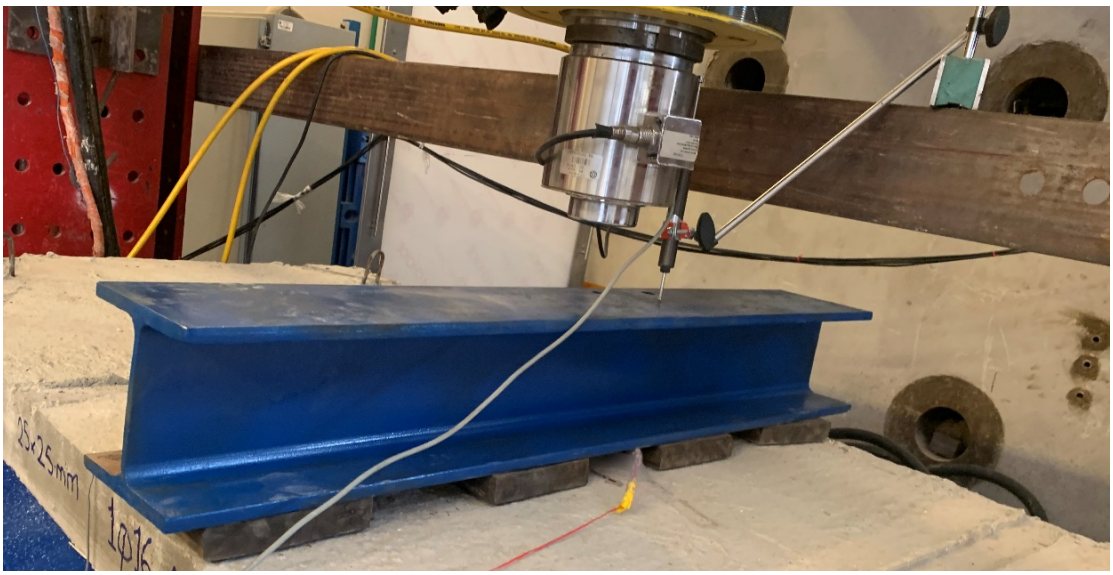

Figure 3.10 Loading beam and rubber pads

3.3 Specimen Design

As per the ACI Code (ACI, 2008), the minimum dimension of the groove for the NSM technique is as shown in Figure 3.11 equal to 1.5 multiplied by the FRP bar diameter, to make sure enough adhesive fills the groove and covers the FRP bar. Therefore, the minimum dimension of the groove (D) is calculated for each bar diameter used, for 8 mm, 12 mm and 16 mm diameters it is equal to 12 mm, 18 mm and 24 mm respectively. Thus, a groove dimension of 20 × 20 mm was used for no. 8 and no. 12, and a groove dimension of 25 × 25 mm was used for no. 16.

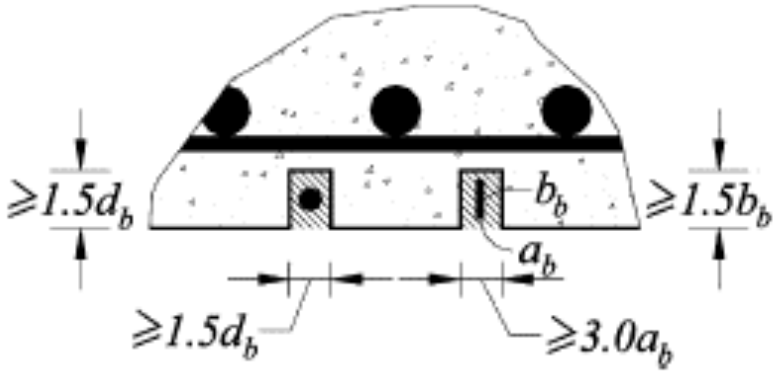

Figure 3.11 Minimum Dimensions of Grooves (ACI, 2008)

Moreover, as per ACI 440.R2.2008, there is a minimum dimension for the FRP bar bonding length, to mitigate premature debonding failure. The purpose for having a limit for the bonding length is to delay the failure of the GFRP bar by detaching from the concrete. This equation is derived from equating the force applied on the bar which is equal to $A_f \times f_{fd}$, to the circumference of the bar in contact with the RC which equals to $\tau_b \times l_{db} \times \pi$ d as shown in Figure 3.12, from which l_{db} for the different used diameters can be calculated.

$$l_{db} = \frac{d_b}{4(\tau_b)} f_{fd} \qquad 3.1$$

where,

l_{db} is the minimum bonding length for the FRP bar

d_b is the used GFRP bar diameter

τ_b is the design value bond strength

f_{fd} is the short term tensile stress

So, for GFRP bars with 8 mm, 12 mm and 16 mm diameters, l_{db} is 811 mm, 1095 mm and 1298 mm, respectively.

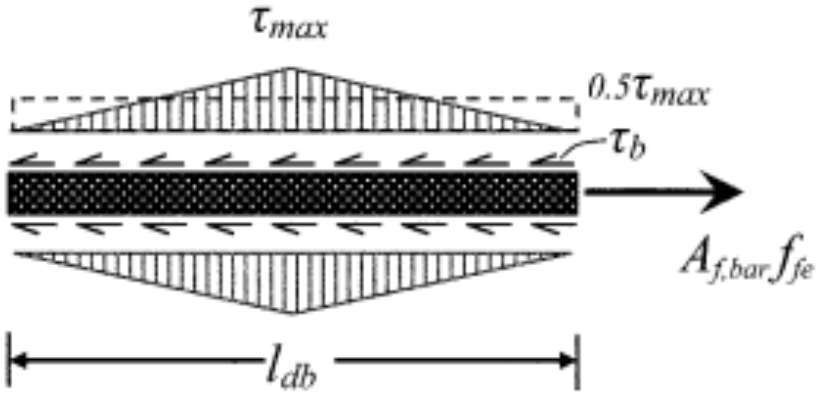

Figure 3.12 Bonding Length of FRP bar (ACI, 2008)

Consequently, the bond length will be 2.0 m for series with GFRP bars of no. 8 and no. 12 mm, which is greater than the accepted minimum, as the main focus for these 3 series is analyzing the effect of using GFRP with different diameters. Moreover, the bonding length will be tested as a variable for series with GFRP bars of no. 16 mm where 3 different dimensions will be used equal to 1.0 m, 1.5 m and 2 m, which are less, equal to and greater than the calculated minimum, in order to be able to analyze the effect of the bonding length on the flexural capacity.

The bonding length is calculated from the point with the maximum moment. Since the slabs will have a moment equal to PL/4, the bonding length is the full bar length.

3.4 Design Calculations for the Tested Slabs

3.4.1 Series 1 (Control Slabs)

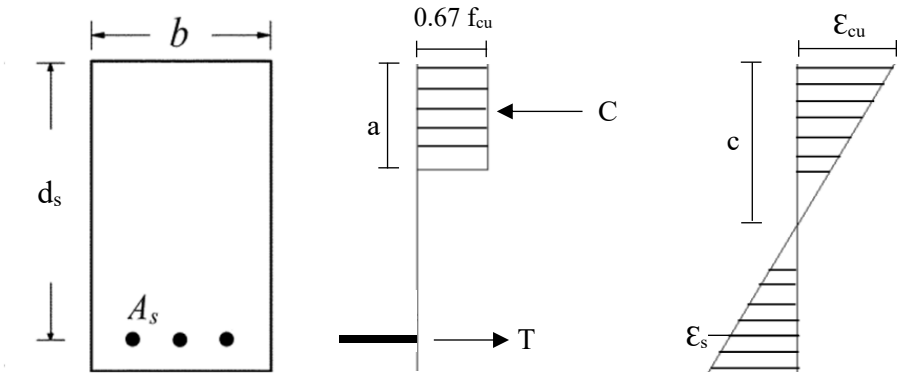

Figure 3.13 Control Sample First Principle Diagram

The failure load for the control samples was calculated using first principle as shown in Figure 3.13, using equilibrium of forces and compatibility of strains concepts, the depth of neutral axis (c) is calculated as:

$$C = 0.67 \times f_{cu} \times b \times a \qquad 3.2$$

where,

C is the compression force

f_{cu} is the concrete compressive strength

a is the depth of compression zone

b is the width of the sample

$$T = F_y \times A_s \qquad 3.3$$

where,

T is the tension force

A_s is the area of the steel reinforcement

F_y is the steel yield strength

$$C = T \qquad 3.4$$

$$0.67 \times f_{cu} \times b \times a = F_y \times A_s$$

$$0.67 \times 36 \times 1000 \times a = 360 \times 6 \times \frac{\pi \times 10^2}{4}$$

Therefore, $a = 7.03$ mm

$$c = \frac{a}{0.85} \quad (3.5)$$

Therefore, $c = 8.27$ mm

$$\frac{\varepsilon s}{ds - c} = \frac{\varepsilon cu}{c} \quad (3.6)$$

where,

ε_s is steel strain

ε_{cu} is concrete strain

d_s is the depth of steel reinforcement

c is the depth of neutral axis

$$\frac{\varepsilon s}{80 - 8.27} = \frac{0.003}{8.27}$$

Therefore, $\varepsilon_s = 0.026 > \varepsilon_y$ ok

After that the resistance moment of the sample is calculated and the ultimate load is obtained

$$M_r = F_y \times A_s \times (ds - \frac{a}{2}) \quad (3.7)$$

where,

M_r is the resistance moment

F_y is the steel yield strength

A_s is the area of the steel reinforcement

d_s is the depth of steel reinforcement

a is the depth of compression zone

$$M_r = 360 \times 6 \times \frac{\pi \times 10^2}{4} \times \left(80 - \frac{7.03}{2}\right)$$

$$M_r = 12.98 \text{ kN} \cdot \text{m}$$

$M_r = \frac{P_u \times L}{4}$ as shown in Figure 3.14 3.8

where,

M_r is the resisting moment

P_u is the ultimate load

L is the length of the sample

Therefore, $P_u = 23.6\ kN$

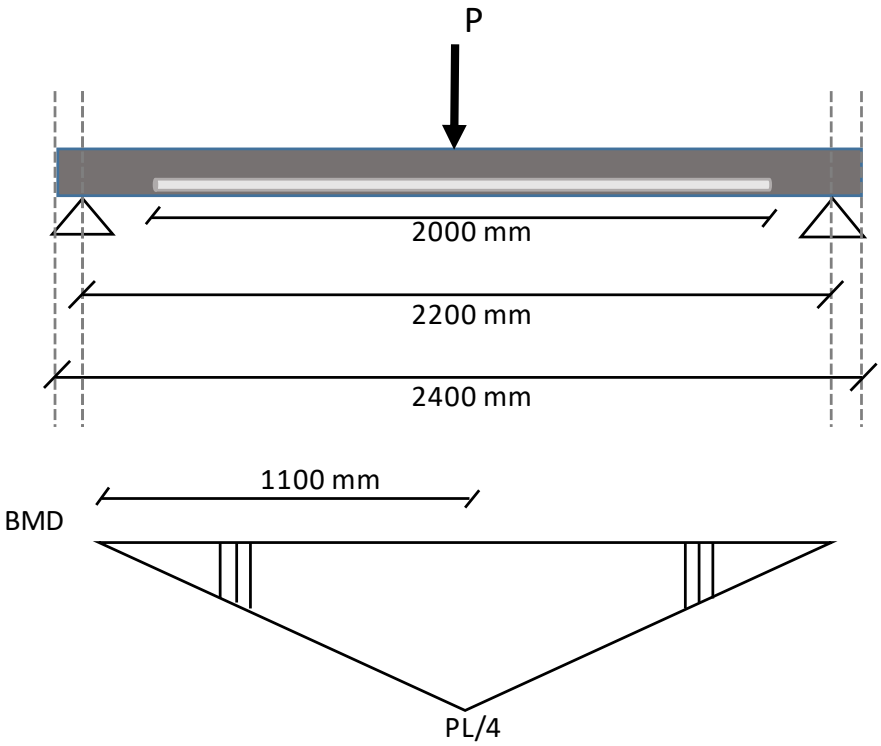

Figure 3.14 Bending Moment Diagram

3.4.2 GFRP Samples

The failure loads for the samples with GFRP were calculated using the first principle as shown in Figure 3.15, where the compression and tension forces from steel reinforcement as well as GFRP are equated as follows

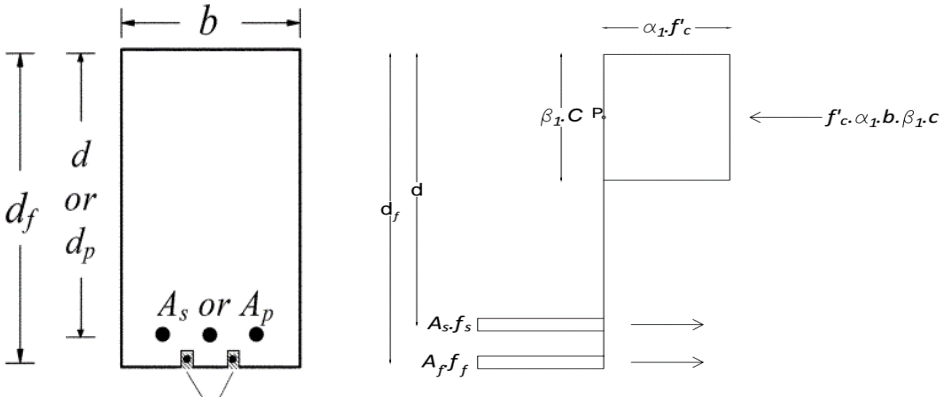

Figure 3.15 GFRP Sections First Principal Diagram (ACI, 2008)

3.4.2.1 Series 2 (1 GFRP bar no. 12)

First, we calculate the FRP system design material properties as well as the materials of concrete

$$f_{fu} = 1350 \text{ MPa}$$

$$E = 60{,}000 \text{ MPa}$$

$$\varepsilon_{cu} = 0.003$$

$$E_c = 4700\sqrt{35} = 27{,}806 \text{ MPa}$$

The existing strain in the sample is assumed to be equals 0 as the slabs are uncracked and are supported on ground at the GFRP installation

$$\varepsilon_{bi} = 0$$

The dimensionless bond-dependent coefficient is based on the manufacturer's recommendation

$$k_m = 0.7$$

The depth of neutral axis (c) is estimated to be 10% the sample's depth, as an initial assumption that will be reiterated and calculated

$$c = 0.1 \times d = 0.1 \times 100 = 10 \text{ mm}$$

After that, we determine the effective level of strain in the FRP reinforcement

$$\varepsilon_{fe} = 0.003 \frac{df-c}{c} - \varepsilon_{bi} \quad 3.9$$

where,

ε_{fe} is the effective level of strain in the GFRP reinforcement

d_f is the depth to the GFRP reinforcement

c is the depth of neutral axis

ε_{bi} is the existing strain in the sample

$$\varepsilon_{fe} = 0.003 \frac{90-10}{10} = 0.024$$

We then check that it is less than or equal to $k_m \varepsilon_{fd}$

$$\varepsilon_{fe} = 0.024 \leq k_m \varepsilon_{fd} = 0.7 \times 0.0225 = 0.01575$$

Therefore, since it is greater than, then the governing failure mode is the debonding. Since GFRP controls failure, concrete strain will not reach 0.003 so it has to be recalculated

$$\varepsilon_c = (\varepsilon_{fd} + \varepsilon_{bi}) \frac{c}{df-c} \quad 3.10$$

where,

ε_c is the strain in the concrete

ε_{fd} is the effective level of strain in the GFRP reinforcement

ε_{bi} is the existing strain in the sample

d_f is the depth to the GFRP reinforcement

c is the depth of neutral axis

$$\varepsilon_c = 0.00197$$

Then, the existing strain in reinforcing steel is calculate using similarity of triangles

$$\varepsilon_s = (\varepsilon_{fe} + \varepsilon_{bi}) \left(\frac{d-c}{df-c}\right) = 0.01180 \quad 3.11$$

where,

ε_s is the strain in the steel reinforcement

ε_{fe} is the effective level of strain in the GFRP reinforcement

ε_{bi} is the existing strain in the sample

d is the depth of the sample

d_f is the depth to the GFRP reinforcement

c is the depth of neutral axis

After the steel and GFRP strain is calculated, the stress level in both of them is calculated and checked to not be greater than f_y and f_f respectively

$$f_s = E_s \times \varepsilon_s = 2362.5 > 360 \text{ MPa} \quad 3.12$$

where,

f_s is the stress in the steel reinforcement

ε_s is the strain in the steel reinforcement

E_s is the modulus of elasticity of steel

Since stress can't be greater than yielding strength, so $f_s = f_y = 360$ MPa

$$f_{fe} = E_f \times \varepsilon_{fe} = 60{,}000 \times 0.01575 = 945 \leq 1350 \text{ MPa}, \quad 3.13$$

where,

f_{fe} is the stress in the GFRP reinforcement

ε_{fe} is the strain in the GFRP reinforcement

E_s is the modulus of elasticity of GFRP

Internal force resultants and equilibrium is checked for the sample,

$$\varepsilon_c' = \frac{1.7 \times fc'}{Ec} = 0.00214 \quad 3.14$$

where,

ε_c' is the yielding strain in concrete

f_c' is the yield compressive strength of concrete

E_c is the modulus of elasticity of concrete

$$\beta_1 = \frac{4 \times \varepsilon c' - \varepsilon c}{6 \times \varepsilon c' - 2 \times \varepsilon c} \quad 3.15$$

where,

β_1 is the first concrete stress block factor calculated based on the parabolic stress strain relationship for concrete

ε_c' is the yielding strain in concrete calculated based on f_c'

ε_c is the strain in concrete

$$\beta_1 = 0.7404$$

$$\alpha_1 = \frac{3\times\varepsilon c\prime\times\varepsilon c-\varepsilon c^2}{3\times\beta 1\times\varepsilon c\prime^2} \quad 3.16$$

where,

α_1 is the second concrete stress block factor calculated based on the parabolic stress strain relationship for concrete

ε_c' is the yielding strain in concrete calculated based on f_c'

ε_c is the strain in concrete

β_1 is the first concrete stress block factor calculated based on the parabolic stress strain relationship for concrete

$$\alpha_1 = 0.8616$$

$$c = \frac{As\times fs+Af\times ffe}{\alpha 1\times fc\prime\times\beta 1\times b} \quad 3.17$$

where,

c is the depth of neutral axis

A_s is the area of steel reinforcement

f_s is the stress in the steel reinforcement

A_f is the area of GFRP reinforcement

f_{fe} is the stress in the GFRP reinforcement

α_1 is the second concrete stress block factor calculated based on the parabolic stress strain relationship for concrete

f_c' is the yield compressive strength of concrete

β_1 is the first concrete stress block factor calculated based on the parabolic stress strain relationship for concrete

b is the width of the RC sample

c = 12.386 mm, not equal to 10 mm (first assumption).

Therefore, re-assume c and iterate using Solver Add-in on Excel to get the value of c when the force equilibrium is satisfied

Using 3.9 $\varepsilon_{fe} = 0.02056 \leq k_m \varepsilon_{fd} = 0.7 \times 0.0225 = 0.01575$

Therefore, the failure mode governing is the debonding, $\varepsilon_{fd} = 0.01575$

Using 3.10 $\varepsilon_c = 0.00230$

Using 3.11 $\varepsilon_s = 0.01174$

Using 3.12 $f_s = 2347.9 > 360$. So, $f_s = f_y = 360$ MPa

Using 3.13 $f_{fe} = 945 \leq 1350$. Ok

Using 3.14 $\varepsilon_c' = 0.00214$

Using 3.15 $\beta_1 = 0.7596$

Using 3.16 $\alpha_1 = 0.9077$

Using 3.17 c = 11.459 mm

After the depth of neutral axis is obtained with force equilibrium, flexural strength components are calculated for the samples

$$M_{ns} = (A_s \times f_s)\left(d_s - \frac{\beta 1 \times c}{2}\right) \quad 3.18$$

where,

M_{ns} is the steel contribution to bending

A_s is the area of steel reinforcement

f_s is the stress in the steel reinforcement

d_s is the depth of the steel reinforcement

c is the depth of neutral axis

β_1 is the first concrete stress block factor calculated based on the parabolic stress strain relationship for concrete

$$M_{ns} = 11.137 \text{ kN·m}$$

$$M_{nf} = (A_f \times f_{fe}) \left(d_f - \frac{\beta 1 \times c}{2}\right) \quad 3.19$$

where,

M_{nf} is the GFRP contribution to bending

A_f is the area of GFRP reinforcement

f_{fe} is the stress in the GFRP reinforcement

d_f is the depth of the GFRP reinforcement

c is the depth of neutral axis

β_1 is the first concrete stress block factor calculated based on the parabolic stress strain relationship for concrete

$$M_{nf} = 13.077 \text{ kN·m}$$

$$M_n = M_{ns} + M_{nf} \quad 3.20$$

where,

M_n is the flexural strength of the section

M_{nf} is the GFRP contribution to bending

M_{ns} is the steel contribution to bending

$$M_n = 24.214 \text{ kN·m}$$

$$P = \frac{M \times 4}{L} \quad 3.21$$

where,

P is the failure load of the section

M_n is the flexural strength of the section

L is the length of the RC sample

$$P = 40.356 \text{ kN}$$

3.4.2.2 Series 3 (1 GFRP bar no. 8)

First, we calculate the FRP system design material properties as well as the materials of concrete

$$f_{fu} = 1350 \text{ MPa}$$

$$E = 60{,}000 \text{ MPa}$$

$$\varepsilon_{cu} = 0.003$$

$$E_c = 4700\sqrt{35} = 27{,}806 \text{ MPa}$$

The existing strain in the sample is assumed to be equals 0 as the slabs are uncracked and are supported on ground at the GFRP installation

$$\varepsilon_{bi} = 0$$

The dimensionless bond-dependent coefficient is based on the manufacturer's recommendation

$$k_m = 0.7$$

The depth of neutral axis (c) is calculated using Solver Add-in on Excel when the force equilibrium is satisfied

$$c = 9.8315 \text{ mm}$$

After that, we determine the effective level of strain in the FRP reinforcement

Using eq. (3.9) $\varepsilon_{fe} = 0.003 \frac{90-9.83}{9.83} = 0.0244$

We then check that it is less than or equal to $k_m \varepsilon_{fd}$

$$\varepsilon_{fe} = \leq k_m \varepsilon_{fd} = 0.7 \times 0.0225 = 0.01575$$

Therefore, since it is greater than, then the governing failure mode is the debonding. Since GFRP controls failure, concrete strain will not reach 0.003 so it has to be recalculated

Using eq. (3.10) $\varepsilon_c = 0.00193$

Then, the existing strain in reinforcing steel is calculate using similarity of triangles

Using 3.11 $\varepsilon_s = 0.01182$

After the steel and GFRP strain is calculated, the stress level in both of them is calculated and checked to not be greater than f_y and f_f respectively

Using 3.12 $f_s = 2364.16 > 360$ MPa

Since stress can't be greater than yielding strength, so $f_s = f_y = 360$ MPa

Using 3.13 $f_{fe} = 60{,}000 \times 0.01575 = 945 \leq 1350$ MPa

Internal force resultants and equilibrium is checked for the sample,

Using 3.14 $\varepsilon_c' = \frac{1.7 \times 35}{27806} = 0.00214$

Using 3.15 $\beta_1 = \frac{4 \times 0.00214 - 0.00193}{6 \times 0.00214 - 2 \times 0.00193} = 0.7384$

Using 3.16 $\alpha_1 = \frac{3 \times 0.00214 \times 0.00193 - 0.00193^2}{3 \times 0.7384 \times 0.00214^2} = 0.8546$

Using 3.17 $c = \frac{471.24 \times 360 + 50.265 \times 945}{0.8546 \times 35 \times 0.7384 \times 1000} = 9.8315$ mm, = to first assumption.

After the depth of neutral axis is obtained with force equilibrium, flexural strength components are calculated for the samples

Using 3.18 $M_{ns} = 11.259$ kN·m

Using 3.19 $M_{nf} = 5.861$ kN·m

Using 3.20 $M_n = 17.120$ kN·m

Using 3.21 $P = 28.534$ kN

3.4.2.3 Series 4 and 5 (1 GFRP bar no. 16)

For series 5, the used length was less than the required minimum specified by the ACI and therefore the available equations will not be applicable as they will show the same value as for series 4.

First, we calculate the FRP system design material properties as well as the materials of concrete

$$f_{fu} = 1350 \text{ MPa}$$

$$E = 60{,}000 \text{ MPa}$$

$$\varepsilon_{cu} = 0.003$$

$$E_c = 4700\sqrt{35} = 27{,}806 \text{ MPa}$$

The existing strain in the sample is assumed to be equals 0 as the slabs are uncracked and are supported on ground at the GFRP installation

$$\varepsilon_{bi} = 0$$

The dimensionless bond-dependent coefficient is based on the manufacturer's recommendation

$$k_m = 0.7$$

The depth of neutral axis (c) is calculated using Solver Add-in on Excel when the force equilibrium is satisfied

$$c = 13.793 \text{ mm}$$

After that, we determine the effective level of strain in the FRP reinforcement

Using eq. (3.9) $\varepsilon_{fe} = 0.003 \frac{90-13.793}{13.793} = 0.01603$

We then check that it is less than or equal to $k_m \varepsilon_{fd}$

$$\varepsilon_{fe} = 0.01603 \leq k_m \varepsilon_{fd} = 0.7 \times 0.0225 = 0.01575$$

Therefore, since it is greater than, then the governing failure mode is the debonding. Since GFRP controls failure, concrete strain will not reach 0.003 so it has to be recalculated

Using 3.10 $\varepsilon_c = 0.00295$

Then, the existing strain in reinforcing steel is calculate using similarity of triangles

Using 3.11 $\varepsilon_s = 0.01201$

After the steel and GFRP strain is calculated, the stress level in both of them is calculated and checked to not be greater than f_y and f_f respectively

Using 3.12 $f_s = 2402.11 > 360$ MPa

Since stress can't be greater than yielding strength, so $f_s = f_y = 360$ MPa

Using 3.13 $f_{fe} = 60{,}000 \times 0.01575 = 945 \leq 1350$ MPa

Internal force resultants and equilibrium is checked for the sample,

Using 3.14 $\varepsilon_c' = \frac{1.7 \times 35}{27806} = 0.00214$

Using 3.15 $\beta_1 = \frac{4 \times 0.00214 - 0.00295}{6 \times 0.00214 - 2 \times 0.00295} = 0.8081$

Using 3.16 $\alpha_1 = \frac{3 \times 0.00214 \times 0.00295 - 0.00295^2}{3 \times 0.8081 \times 0.00214^2} = 0.9219$

Using 3.17 $c = \frac{471.24 \times 360 + 201 \times 945}{0.9219 \times 35 \times 0.8081 \times 1000} = 13.793$ mm, = to first assumption.

After the depth of neutral axis is obtained with force equilibrium, flexural strength components are calculated for the samples

Using 3.18 $M_{ns} = 10.930$ kN·m

Using 3.19 $M_{nf} = 22.238$ kN·m

Using 3.20 $M_n = 33.167$ kN·m

Using 3.21 $P = 55.279$ kN

3.4.2.4 Series 6 (2 GFRP bars no. 16)

First, we calculate the FRP system design material properties as well as the materials of concrete

$$f_{fu} = 1350 \text{ MPa}$$

$$E = 60{,}000 \text{ MPa}$$

$$\varepsilon_{cu} = 0.003,\ E_c = 4700\sqrt{35} = 27{,}806 \text{ MPa}$$

The existing strain in the sample is assumed to be equals 0 as the slabs are uncracked and are supported on ground at the GFRP installation

$$\varepsilon_{bi} = 0$$

The dimensionless bond-dependent coefficient is based on the manufacturer's recommendation

$$k_m = 0.7$$

The depth of neutral axis (c) is calculated using Solver Add-in on Excel when the force equilibrium is satisfied

$$c = 17.54 \text{ mm}$$

After that, we determine the effective level of strain in the FRP reinforcement

Using 3.9 $$\varepsilon_{fe} = 0.003 \frac{90-17.54}{17.54} = 0.01197$$

We then check that it is less than or equal to $k_m \varepsilon_{fd}$

$$\varepsilon_{fe} = 0.024 \leq k_m \varepsilon_{fd} = 0.7 \times 0.0225 = 0.01575$$

Therefore, since it is less than, then the governing failure mode is the concrete crushing. Since GFRP controls failure, concrete strain will reach 0.003

Using 3.10 $$\varepsilon_c = 0.003$$

Then, the existing strain in reinforcing steel is calculate using similarity of triangles

Using 3.11 $$\varepsilon_s = 0.00897$$

After the steel and GFRP strain is calculated, the stress level in both of them is calculated and checked to not be greater than f_y and f_f respectively

Using 3.12 $$f_s = 1794.84 > 360 \text{ MPa}$$

Since stress can't be greater than yielding strength, so $f_s = f_y = 360$ MPa

Using 3.13 $$f_{fe} = 60{,}000 \times 0.01197 = 718.1 \leq 1350 \text{ MPa}$$

Internal force resultants and equilibrium is checked for the sample,

Using 3.14 $$\varepsilon_c' = \frac{1.7 \times 35}{27806} = 0.00214$$

Using 3.15 $\beta_1 = \frac{4\times0.00214-0.003}{6\times0.00214-2\times0.003} = 0.8129$

Using 3.16 $\alpha_1 = \frac{3\times0.00214\times0.003-0.003^2}{3\times0.8129\times0.00214^2} = 0.9187$

Using 3.17 $c = \frac{471.24\times360+402\times718}{0.9187\times35\times0.8129\times1000} = 17.54$ mm, = to first assumption.

After the depth of neutral axis is obtained with force equilibrium, flexural strength components are calculated for the samples

Using 3.18 $M_{ns} = 10.666$ kN·m

Using 3.19 $M_{nf} = 43.631$ kN·m

Using 3.20 $M_n = 54.297$ kN·m

Using 3.21 $P = 90.495$ kN

3.4.3 Cracking Load and Moment

The expected cracking moment is calculated using the below equation, to compare it to the actual cracking moment from the tested slabs

$$S = \frac{I}{y} = \frac{b \times d^2}{6} \quad 3.22$$

$$M_{cr} = S \times 0.6\sqrt{fcu} \quad 3.23$$

where,

M_{cr} is the cracking moment

S is the elastic section modulus of the section

I is the moment of inertia of the section

b is the width of the RC sample

d is the depth of the RC sample

f_{cu} is the concrete compressive strength

$M_{cr} = 6$ kN·m

The expected cracking load is calculated

Using eq. (3.21) $P_{cr} = \frac{6 \times 4}{2.2} = 10.91$ kN

3.4.4 Design Calculations Summary

Table 3.5 Design Calculations Summary

Series	Failure Moment (kN·m)	Failure Load (kN)	Governing Mode of Failure
S1	12.98	23.60	Flexural
S2	24.21	40.36	Debonding
S3	17.12	28.53	Debonding
S4	33.17	55.28	Debonding
S5	-	-	-
S6	54.30	90.50	Concrete Crushing

3.5 Test Setup

The test setup is as shown in Figure 3.16 and Figure 3.17, the slab will be simply supported on the short dimension, a line load is applied perpendicular to the GFRP bar, parallel to the short dimension of the slabs, therefore there will be a one-way distribution of load parallel to the long dimension.

Figure 3.16 Actual Test Setup

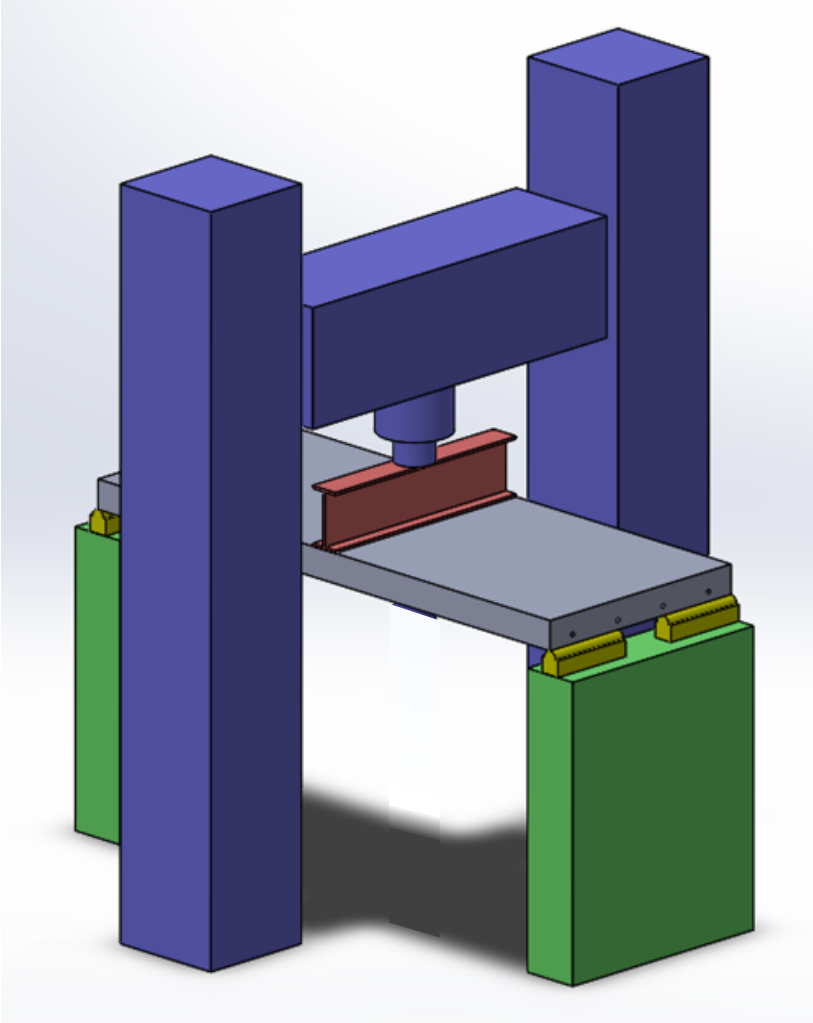

Figure 3.17 Model Test Setup (Makhlouf et al. 2015)

3.5.1 LVDTs

LVDTs were used to measure deflection. As shown in Figure 3.18, LVDT 1 is located at the top of the concrete surface, LVDT 2 located at the midspan to measure the maximum deflection and LVDT 3 below the beam used as a support, to monitor its movement.

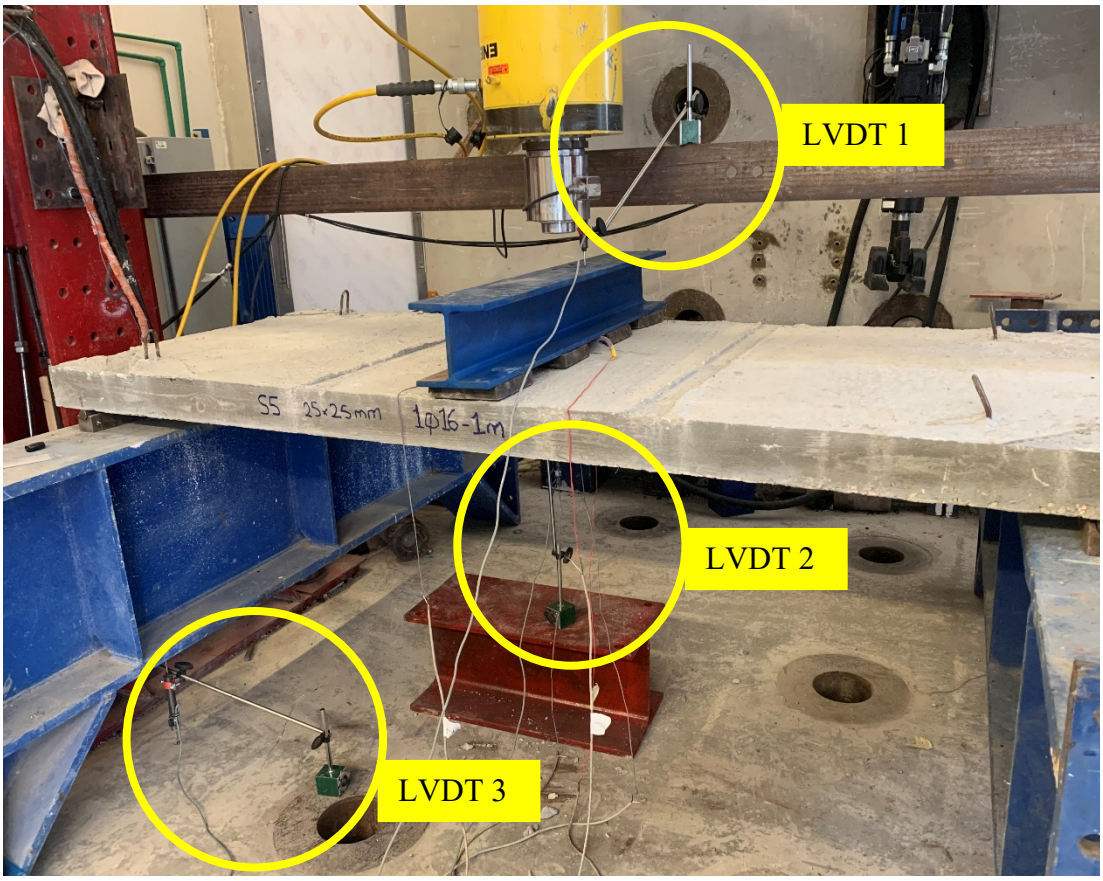

Figure 3.18 Location of LVDTs

3.5.2 Strain Gauges

Strain gauges were used to measure the strain. As shown in Figure 3.19, strain gauge 1 size 10 mm is placed at the steel reinforcement primary bar in the middle of the sample, this will be helpful to be able to compare it to the calculated strain and to check if the steel reached the yielding strength or not. Strain gauge 2 size 30 mm is added at the top surface of concrete, to measure the concrete's strain in compression. Strain gauge 3 size 60 mm is added at the bottom surface of concrete, to measure the concrete's strain in tension. Moreover, strain gauge 4 size 30 mm at the epoxy surface, to measure its performance in relevance to the GFRP. Strain gauges 5 and 6 at the GFRP bars, size 10 mm was used for no. 12 and 16, while size 6 mm was used for no. 8.

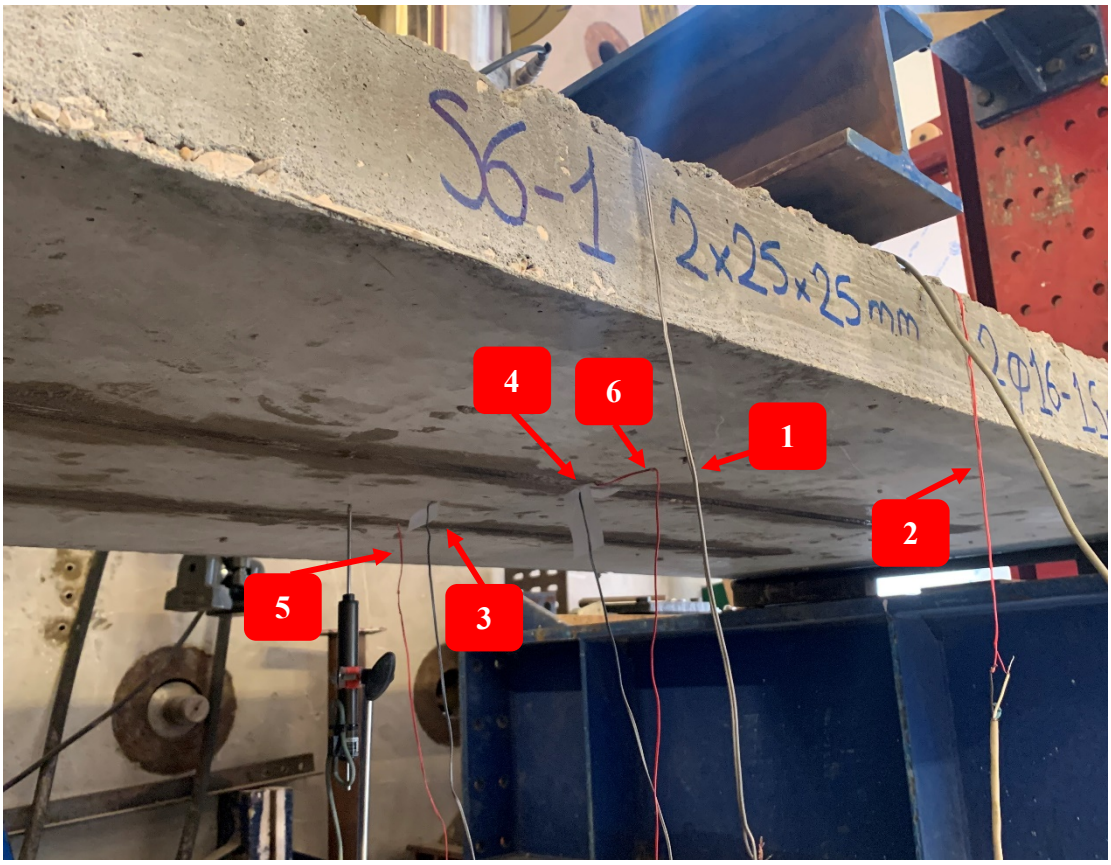

Figure 3.19 Location of Strain Gauges

3.5.3 Supports

The slabs are supported on a 1 m rod that supports the entire span, as shown in Figure 3.20, the circular metal rod is used to act as a hinge and ensure the slabs flexible movement with its deformation.

Figure 3.20 Slabs Supports

3.5.4 Loading and Load Cell

The load cell was used to apply the load on a main loading beam shown in Figure 3.21, which then applied the load on four rubber pads to ensure uniform distribution of the load on the slab due to its uneven surface. Then the rubber pads transferred the load on the slab.

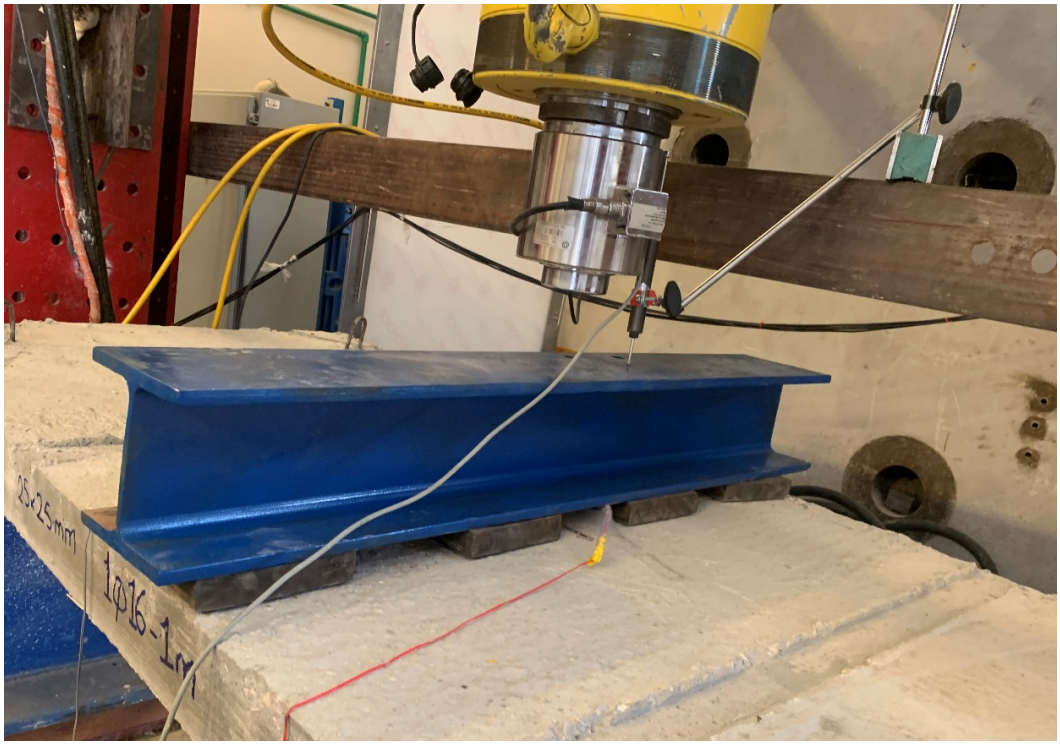

Figure 3.21 Loading

Chapter 4 – Results and Discussion

This chapter demonstrates the results of the flexural tests conducted on the twelve samples, as well as the detailed analysis conducted for each sample, elaborating the mechanical properties of GFRP and comparing between the different series.

4.1 Concrete Compressive Strength

On the day of testing the samples, 12 cubes 150 × 150 × 150 mm were tested as shown in Figure 4.1 to know the concrete compressive strength; the results shown in Table 4.1, reveal that the concrete compressive strength f_{cu} is 36 MPa.

Figure 4.1 Concrete Cube Testing

Table 4.1 Cube Testing - Concrete Compressive Strength

	Peak Load (kN)	Stress (MPa)
Cube 1	734.5	32.64
Cube 2	806.9	35.86
Cube 3	949.3	42.19
Cube 4	807.3	35.88
Cube 5	709.5	31.53
Cube 6	789.7	35.1
Cube 7	811.8	36.08
Cube 8	889.9	39.55
Cube 9	947.6	42.11
Cube 10	770.3	34.24
Cube 11	869.4	38.64
Cube 12	840	37.33

Max	42.19
Min	31.53
Average	36.76
Median	35.98
St. Dev.	3.37

The standard deviation of the samples was reasonable, which did not require excluding any of the samples while calculating the average.

4.2 Results of the Experimental Investigation

The failure load for each conducted test is recorded and the results of the strengthened slabs are analyzed. This is done by checking the cracks and the mode of failure of each sample and plotting the load vs. strain graphs.

There was a fault in the LVDTs used and the load-deformation graphs could not be used in the analysis. However, the maximum deflection was used in the analysis.

4.2.1 Series 1

The first sample is Series 1 Sample 1, without the use of GFRP bars, which will act as a control sample to compare with other samples and know the effect of strengthening using GFRP. There were 3 main cracks that formed at the mid span of the slab as shown in Figure 4.2, the cracks increased as the load increased, concrete started spalling and one crack propagated and was the reason for failure at a load P_f of 32 kN. The mode of failure was due to flexural failure as shown in Figure 4.3, the deflection was maximum at the mid span with a value equal to 64 mm.

Figure 4.2 Series 1-1 – Cracks

Figure 4.3 Series 1-1 - Sample Failure

The second sample is Series 1 Sample 2, without the use of GFRP bars, which will act as a control sample to compare with other samples and know the effect of strengthening using GFRP. It was similar to sample 1, but there was 1 main crack that formed at the mid span of the slab as shown in Figure 4.4. Microcracks generated and increased as the load increased, the crack propagated and was the reason for failure at a load P_f of 31 kN. The mode of failure was due to flexural failure as shown in Figure 4.5, the deflection was maximum at the mid span with a value equal to 58 mm.

Figure 4.4 Series 1-2 - Cracks

Figure 4.5 Series 1-2 - Sample Failure

As shown in Figure 4.6 for sample 1, the cracking load P_{cr} is equal to 10 kN and the concrete strain at failure ε_{cu} is equal to 0.003 at a load of 32 kN. For the steel reinforcement, the strain is equal to 0.007. Also, Figure 4.7 shows the load strain graph for sample 2, the cracking load P_{cr} is equal to 5 kN and the concrete strain at failure ε_{cu} is equal to 0.003 at a load of 31 kN. For the steel reinforcement, the strain is equal to 0.0058.

Therefore, M_{cr} and M_f are calculated for both samples as follows:

$$M_{cr\ S1\text{-}1} = \frac{Pcr \times L}{4} = 5.50\ kN{\cdot}m$$

$$M_{cr\ S1\text{-}2} = \frac{Pcr \times L}{4} = 2.75\ kN{\cdot}m$$

$$M_{f\ S1\text{-}1} = \frac{Pf \times L}{4} = 17.60\ kN{\cdot}m$$

$$M_{f\ S1\text{-}2} = \frac{Pf \times L}{4} = 17.05\ kN{\cdot}m$$

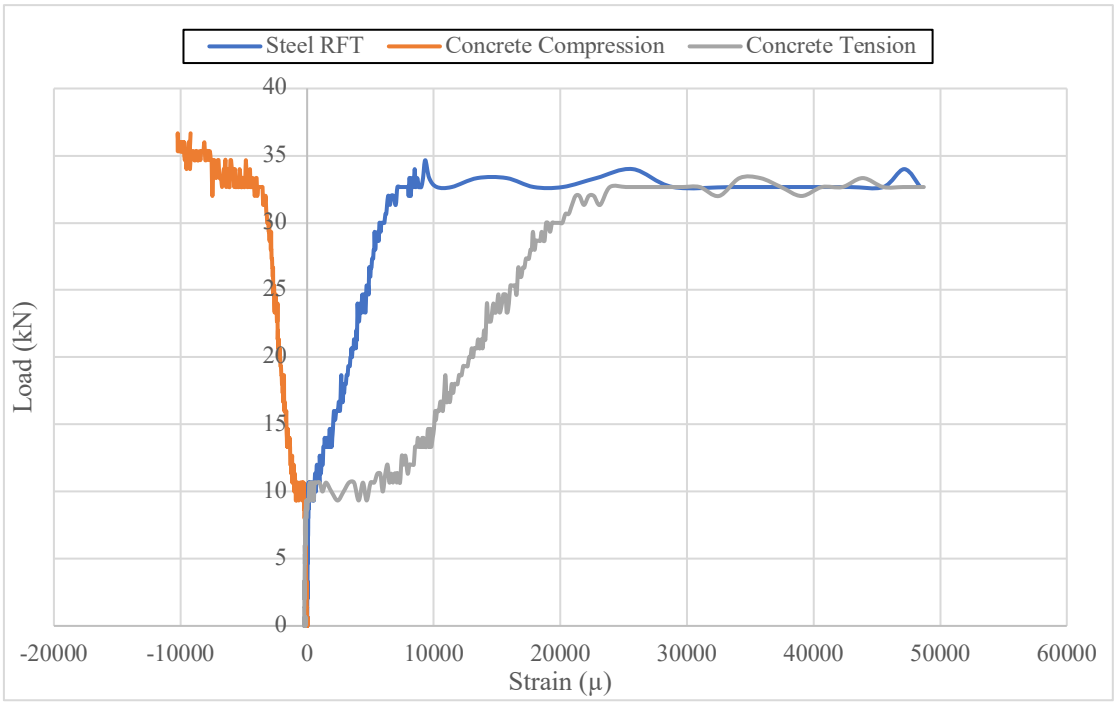

Figure 4.6 Series 1-1 - Load-Strain Graph

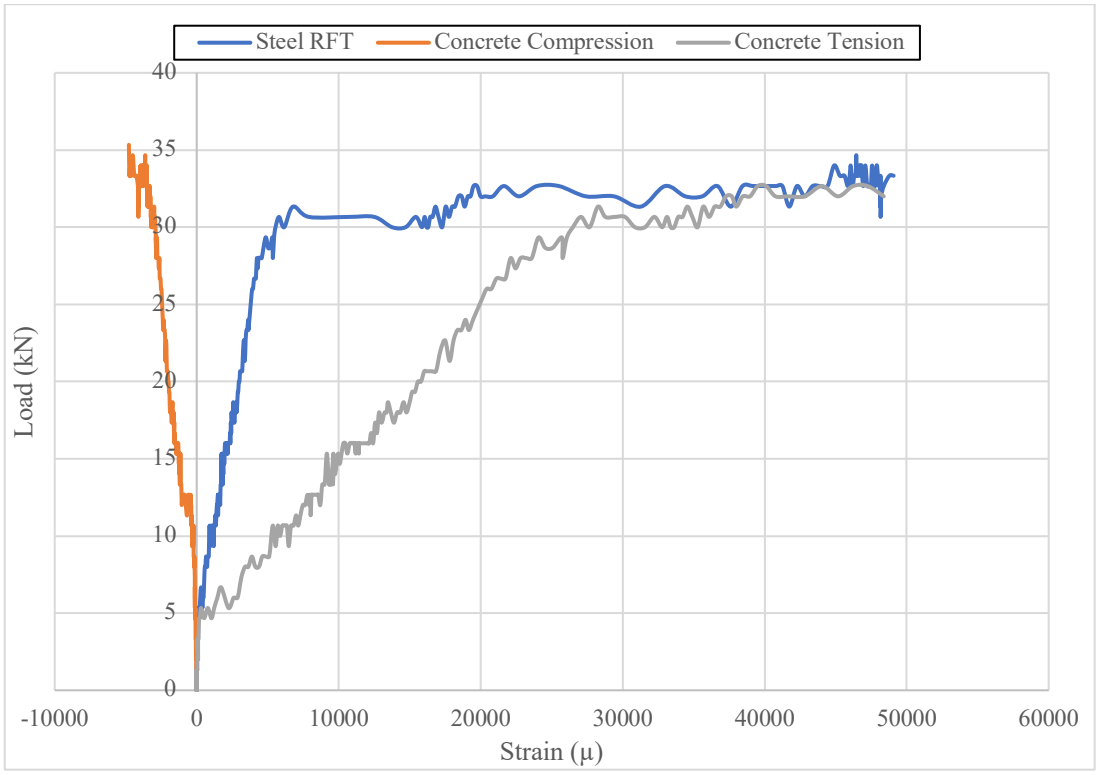

Figure 4.7 Series 1-2 - Load Strain Graph

4.2.2 Series 2

The third sample is Series 2 Sample 1, with the use of 1 GFRP bar 12 mm diameter and 2m long, to see the effect of strengthening using GFRP. There were 2 main cracks that formed at the mid span of the slab as shown in Figure 4.8, the cracks increased as the load increased, and they propagated and drifted around the location of the GFRP bar. The mode of failure was due to flexural failure as shown in Figure 4.9 at a load P_f of 40 kN, the deflection was maximum at the mid span with a value equal to 49 mm.

Figure 4.8 Series 2-1- Cracks

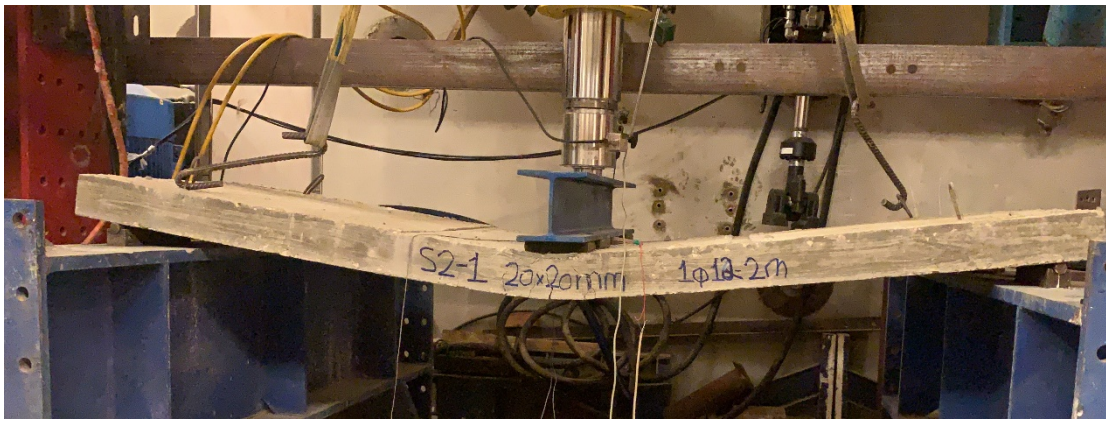

Figure 4.9 Series 2-1- Sample Failure

The fourth sample is Series 2 Sample 2, with the use of 1 GFRP bar 12 mm diameter and 2m long, to see the effect of strengthening using GFRP. There were multiple cracks that formed at the mid span of the slab as shown in Figure 4.10, the cracks increased as the load increased, but there were almost no cracks at the epoxy surface at the location of the GFRP bar. One crack right under the loading beam propagated and was the reason for failure at a load of 40 kN. The mode of failure was due to flexural failure as shown in Figure 4.11, the deflection was maximum at the mid span with a value equal to 77 mm.

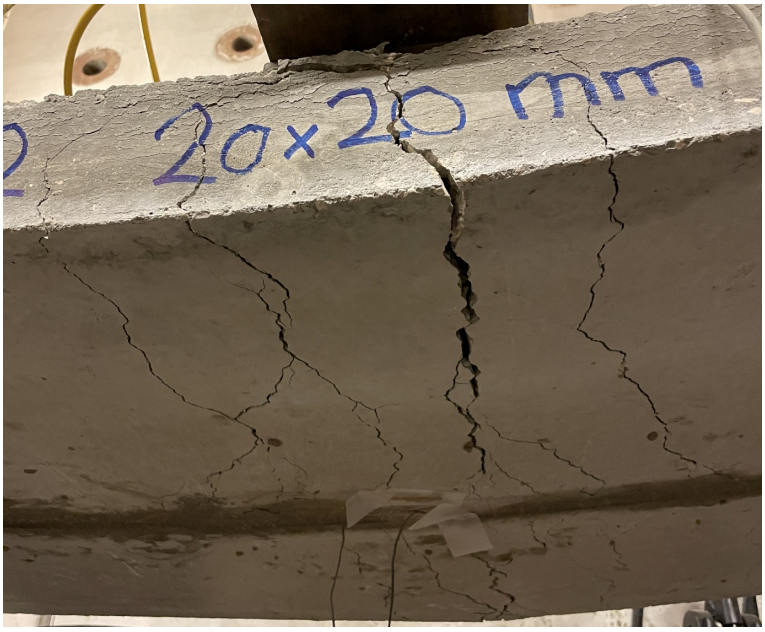

Figure 4.10 Series 2-2- Cracks

Figure 4.11 Series 2-2- Sample Failure

As shown in Figure 4.12 for sample 1, the cracking load P_{cr} is equal to 10 kN and the concrete strain at failure ε_{cu} is equal to 0.0035 at a load of 40 kN. For the steel reinforcement, the strain is equal to 0.009. Also, Figure 4.11, shows the load strain graph for sample 2, the cracking load P_{cr} is equal to 10 kN and the concrete strain at failure ε_{cu} is equal to 0.003 at a load of 40 kN. For the steel reinforcement, the strain is equal to 0.007. Strain gauges on the GFRP bars in both samples didn't work.

Therefore, M_{cr} and M_f are calculated for both samples as follows:

$$M_{cr\ S2\text{-}1} = \frac{Pcr \times L}{4} = 5.50\ \text{kN·m}$$

$$M_{cr\ S2\text{-}2} = \frac{Pcr \times L}{4} = 5.50\ \text{kN·m}$$

$$M_{f\ S2\text{-}1} = \frac{Pf \times L}{4} = 22.0\ \text{kN·m}$$

$$M_{f\ S2\text{-}1} = \frac{Pf \times L}{4} = 22.0\ \text{kN·m}$$

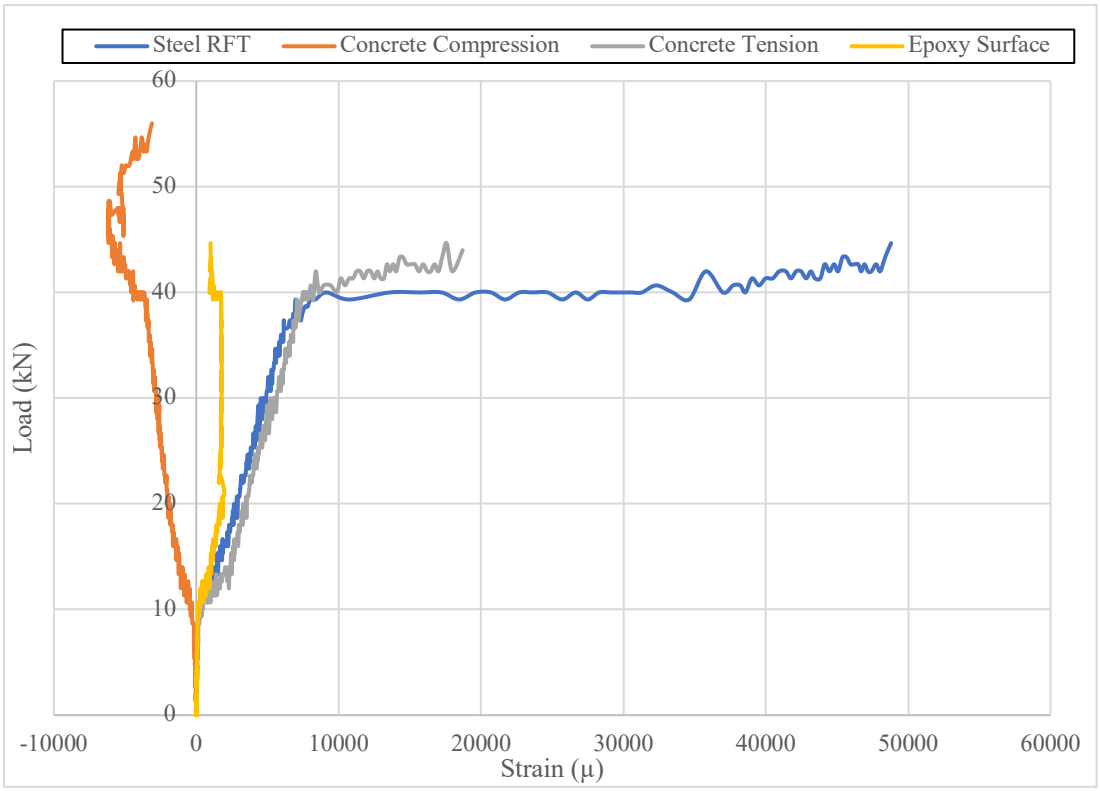

Figure 4.12 Series 2-1 - Load Strain Graph

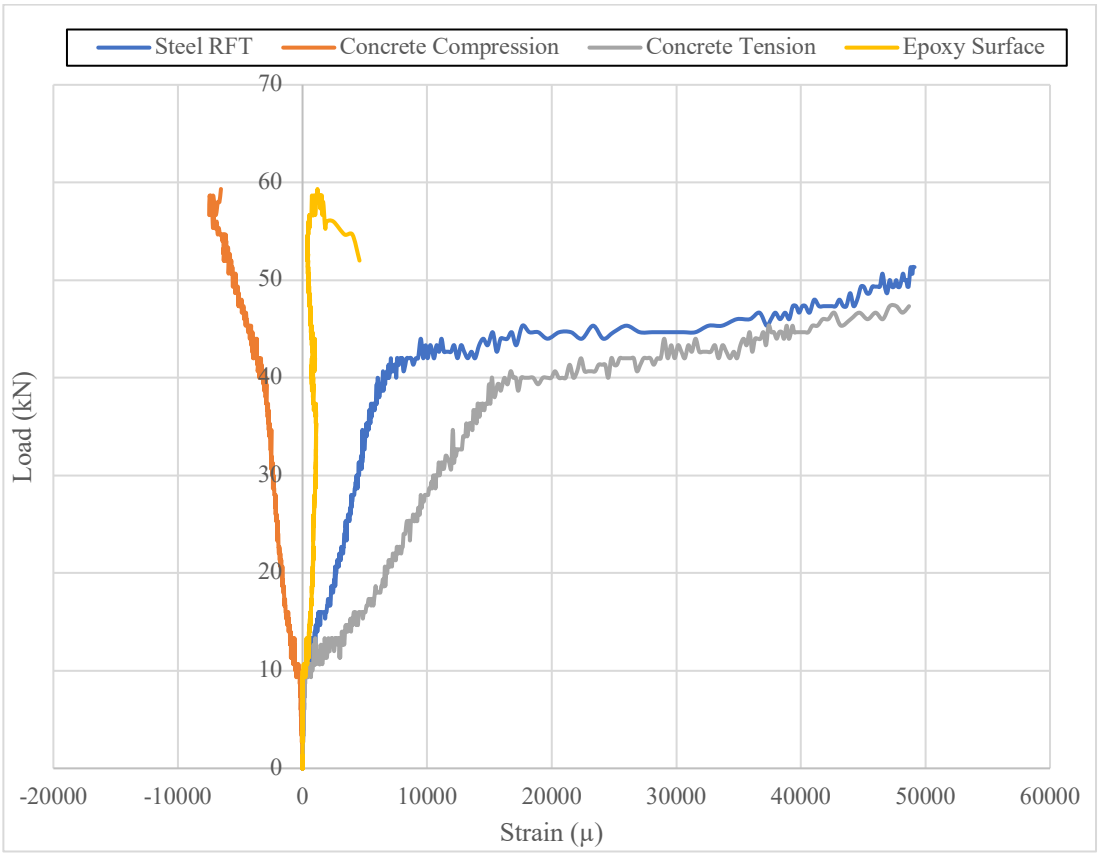

Figure 4.13 Series 2-2- Load Strain Graph

4.2.3 Series 3

The fifth sample is Series 3 Sample 1, with the use of 1 GFRP bar 8 mm diameter and 2m long, to see the effect of strengthening using GFRP. There were multiple cracks that formed at mid span of the slab as shown in Figure 4.14, the cracks increased as the load increased, and they propagated and passed through the epoxy surface at the location of the GFRP bar. The mode of failure was due to flexural failure as shown in Figure 4.15 at a load of 34 kN, the deflection was maximum at the mid span with a value equal to 50 mm.

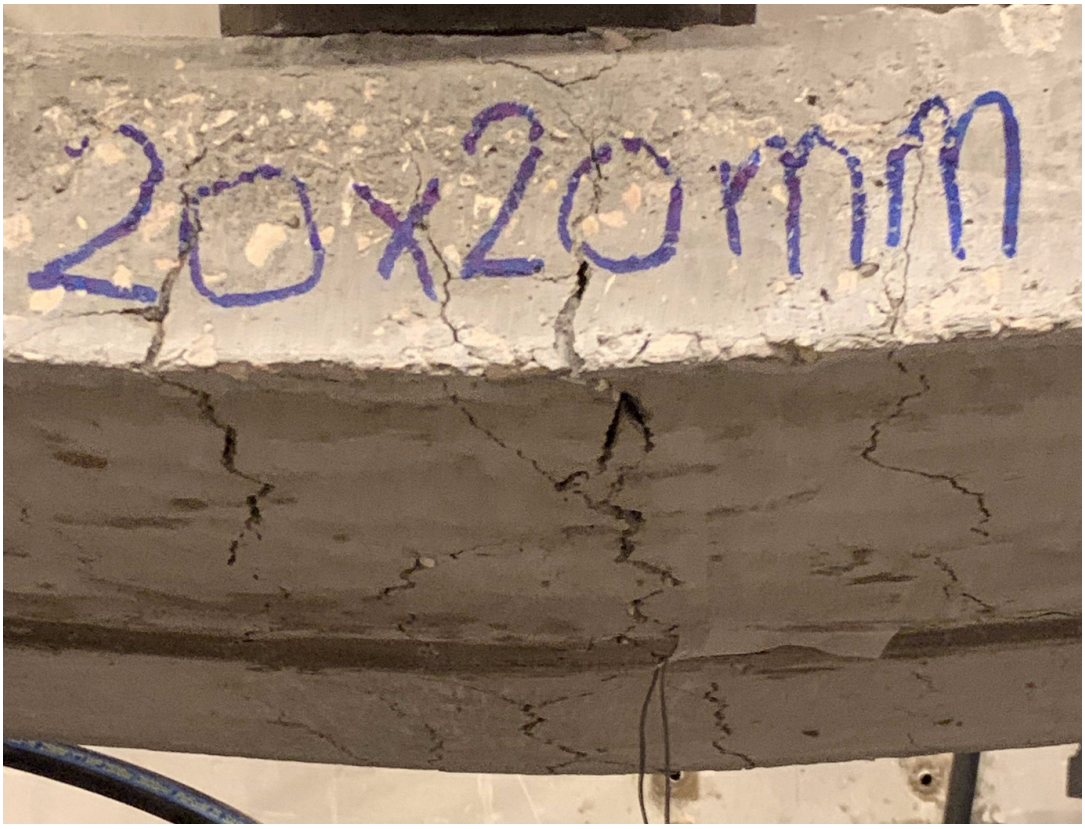

Figure 4.14 Series 3-1- Cracks

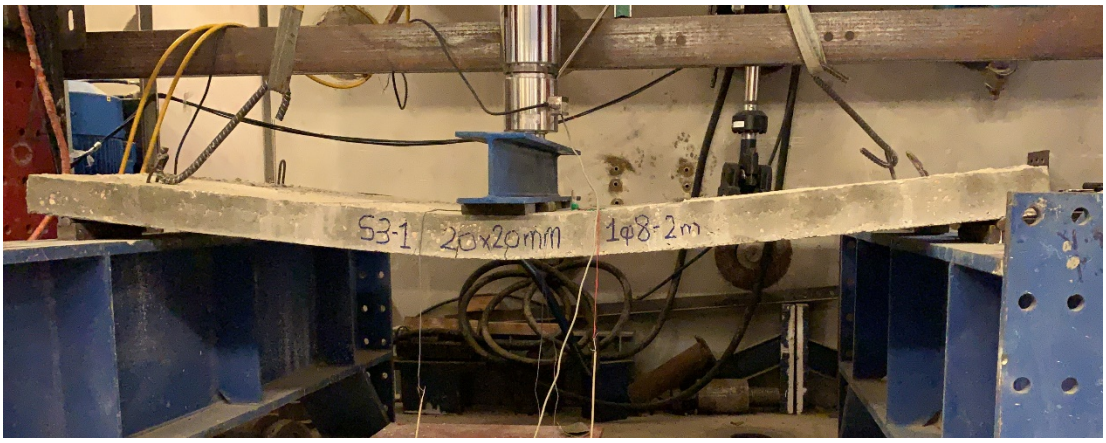

Figure 4.15 Series 3-1- Sample Failure

The sixth sample is Series 3 Sample 2, with the use of 1 GFRP bar 8 mm diameter and 2m long, to see the effect of strengthening using GFRP. There were three main cracks that formed at mid span of the slab as shown in Figure 4.16, the cracks increased as the load increased, and they propagated and passed through the epoxy surface at the location of the GFRP bar. The mode of failure was due to flexural failure as shown in Figure 4.17 at a load of 37 kN, the deflection was maximum at the mid span with a value equal to 50 mm.

Figure 4.16 Series 3-2- Cracks

Figure 4.17 Series 3-2- Sample Failure

As shown in Figure 4.18 for sample 1, the cracking load P_{cr} is equal to 11 kN and the steel reinforcement strain is equal to 0.0074. Also, Figure 4.19 shows the load strain graph for sample 2, the strain gauge at the concrete bottom surface was not working. The cracking load P_{cr} is equal to 10 kN and the steel reinforcement strain is equal to 0.008. Strain gauges on the GFRP bars in both samples didn't work.

Therefore, M_{cr} and M_f are calculated for both samples as follows:

$$M_{cr\ S3\text{-}1} = \frac{Pcr \times L}{4} = 6.05\ \text{kN·m}$$

$$M_{cr\ S3\text{-}2} = \frac{Pcr \times L}{4} = 5.50\ \text{kN·m}$$

$$M_{f\ S3\text{-}1} = \frac{Pf \times L}{4} = 18.70\ \text{kN·m}$$

$$M_{f\ S3\text{-}2} = \frac{Pf \times L}{4} = 20.35\ \text{kN·m}$$

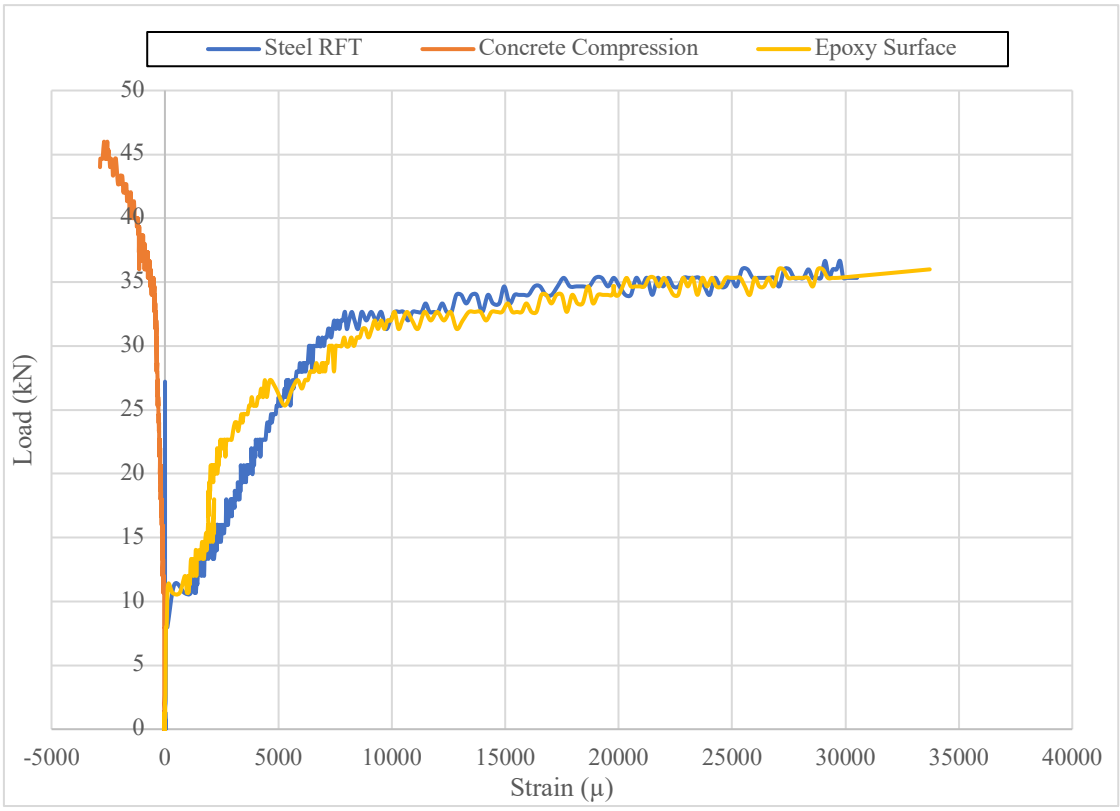

Figure 4.18 Series 3-1- Load Strain Graph

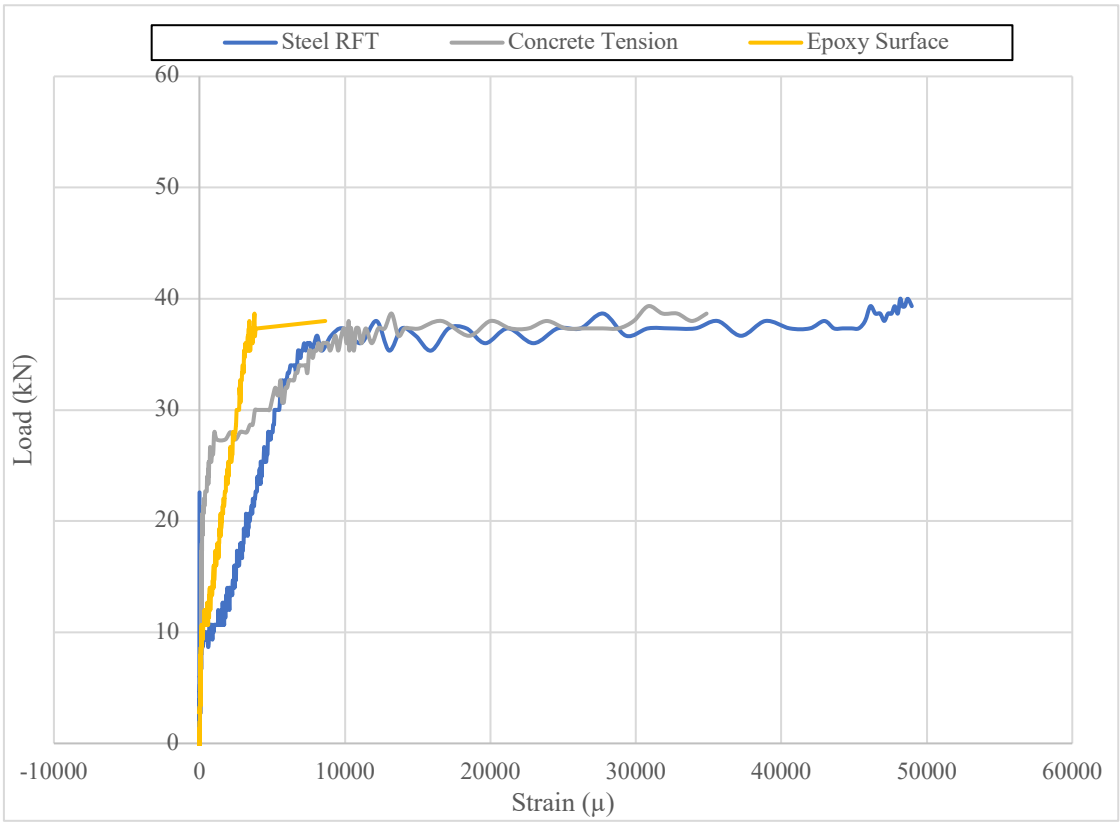

Figure 4.19 Series 3-2- Load Strain Graph

4.2.4 Series 4

The seventh sample is Series 4 Sample 1, with the use of 1 GFRP bar 16 mm diameter and 2m long, to see the effect of strengthening using GFRP. There were multiple cracks that formed at mid span of the slab as shown in Figure 4.20, the cracks increased as the load increased, but there were almost no cracks at the epoxy surface at the location of the GFRP bar, as they drifted parallel to the GFRP bar. Two cracks under the loading beam propagated and were the reason for failure at a load of 43 kN. The mode of failure was due to flexural failure as shown in Figure 4.21 and the deflection was maximum at the mid span with a value equal to 69 mm.

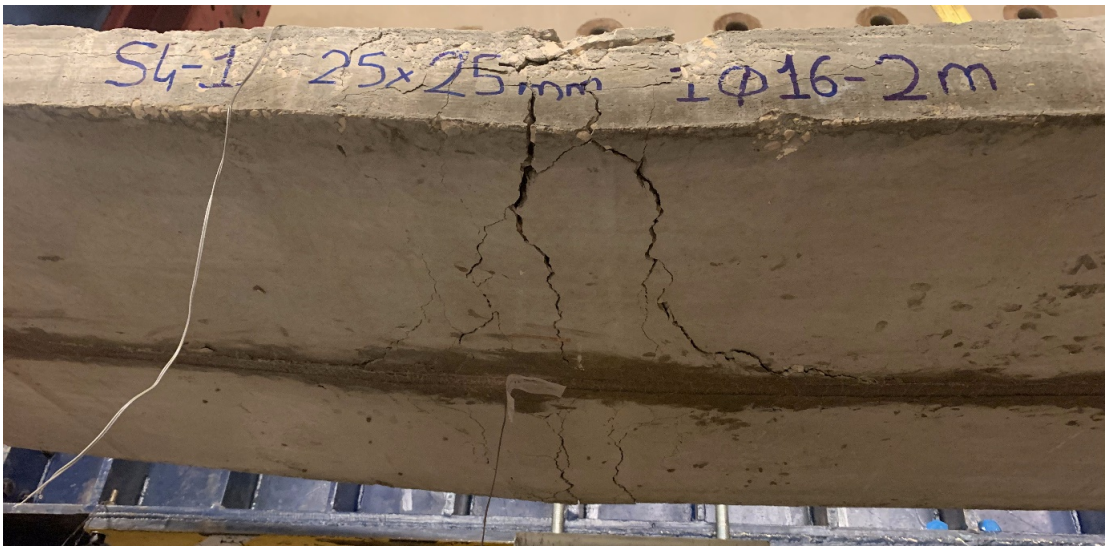

Figure 4.20 Series 4-1- Cracks

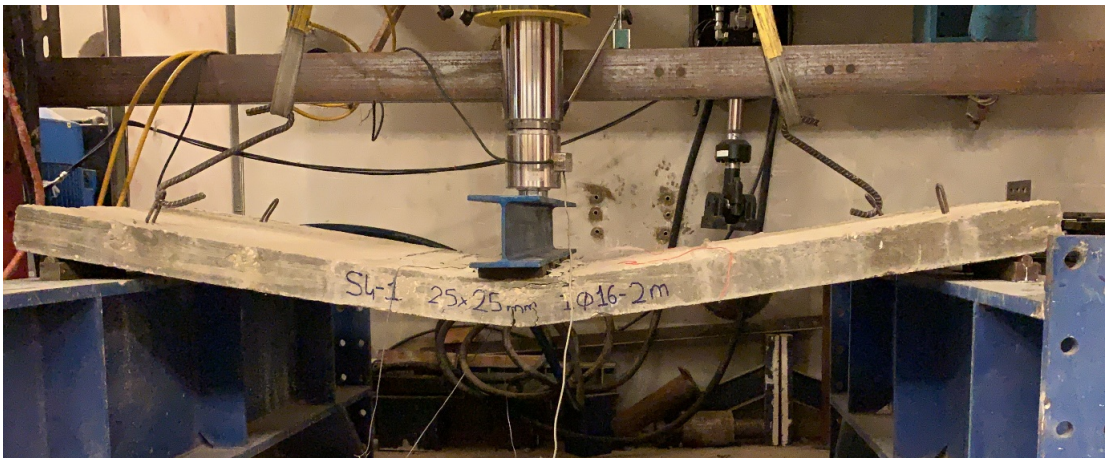

Figure 4.21 Series 4-1- Sample Failure

The eighth sample is Series 4 Sample 2, with the use of 1 GFRP bar 16 mm diameter and 2m long, to see the effect of strengthening using GFRP. There was a problem with this sample as part of it was broken due to a concrete block falling on it as shown in Figure 4.22. However, it was repaired using Grout as shown in Figure 4.23 and was tested.

Figure 4.22 Series 4-2 Broken sample before repair

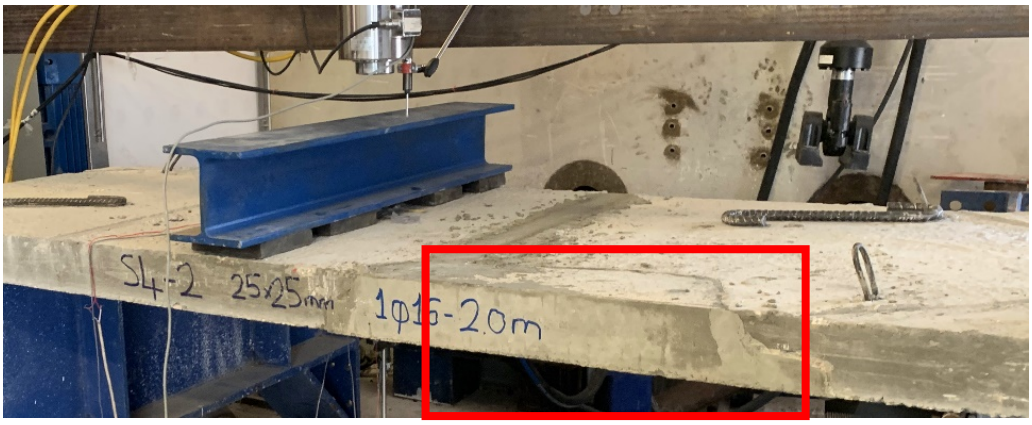

Figure 4.23 Series 4-2 Broken sample after repair

There were multiple cracks that formed at mid span of the slab as shown in Figure 4.24, the cracks increased as the load increased, and there were cracks at the location of the GFRP bar, but there were no cracks at the location of the repaired grout,

since it has higher strength than concrete, non-shrinkage grout. Cracks under the loading beam propagated and were the reason for failure at a load of 50 kN. The mode of failure was due to debonding as the epoxy surface spalled and the GFRP fully detached from the concrete slab as shown in Figure 4.25. The failure mode was due to debonding unlike the first sample in series 4, due to the grout used in repair. As no cracks occurred at the grout and there was no deflection at the repaired part, increasing the stress on the epoxy surface and GFRP bar. The deflection was maximum at the mid span with a value equal to 60 mm.

Figure 4.24 Series 4-2 Cracks

Figure 4.25 Series 4-2- Sample Failure

As shown in Figure 4.26 for sample 1, the cracking load P_{cr} is equal to 10 kN. For the steel reinforcement and GFRP, the strain gauges weren't working. Also, Figure 4.27 shows the load strain graph for sample 2, the cracking load P_{cr} is equal to 11 kN and the concrete strain at failure ε_{cu} is equal to 0.0028 at a load of 34 kN. For the steel reinforcement, the strain is equal to 0.009. Additionally, the strain for the GFRP bar is equal to 0.023.

Therefore, M_{cr} and M_f are calculated for both samples as follows:

$$M_{cr\ S4\text{-}1} = \frac{Pcr \times L}{4} = 5.50\ kN{\cdot}m$$

$$M_{cr\ S4\text{-}2} = \frac{Pcr \times L}{4} = 6.05\ kN{\cdot}m$$

$$M_{f\ S4\text{-}1} = \frac{Pf \times L}{4} = 23.65\ kN{\cdot}m$$

$$M_{f\ S4\text{-}2} = \frac{Pf \times L}{4} = 27.50\ kN{\cdot}m$$

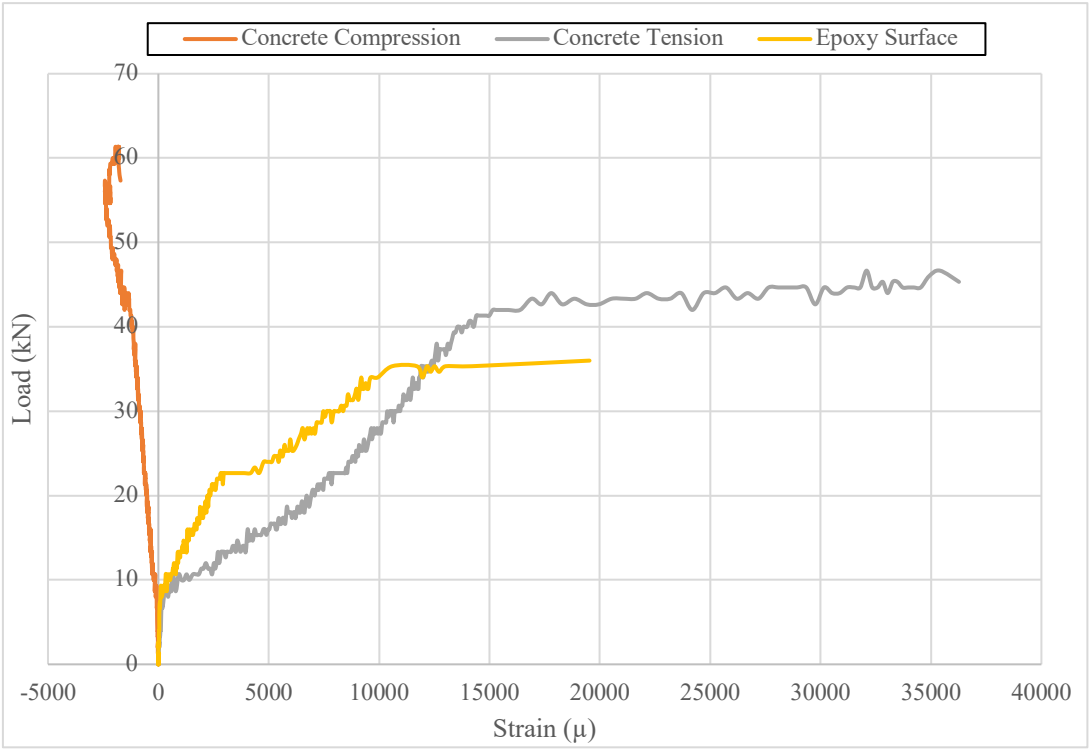

Figure 4.26 Series 4-1- Load Strain Graph

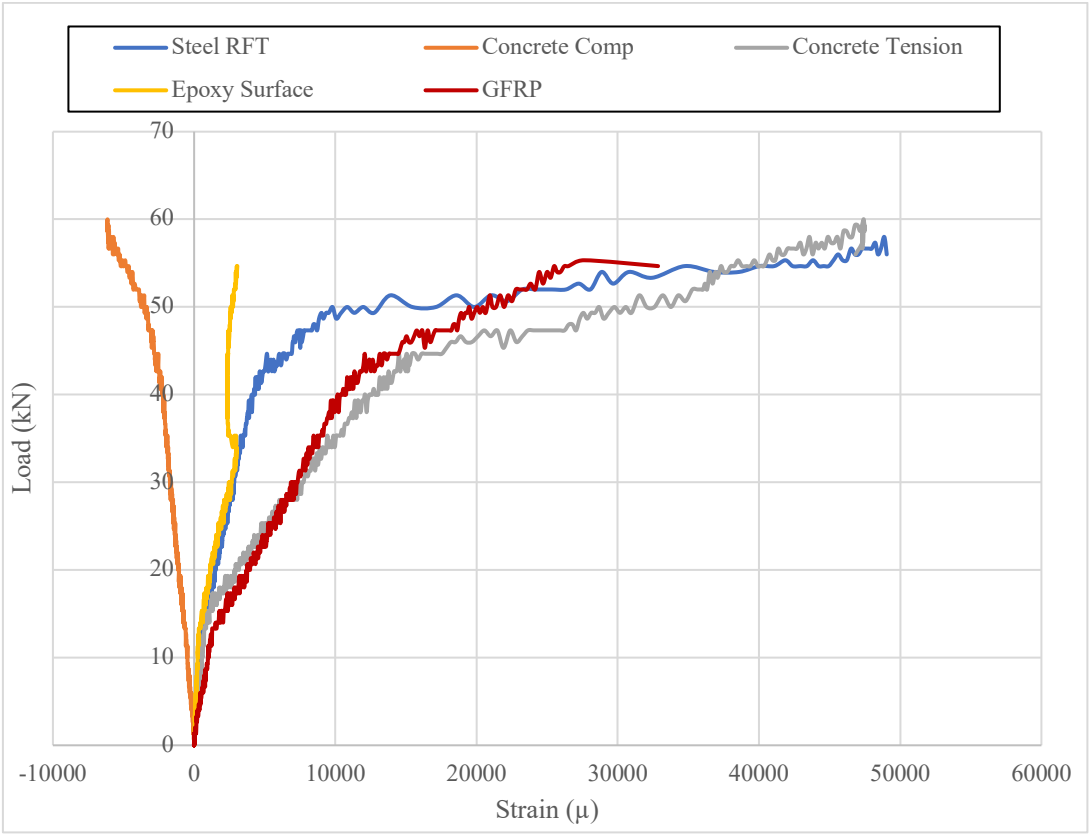

Figure 4.27 Series 4-2 Load Strain Graph

4.2.5 Series 5

The nineth sample is Series 5 Sample 1, with the use of 1 GFRP bar 16 mm diameter and 1m long, to see the effect of the bonding length of GFRP. Multiple cracks formed at the location of the edge of the GFRP bar 0.5 m from mid span as shown in Figure 4.28, the cracks increased as the load increased. One crack at the edge of the GFRP bar propagated and was the reason for failure at a load of 47 kN. The mode of failure was due to concrete crushing as shown in Figure 4.29 at the end of the GFRP bar as shown in Figure 4.30 and the deflection at the mid span was equal to 62 mm.

Figure 4.28 Series 5-1- Cracks

Figure 4.29 Series 5-1- Concrete Surface

Figure 4.30 Series 5-1- Sample Failure

The tenth sample is Series 5 Sample 2, with the use of 1 GFRP bar 16 mm diameter and 1m long, to see the effect of the bonding length of GFRP. Multiple cracks formed at the location of the edge of the GFRP bar 0.5 m from mid span as shown in Figure 4.31, the cracks increased as the load increased. One crack at the edge of the GFRP bar propagated and was the reason for failure at a load of 40 kN. The mode of failure was due to concrete crushing at the end of the GFRP bar as shown in Figure 4.32 and the deflection at the mid span was equal to 54 mm.

Figure 4.31 Series 5-2- Cracks

Figure 4.32 Series 5-2- Sample Failure

As shown in Figure 4.33 for sample 1, the cracking load P_{cr} is equal to 10 kN and the concrete strain at failure ε_{cu} is equal to 0.0035 at a load of 47 kN. For the steel reinforcement, the strain is equal to 0.006 at a load of 41 kN. Moreover, the strain for the GFRP bar is equal to 0.021. Also, Figure 4.34 shows the load strain graph for sample 2, the cracking load P_{cr} is equal to 11.5 kN and the steel reinforcement strain is equal to 0.007. Strain gauge on the GFRP bar in this sample didn't work.

Therefore, M_{cr} and M_f are calculated for both samples as follows:

$$M_{cr\ S5\text{-}1} = \frac{Pcr \times L}{4} = 5.50\ \text{kN·m}$$

$$M_{cr\ S5\text{-}2} = \frac{Pcr \times L}{4} = 6.33\ \text{kN·m}$$

$$M_{f\ S5\text{-}1} = \frac{Pf \times L}{4} = 25.85\ \text{kN·m}$$

$$M_{f\ S5\text{-}2} = \frac{Pf \times L}{4} = 22.00\ \text{kN·m}$$

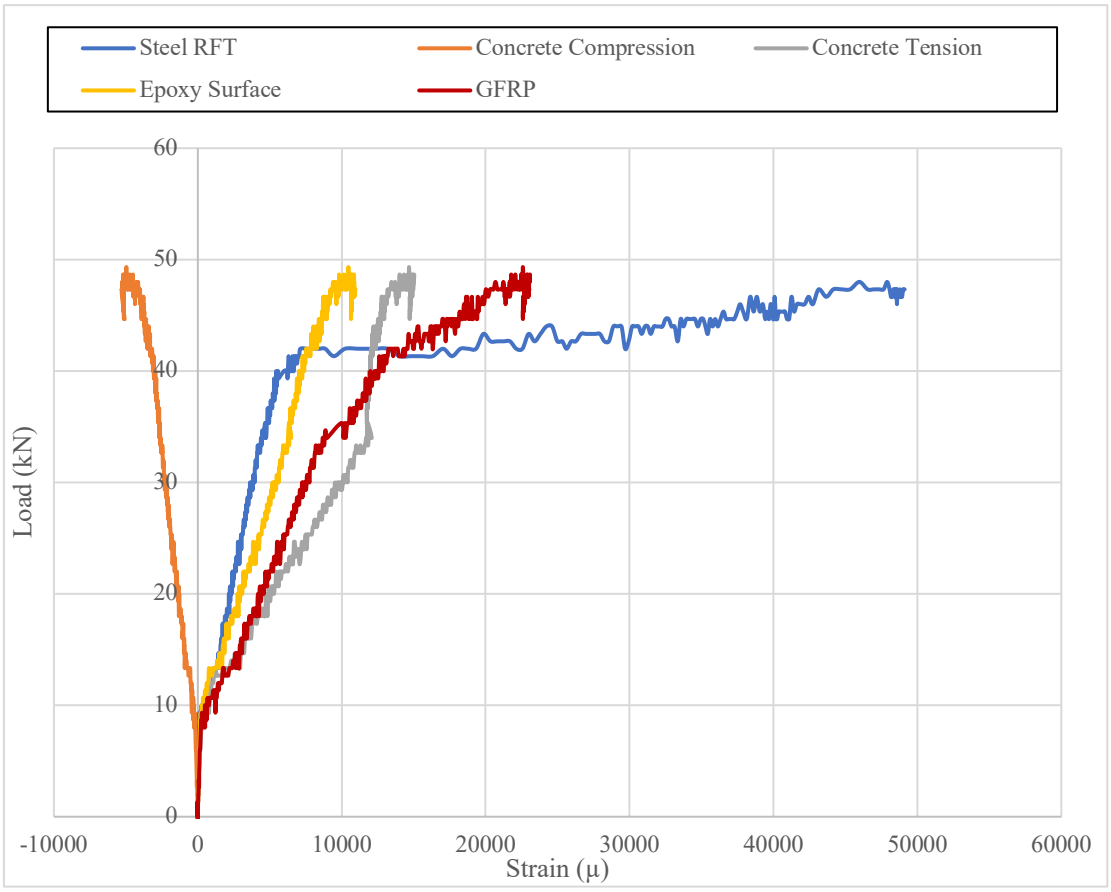

Figure 4.33 Series 5-1 Load Strain Graph

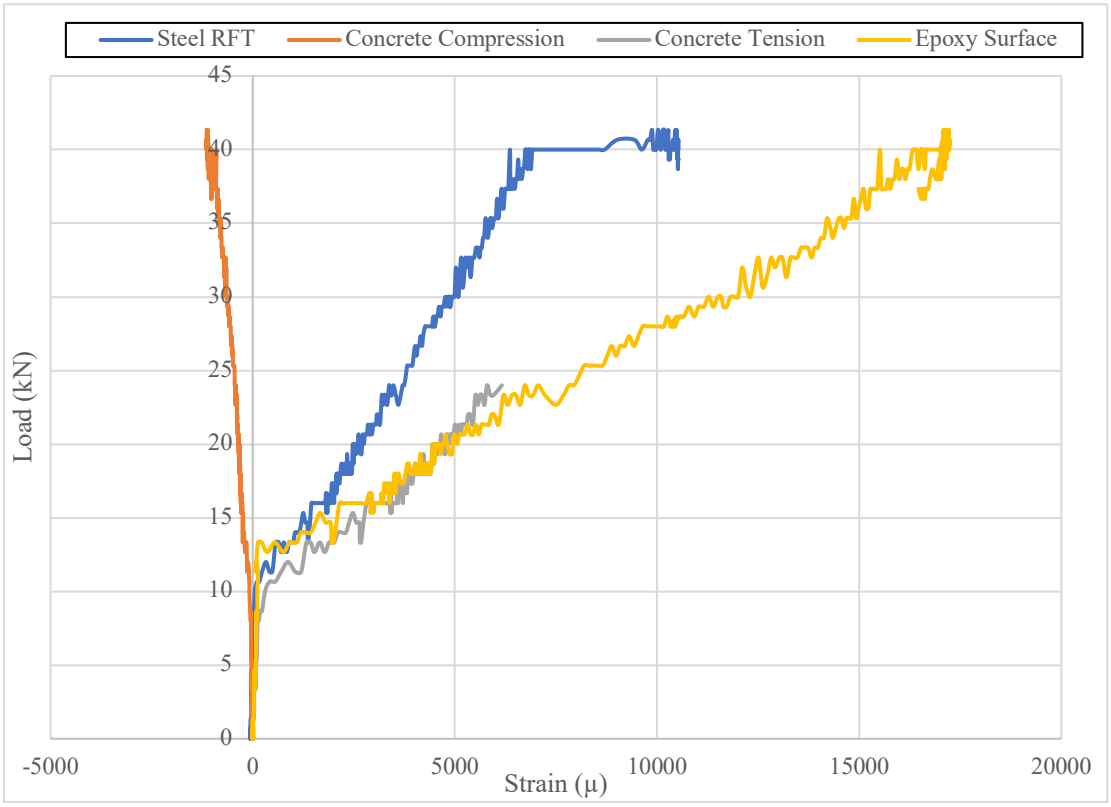

Figure 4.34 Series 5-2 Load Strain Graph

4.2.6 Series 6

The eleventh sample is Series 6 Sample 1, with the use of 2 GFRP bars 16 mm diameter and 1.5m long, to see the effect of the bonding length of GFRP as well as the number of bars. Multiple cracks formed and propagated parallel to the edge of the GFRP bar as shown in Figure 4.35, the cracks increased as the load increased. Cracks started to show at the epoxy surface and both bars started debonding from concrete, one bar fully de-bonded and was detached from the sample causing failure at a load of 63 kN. The mode of failure was due to debonding as shown in Figure 4.36 at the end of the GFRP bar and the deflection at the mid span was equal to 78 mm.

Figure 4.35 Series 6-1- Cracks

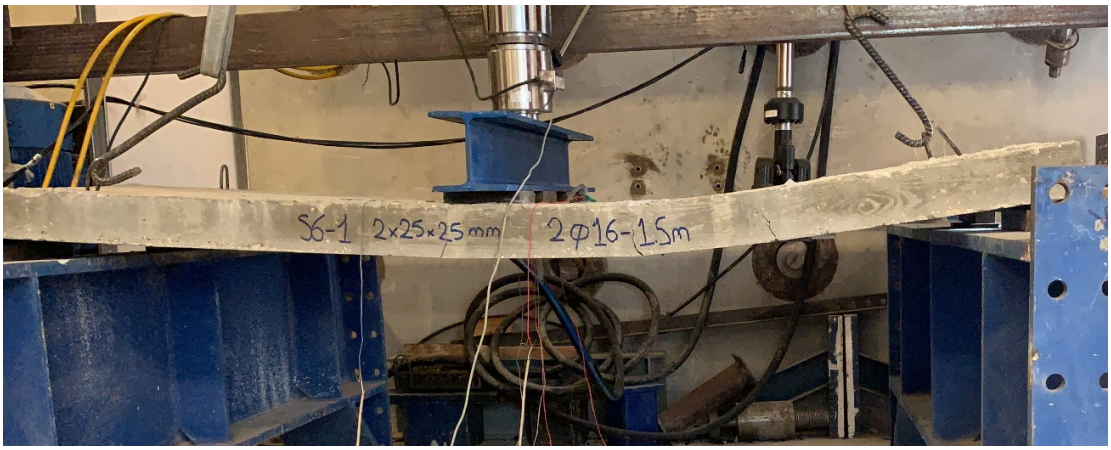

Figure 4.36 Series 6-1- Sample Failure

The last and twelfth sample is Series 6 Sample 2, with the use of 2 GFRP bars 16 mm diameter and 1.5m long, to see the effect of the bonding length of GFRP as well as the number of bars. Multiple cracks formed and propagated parallel to the edge of the GFRP bar as shown in Figure 4.37, the cracks increased as the load increased. Cracks started to show at the epoxy surface, and one bar started debonding from concrete. The bar fully de-bonded and was detached from the sample causing failure at a load of 65 kN. The mode of failure was due to debonding as shown in Figure 4.38 at the end of the GFRP bar and the deflection at the mid span was equal to 56 mm.

Figure 4.37 Series 6-2- Cracks

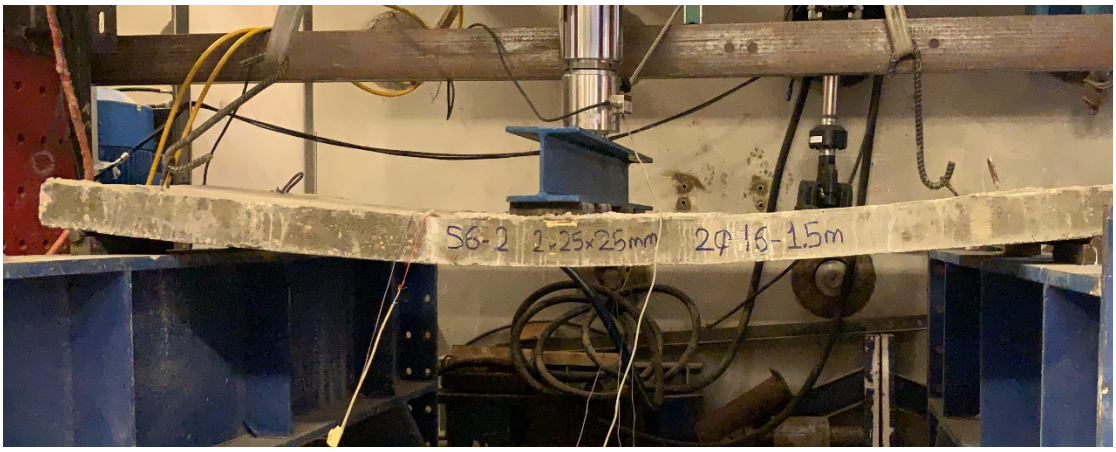

Figure 4.38 Series 6-2- Sample Failure

As shown in Figure 4.39 for sample 1, the cracking load P_{cr} is equal to 11 kN and the concrete strain at failure ε_{cu} is equal to 0.0027 at a load of 63 kN. For the steel reinforcement, the strain is equal to 0.0065. Additionally, the strain for both GFRP bars is equal to 0.021. Both GFRP bars had the same behavior and pattern, however, one bar failed earlier than the other as it de-bonded from the sample.

Also, Figure 4.40 shows the load strain graph for sample 2, the cracking load P_{cr} is equal to 11 kN and the concrete strain at failure ε_{cu} is equal to 0.0025 at a load of 65 kN. For the steel reinforcement, the strain is equal to 0.007. Strain gauges on the 2 GFRP bars in this samples didn't work.

Therefore, M_{cr} and M_f are calculated for both samples as follows:

$$M_{cr\ S6\text{-}1} = \frac{Pcr \times L}{4} = 6.05\ kN{\cdot}m$$

$$M_{cr\ S6\text{-}2} = \frac{Pcr \times L}{4} = 6.05\ kN{\cdot}m$$

$$M_{f\ S6\text{-}1} = \frac{Pf \times L}{4} = 34.65\ kN{\cdot}m$$

$$M_{f\ S6\text{-}2} = \frac{Pf \times L}{4} = 35.75\ kN{\cdot}m$$

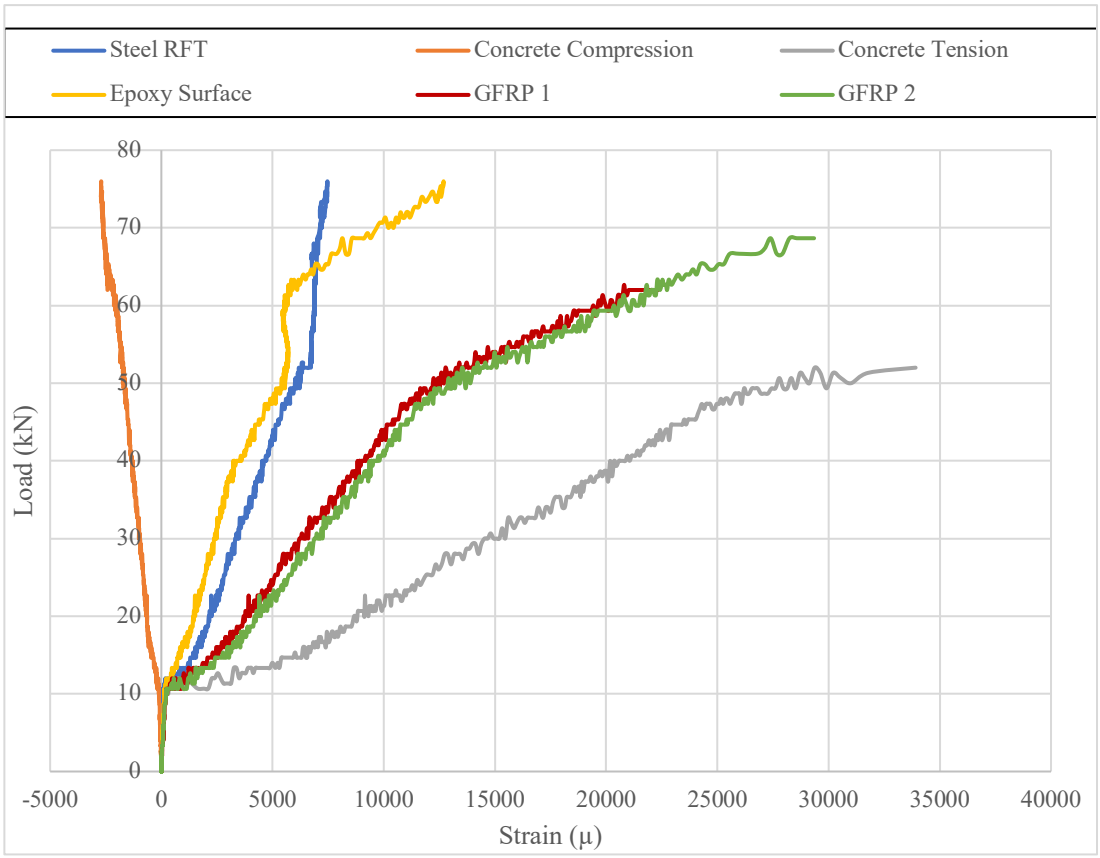

Figure 4.39 Series 6-1 Load Strain Graph

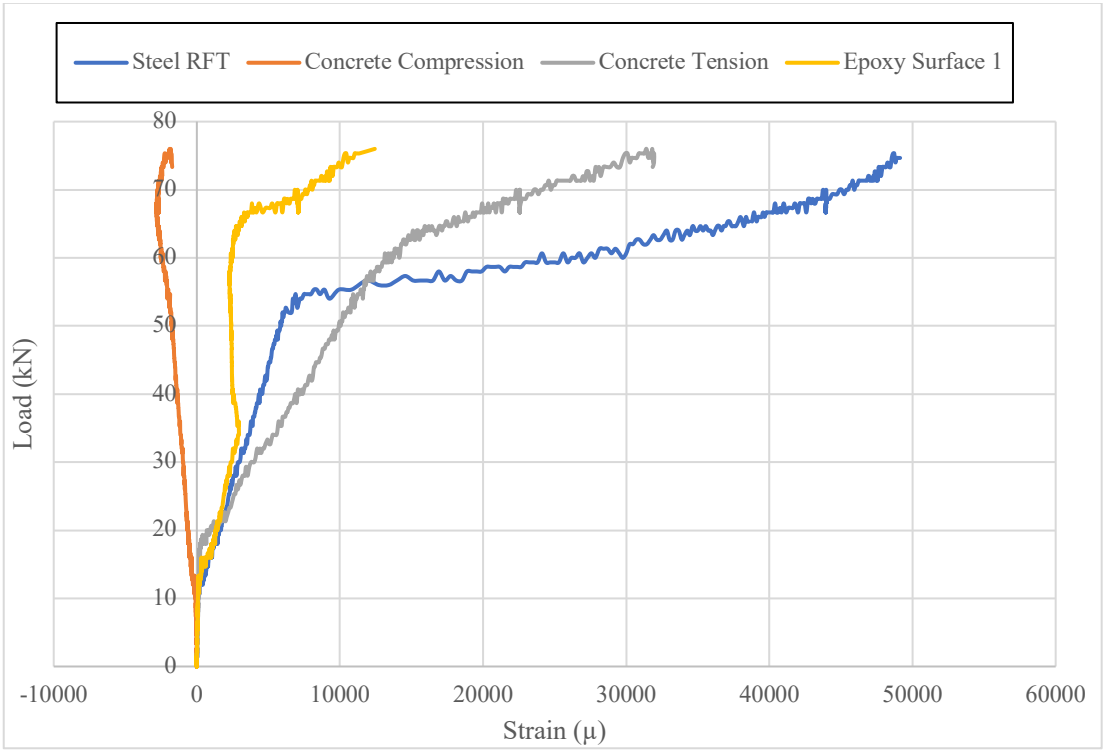

Figure 4.40 Series 6-2 Load Strain Graph

4.2.7 Summary

Table 4.2 Failure load for each sample

Failure Load	Sample 1 (kN)	Sample 2 (kN)	Average (kN)	Max. Deviation from Average (%)
S1 (Control)	32.0	31.0	31.5	1.59%
S2 (1 no. 12 - 2 m)	40.0	40.0	40.0	0.00%
S3 (1 no. 8 - 2 m)	34.0	37.0	35.5	4.23%
S4 (1 no. 16 - 2 m)	43.0	50.0	46.5	7.53%
S5 (1 no. 16 - 1 m)	47.0	40.0	43.5	8.05%
S6 (2 no. 16 - 1.5 m)	63.0	65.0	64.0	1.56%

The failure loads for each sample is shown in Table 4.2 and Figure 4.41, the maximum deviation from the average of the 2 samples in each series is calculated. It is shown that the deviation is less than 10% for all the series, that might be due to change in workmanship, change in concrete specs, changes in the test setup, or changes in the installation of the GFRP bars.

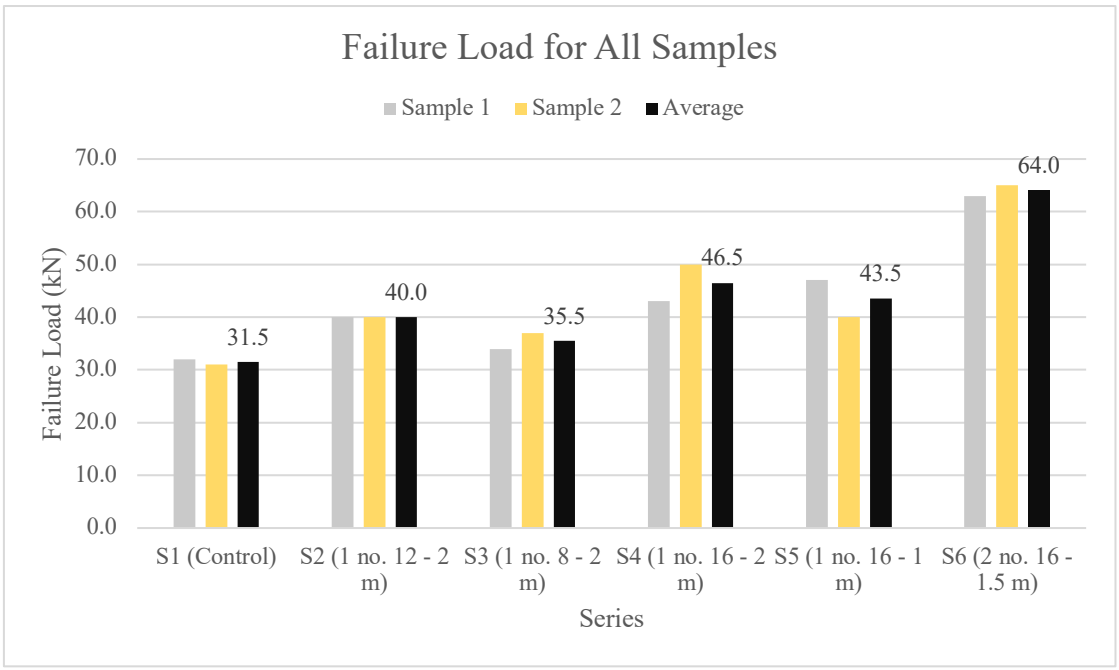

Figure 4.41 Failure Loads for all Samples

Table 4.3 Calculated and Experimental Loads and Moment Comparison

Sample	GFRP bars	Exp. Pf (kN)	Calc. Pf (kN)	Exp. Mf (kN·m)	Calc. Mf (kN·m)	Exp. Mcr (kN·m)	Calc. Mcr (kN·m)	Mexperimental / Mcontrol	Mexperimental / Manalytical
S1-1	Control	32.0	23.6	17.6	13.0	5.5	6.0	100%	136%
S1-2	Control	31.0	23.6	17.1	13.0	2.8	6.0	100%	131%
S2-1	1 no.12 - 2 m	40.0	40.4	22.0	22.2	5.5	6.0	127%	99%
S2-2	1 no.12 - 2 m	40.0	40.4	22.0	22.2	5.5	6.0	127%	99%
S3-1	1 no.8- 2 m	34.0	28.5	18.7	15.7	6.1	6.0	108%	119%
S3-2	1 no.8- 2 m	37.0	28.5	20.4	15.7	5.5	6.0	117%	130%
S4-1	1 no.16- 2 m	43.0	55.3	23.7	30.4	5.5	6.0	137%	78%
S4-2	1 no.16- 2 m	50.0	55.3	27.5	30.4	6.1	6.0	159%	90%
S5-1	1 no.16- 1 m	47.0	-	25.9	-	5.5	6.0	149%	-
S5-2	1 no.16- 1 m	40.0	-	22.0	-	6.3	6.0	127%	-
S6-1	2 no.16- 1.5 m	63.0	90.5	34.7	49.8	6.1	6.0	200%	70%
S6-2	2 no.16- 1.5 m	65.0	90.5	35.8	49.8	6.1	6.0	206%	72%

In Table 4.3, the experimental and calculated failure load and moment for each sample are listed. A comparison is made between the experimental moment and the control experimental moment, to check the occurred increase in moment when adding GFRP bars with different diameters, numbers and lengths. As shown in Figure 4.42, series 2 has a 27% increase, series 3 a 13% increase, series 4 a 48% increase, series 5 a 38% and series 6 a 103% increase. Which proves the efficiency of strengthening using NSM GFRP bars, even when there was premature debonding in series 5, there is an increase in moment.

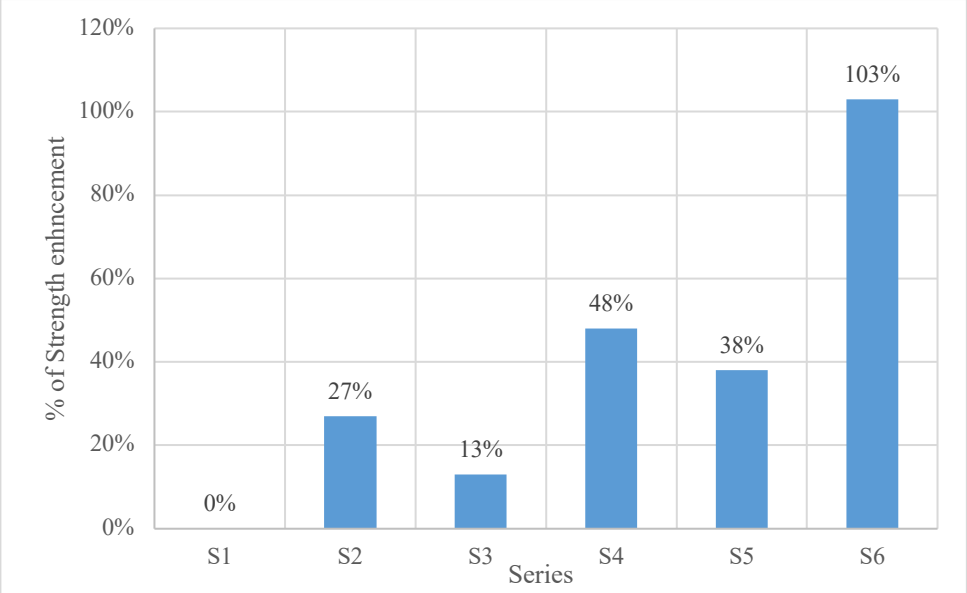

Figure 4.42 Percentage Increase in Experimental Moment from Control Sample Moment

Moreover, in Table 4.3, a comparison is made between the experimental moment and the calculated moment for each sample. As shown in Figure 4.43, series 1 has a +33% difference, this shows that the calculated moment was less than the experimented moment, which can be due to the steel reinforcement having a yield strength greater than 360 MPa, or due to differences in the dimensions due to workmanship i.e. concrete cover, sample dimension, etc. Also, series 2 has no difference and series 3 has a +24% difference between the experimental and calculated moment, which means that the code is underestimated for smaller GFRP diameters and

that the specifications of the no.8 diameter is higher than calculated. However, for series 4 and 6 there is a difference of -16%, -21% and -29% respectively. For series 4, this shows that the calculations were higher than the experimental and that the code is overestimated for higher GFRP diameters. Additionally, for series 6, the difference is mainly due to the premature debonding that occurred in both series, as their bonding length was less and equal to the minimum specified by the code. Which proves that the bonding length equation in the ACI code is accurate and important to mitigate failure due to debonding.

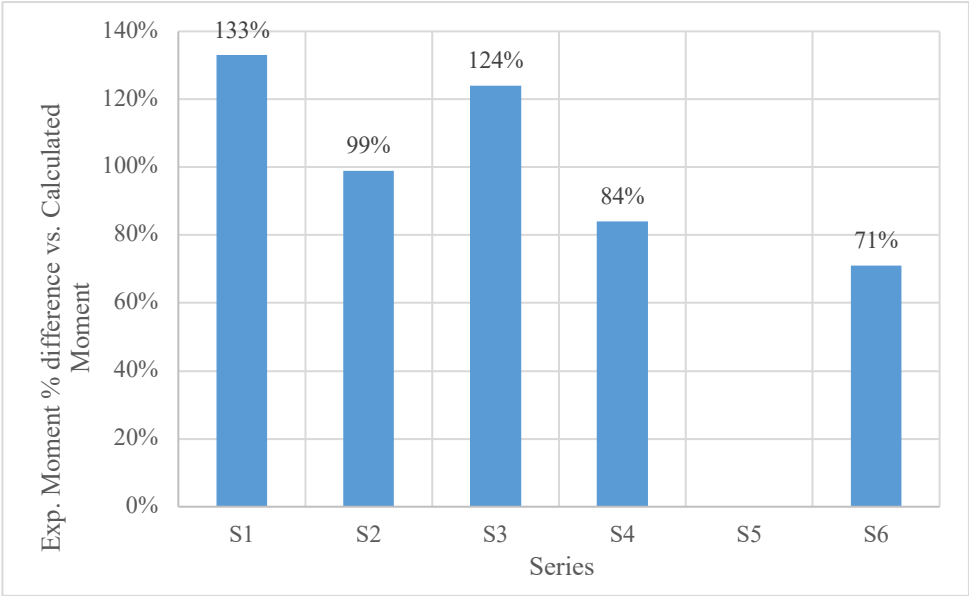

Figure 4.43 Experimental Moment Percentage Difference vs Calculated Moment

Therefore, it is recommended to have a relation between the bonding length and the decrease in strength, to be able to know the expected failure load of the sample with different bonding lengths that are less than and equal to the minimum specified in the code, as series 5 could not be compared to the calculations as its bonding length was less than the minimum. As Figure 4.43 shows that there is a 16% - 29% reduction in the calculated load carrying capacity due to premature debonding

Moreover, Table 4.4 shows the experimental and calculated strain for concrete, steel and GFRP, where the strain gauges obtained readings. For all series, the steel experimental strain is less than the calculated strain, which is due to the steel not reaching its yielding value. For series 2, 3, 4, 5 and 6, the concrete experimental strain was greater than the calculated strain, but it didn't exceed 0.0035. For the GFRP bars' strain, the experimental strain was higher than the calculated strain.

Table 4.4 Experimental Maximum Strain Values

Sample	GFRP bars	Exp. Ɛs	Calc. Ɛs	Exp. Ɛc	Cal. Ɛc	Exp. Ɛf	Cal. Ɛf
S1-1	Control	0.0070	0.0399	0.0030	0.0030	-	-
S1-2	Control	0.0058	0.0399	0.0030	0.0030	-	-
S2-1	1 no.12 - 2 m	0.0090	0.0117	0.0035	0.0021	-	0.0158
S2-2	1 no.12 - 2 m	0.0070	0.0117	0.0030	0.0021	-	0.0158
S3-1	1 no.8- 2 m	0.0074	0.0117	-	0.0021	-	0.0158
S3-2	1 no.8- 2 m	0.0080	0.0117	-	0.0021	-	0.0158
S4-1	1 no.16- 2 m	-	0.0120	-	0.0021	-	0.0158
S4-2	1 no.16- 2 m	0.0090	0.0120	0.0028	0.0021	0.0230	0.0158
S5-1	1 no.16- 1 m	0.0060	-	0.0035	-	0.0210	-
S5-2	1 no.16- 1 m	0.0070	-	-	-	-	-
S6-1	2 no.16- 1.5 m	0.0065	0.0090	0.0027	0.0021	0.0210	0.0120
S6-2	2 no.16- 1.5 m	0.0070	0.0090	0.0025	0.0021	-	0.0120

4.3 Analysis

Code Calculations vs. Experimental Values

To analyze the validity of the Code design equations, the equations were used to calculate the expected failure load for all the series and they were compared to the actual failure loads from the experimental work. As shown in Figure 4.44 and Table 4.5, for series 1 and series 3 the calculated failure load is less than the actual failure load, in series 1 this is due to differences in the dimensions or steel reinforcement yield strength and in series 3 it shows that the calculations are underestimated for no.8 GFRP bar diameter.

However, for Series 4 and 6 the calculated failure load is more than the actual failure load, which means that the code design equations are overestimated for no.16 GFRP bar diameter and for the series where the used bonding length is equal to the minimum bonding length, this is due to their rapid premature failure due to debonding. As for series 5 the bonding length is less than the minimum bonding length set in the code and the available equations will not be applicable to use and compare as they don't take into consideration the bonding length, assuming they are not violating the set minimum using the bonding length equation

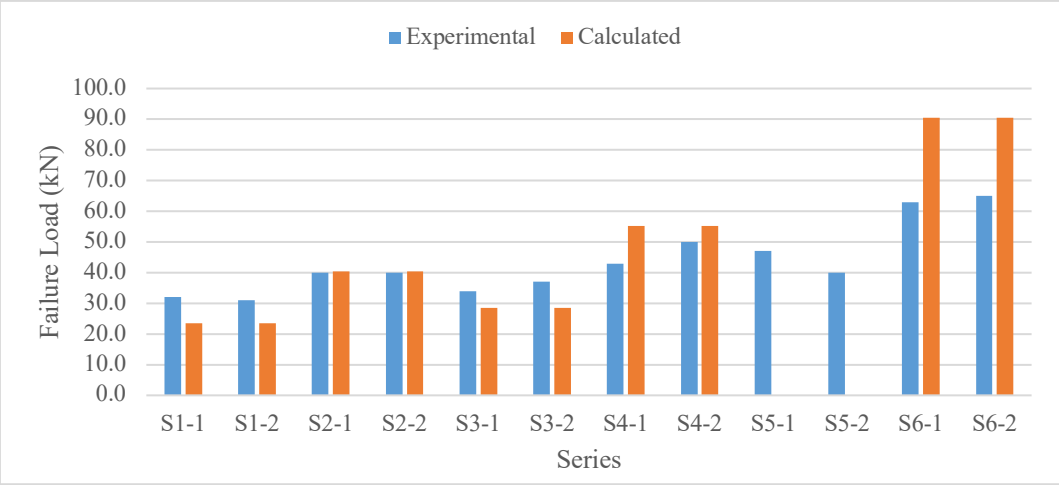

Figure 4.44 Comparison between Actual and Calculated Failure Loads

Table 4.5 Experimental and Calculated Failure Loads

	Sample	Exp. Failure Load (kN)	Calc. Failure Load (kN)	% Exp. from Calc. failure load
Series 1	S1-1	32.0	23.6	136%
	S1-2	31.0	23.6	131%
Series 2	S2-1	40.0	40.4	99%
	S2-2	40.0	40.4	99%
Series 3	S3-1	34.0	28.5	119%
	S3-2	37.0	28.5	130%
Series 4	S4-1	43.0	55.3	78%
	S4-2	50.0	55.3	90%
Series 5	S5-1	47.0	-	-
	S5-2	40.0	-	-
Series 6	S6-1	63.0	90.5	70%
	S6-2	65.0	90.5	72%

No GFRP vs. Use of GFRP no. 8

To analyze the increase in strength due to adding NSM GFRP bar no. 8, comparison between Series 1 with Series 3 is made. As shown in Figure 4.45, one GFRP bar no. 8 increased the strength to 113%, from a failure load of 31.5 kN without the use of GFRP to a failure load of 35.5 kN

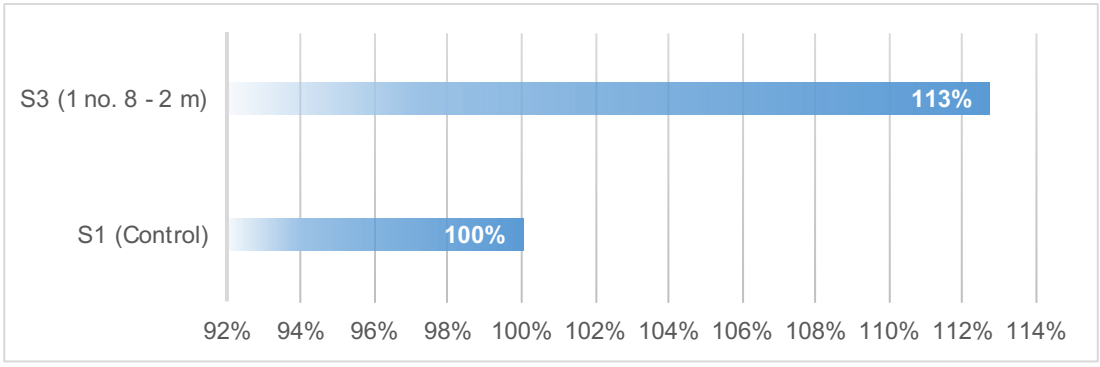

Figure 4.45 Percentage increase in strength due to the use of GFRP no.8

No GFRP vs. Use of GFRP no. 12

To analyze the increase in strength due to adding NSM GFRP bar no. 12, comparison between Series 1 with Series 2 is made. As shown in Figure 4.46, one GFRP bar no. 12 increased the strength to 127%, from a failure load of 31.5 kN without the use of GFRP to a failure load of 40 kN

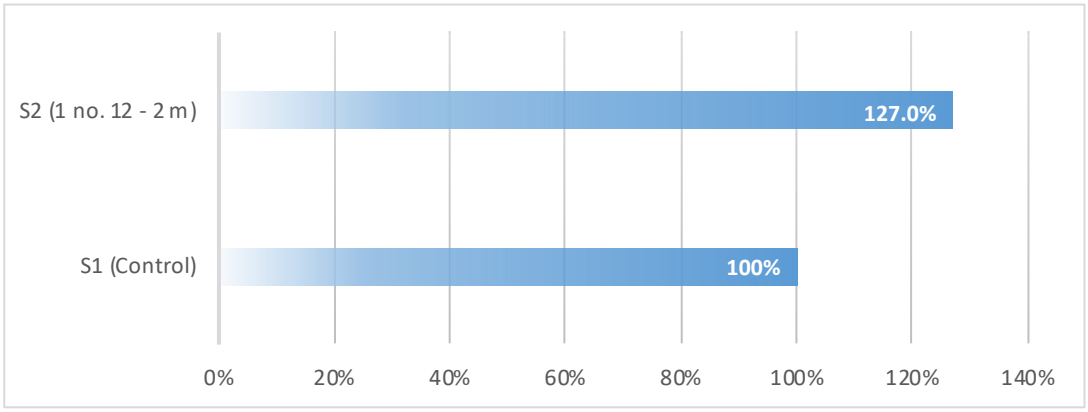

Figure 4.46 Percentage increase in strength due to the use of GFRP no.12

No GFRP vs. Use of GFRP no. 16

To analyze the increase in strength due to adding NSM GFRP bar no. 16, comparison between Series 1 with Series 4 is made. As shown in Figure 4.47, one GFRP bar no. 16 increased the strength to 148%, from a failure load of 31.5 kN without the use of GFRP to a failure load of 46.5 kN, which is a significant increase in the strength

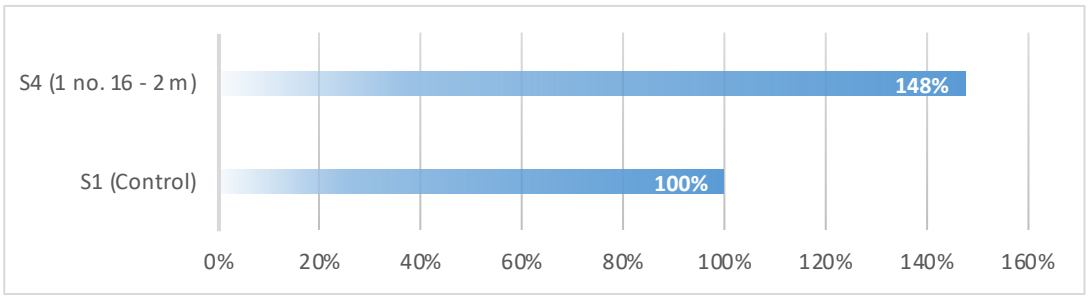

Figure 4.47 Percentage increase in strength due to the use of GFRP no.16

Percentage increase in failure load vs. GFRP reinforcement ratio

The GFRP reinforcement ratio is calculated for each sample, where the GFRP reinforcement area is divided by the concrete sample area. As shown in Figure 4.48, the higher the GFRP reinforcement ratio, the higher increase in failure load with a linear behavior.

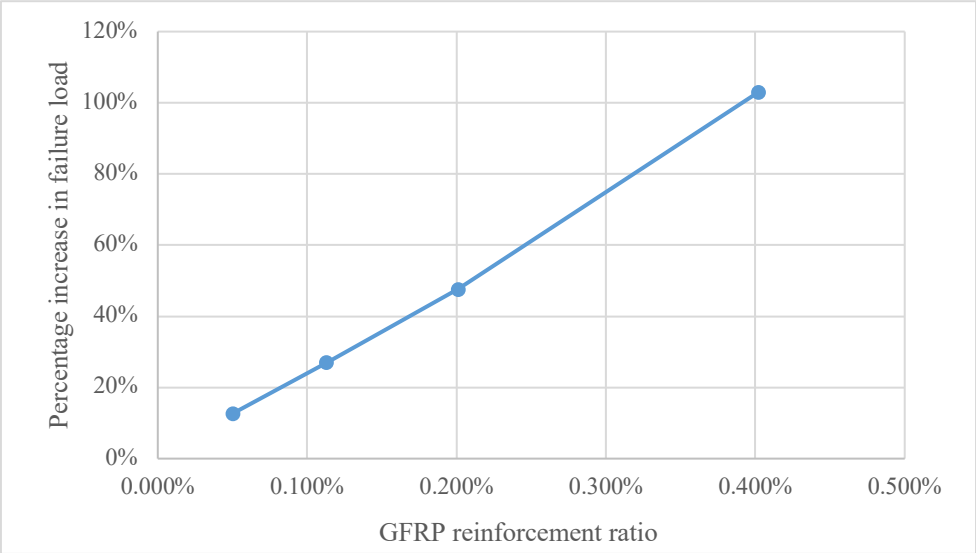

Figure 4.48 Percentage increase in failure load vs. GFRP reinforcement ratio

Percentage increase in failure load vs. GFRP development length over the GFRP diameter

The GFRP development length to the GFRP bar diameter is calculated. As shown in Figure 4.49 the higher the GFRP length to diameter ratio, the lower increase in failure load. However, for the series with the lowest length to diameter ratio equal to 62.5 and development length 1000 mm, the percentage increase was lower than series with higher length to diameter ratio. As its development length is smaller than the minimum specified by the code and its mode of failure was due to debonding.

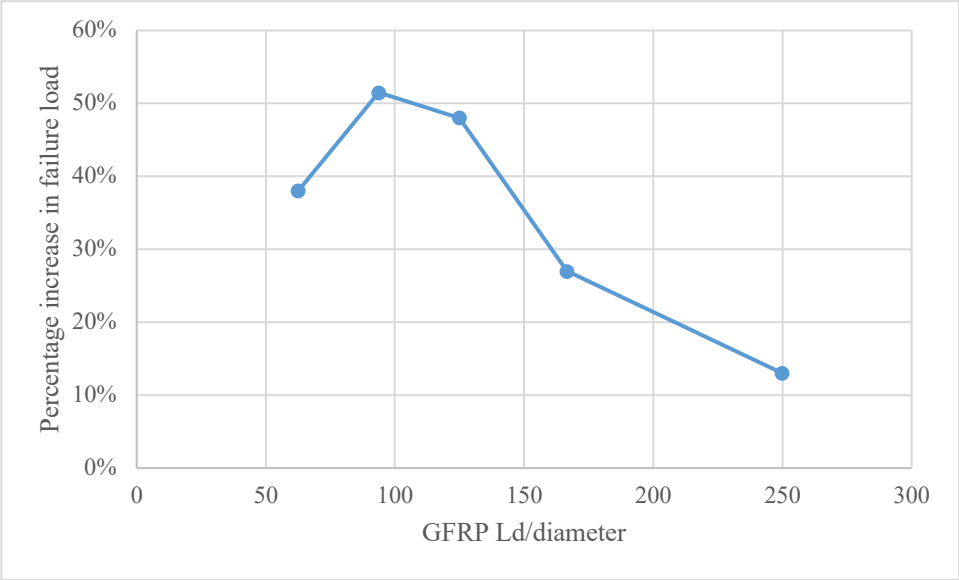

Figure 4.49 Percentage increase in failure load vs. the GFRP development length to diameter ratio

Use of different GFRP diameters

To analyze the increase in strength due to using different diameters of GFRP bars, comparison between Series 1 with Series 2, 3 and 4 is made. One GFRP bar no. 12 increased the strength 13% than of when using GFRP no.8 and one GFRP bar no. 16 increased the strength 16% that of when using GFRP no.12. Therefore, as shown in Figure 4.50, a trendline was drawn to find an equation correlating the load to the GFRP diameter/area. The correlation was found to be with linear behavior.

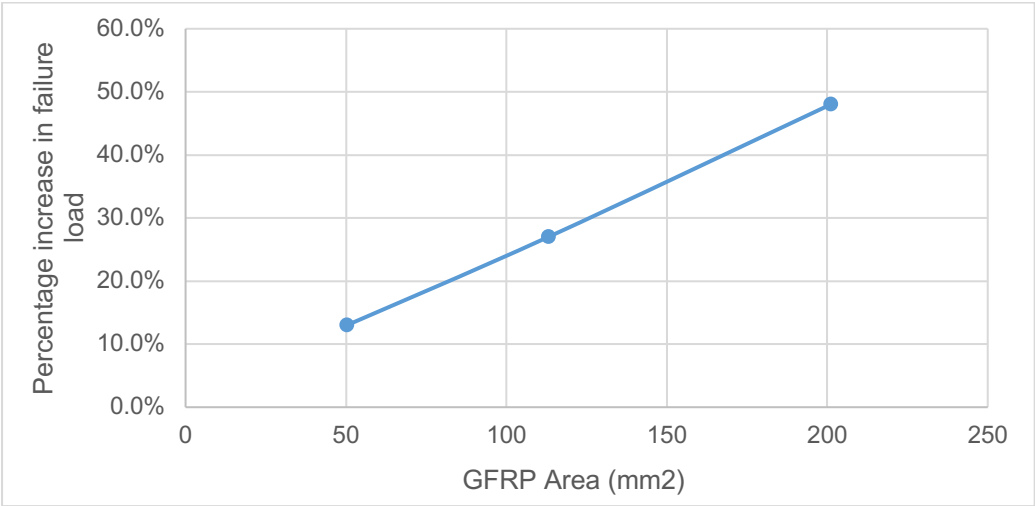

Figure 4.50 Load vs GFRP bar area

Use of different GFRP bar lengths

To analyze the increase in strength due to using different length of GFRP bars, comparison between Series 4 with Series 5 is made. Therefore, as shown in Figure 4.51, a trendline was drawn to find an equation correlating the load to the GFRP length. For GFRP length 1500 mm, the used number of bars was 2 bars, whereas for the other length the used number of bars was only 1 bar, so to be able to compare equitably the percentage increase in failure load for the 1500 mm length was divided by 2. Consequently, in Figure 4.51 it might show that the 1500 mm showed a higher percentage increase in failure load. Apart from the mode of failure, the correlation was found to be with polynomial behavior.

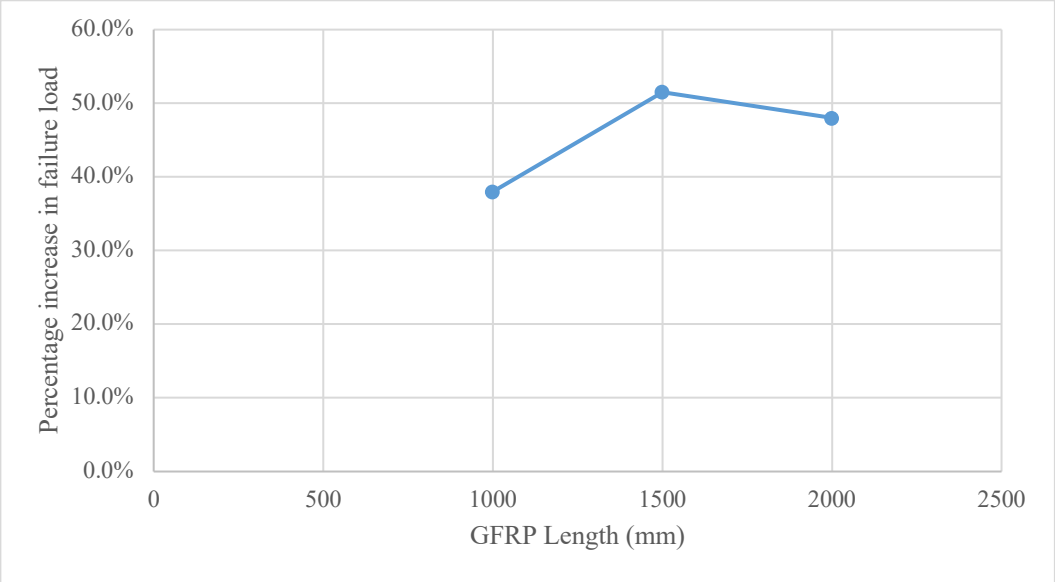

Figure 4.51 Load vs GFRP bar length

Use of different numbers of GFRP bars

To analyze the increase in strength due to using different number of GFRP bars, comparison between series 2,3,4,5 & 6 is made. However, since that series 2,3 & 4 GFRP bar length is 2 m, series 5 GFRP bar length is 1 m and Series 6 GFRP bar length is 1.5 m, the comparison is done in terms on total GFRP bars volume (no. bars * bar area * length). Therefore, as shown in Figure 4.52, a trendline was drawn to find an

equation correlating the load to the GFRP volume. The correlation was found to be with polynomial behavior of second degree. However, the results of series 5 do not match the trendline as its length is 1 m which is less than the allowed minimum bonding length specified by the code, and its mode of failure was due to debonding.

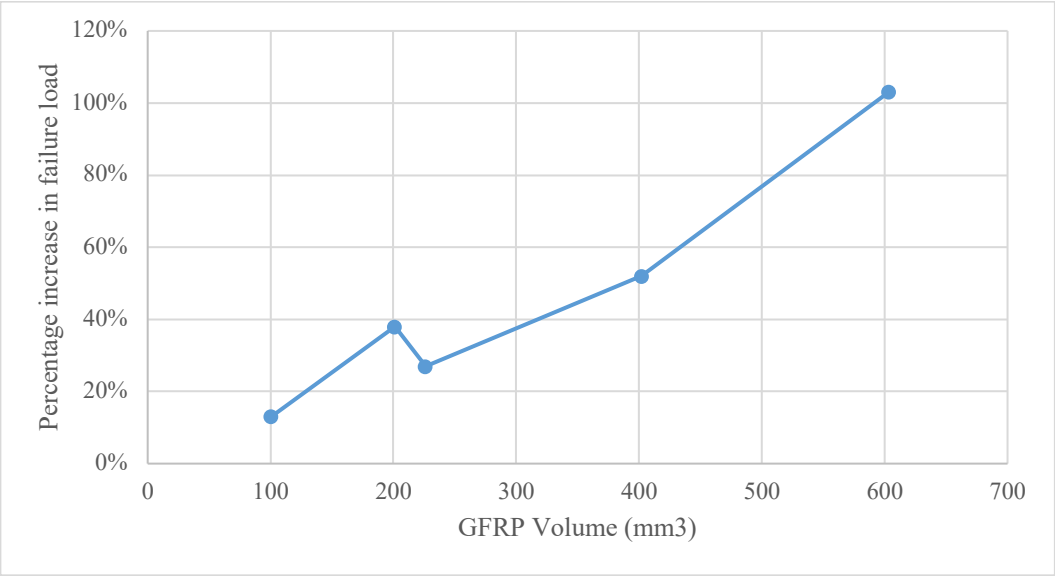

Figure 4.52 Load vs GFRP bar volume

Chapter 5 – Conclusions

Presents the conclusions reached throughout the conducted experimental work. Followed by a set of recommendations for possible future work that would add to the thesis topic or that the studied topic would be of benefit to.

5.1 Conclusions

In light of the materials used, sample design, steps of execution and test parameters associated with this study, the following conclusion can be stated:

1. Strengthening of RC Slabs using NSM GFRP showed a significant increase in strength and load carrying capacity. Where μGFRP 0.05% increased the load by 13%, μGFRP 0.1% by 27%, μGFRP 0.2% by 48% and μGFRP 0.4% by 103%.
2. The larger the GFRP bar diameter, the higher the strength of the RC slab.
3. The more numbers of GFRP bars used, the higher the strength of the RC slab. Moreover, the volume of the GFRP bars used is proportional to the increase in strength
4. For a bonding length greater than the minimum specified by the ACI code, the mode of failure was due to flexural failure. The calculated failure load was less than the experimental for GFRP diameter no.8, equals to the experimental for GFRP diameter no.12 and was more than the experimental for GFRP diameter no.16.
5. For a bonding length equals to the minimum specified by the ACI code, the mode of failure was due to debonding of the GFRP bars. The calculated failure load is more than the experimental load.

6. For a bonding length less than the minimum specified by the ACI code, the calculated failure load could not be calculated as the available equations do not take into consideration the bonding length, assuming the used length will be greater than the minimum specified. This would result in having the same calculated failure load with the sample with bonding length greater than the minimum specified. Accordingly, the comparison was not done as it will not be applicable and won't give a reasonable estimation.

5.2 Recommendations for Future Work

Since the findings of this study yielded promising results, while many questions remain unanswered, future research work is highly recommended including the following tasks:

1. Expanding this study by experimenting two-way slabs with different dimensions
2. Running a finite element model and comparing the results to the conducted experimental work
3. Studying the use of other adhesive materials to enhance the bonding between the RC and the GFRP bars
4. Enhancing the equation for the minimum bonding length and incorporating it in the calculation for the load carrying capacity, to be able to know the expected failure load of the sample with different bonding lengths that are less than and equal to the minimum specified in the code. As this work shows that there is a 16% - 29% reduction in the calculated load carrying capacity due to premature debonding

5. Investigating the equation for the minimum groove dimension to enhance bonding between the GFRP bar and the RC
6. Testing and examining the durability of GFRP

References

Abbood, Imad S., Odaa, Sief aldeen, Hasan, Kamalaldin F. and Jasim, Mohammed A., "Properties evaluation of fiber reinforced polymers and their constituent materials used in structures – A review", Materials Today: Proceedings, July 2020. Accessed on 19, September 2019.

ACI Committee 440.2. "Guide For The Design And Construction Of Externally Bonded FRP Systems For Strengthening Concrete Structure". ACI American Concrete Institute. 2008. Accessed on 19, September 2019.

Aydin, F. and M. Saribiyik. "Compressive and Flexural Behavior of Hybrid Use of GFRP Profilewith Concrete." International Symposium on Sustainable Development. Materials Science. 2010. Accessed on 2, May 2021.

Behzard, Pejman, Sharbatdar, Mohammad and Kheyroddin, Ali. "Different NSM FRP technique for strengthening of RC two-way slabs with low clear cover thickness". Scientia Iranica. 23. 2016. Accessed on 19, September 2019.

Bilotta, Antonio, Ceroni, Francesca, et al. "Bond of NSM FRP-Strengthened Concrete: Round Robin Test Initiative". Journal of Composites for Construction, American Society for Civil Engineering. 2015. Accessed on 18 April 2021.

Carolin, Anders. "Carbon Fibre Reinforced Polymers for Strengthening of Structural Elements." Luleå University of Technology, Department of Civil, Environmental and Natural Resources Engineering., Luleå Tekniska Universitet, 2003. Accessed on 18, May 2021.

Coelho, Mário, Sena-Cruz, Jose and Neves, Luis. “A review on the bond behavior of FRP NSM systems in concrete”. Construction and Building Materials. 93. 2015. Accessed on 19, September 2019.

De Lorenzis, Laura, Nanni, Antonio and La Tegola, Antonio. “Strengthening of Reinforced Concrete Structures with Near Surface Mounted FRP Rods”. International Meeting on Composity Materials, PLAST 2000. 2000. Italy. Accessed on 19, September 2019.

De Lorenzis, Laura and Teng, J.G.. “Near-Surface Mounted FRP Reinforcement: An Emerging Technique For Strengthening Structures”. Composites Part B: Engineering. 2007. Accessed on 23, September 2019.

El-Hacha, Raafat and Rizkalla, S.H.. “Near-surface-mounted fiber-reinforced polymer reinforcements for flexural strengthening of concrete structures”. ACI Structural Journal. 101. 2004. Accessed on 19, September 2019.

Gunaslan, Sultan Erdemlı, and Abdulhalim Karasin. “Confining Concrete Columns with FRP Materials.” European Scientific Journal, ISSN: 1857 – 7881, Apr. 2017, pp. 464–470. Accessed on 2, May 2021.

Hosen, Md Akter, U. Johnson Alengaram, Mohd Zamin Jumaat and N. H. Ramli Sulong, Kh. Mahfuz ud Darain. “Glass Fiber Reinforced Polymer (GFRP) Bars for Enhancing the Flexural Performance of RC Beams Using Side-NSM Technique.” Polymers vol. 9,5 180. 19 May. 2017. Accessed on 19, September 2019.

Hsieh, Chia-Tsung and Lin, Yiching, “Detecting debonding flaws at the epoxy–concrete interfaces in near- surface mounted CFRP strengthening beams using the impact–echo method” NDT&E International. May 2016. Accessed on 19, September 2019.

Kang, T.HK., Howell, J., Kim, S. et al. A State-of-the-Art Review on Debonding Failures of FRP Laminates Externally Adhered to Concrete. Int J Concr Struct Mater 6, 123–134 (2012). https://doi.org/10.1007/s40069-012-0012-1. Accessed on 19, September 2019.

Makhlouf, Aly. Kareem Mostafa, Sarah Rezk, Seif Eteifa and Ziad El Abd. “Testing Near-Surface Mounted Reinforcement in Concrete Using Glass Fibre-Reinforced Polymer”. American University in Cairo. Department of Construction Engineering. Supervised by Dr. Ezzeldin Yazeed and Dr. Mohamed AbouZeid. 2015. Accessed on 19, September 2019.

Mohamedien, Mohamed A., Hosny, Abdel-Hady and Abdelrahman, Amr. “Use of FRP in Egypt, Research Overview and Applications”. Procedia Engneering 54 2-21, 2013. Accessed on 19, September 2019.

Parvin, Azadeh and Taqiuddin Syed Shah. "Fiber Reinforced Polymer Strengthening of Structures by Near-Surface Mounting Method." Polymers: 1-4. 2016. Accessed on 19 September 2019.

Pultron Composites. “World's Largest GFRP Rebar Project Embraces Corrosion-Free Future.” Pultron Composites. 13 Aug. 2019, www.pultron.com/composite-blog/worlds-largest-gfrp-project/ Accessed on 2, May 2021.

Salman, Wissam. “Strengthening of Reinforced Concrete One-Way Slabs with Opening using CFRP Strips in Flexural”. International Journal of Science and Research (IJSR) Volume 4 Issue 5. May 2015. Accessed on 25 September 2019.

Sathishkumar, TP., Satheeshkumar, S. and Naveen, J. “Glass fiber-reinforced polymer composites – a review”. Journal of Reinforced Plastics and Composites. Vol. 33 (13) 1258–1275. 2014. Accessed on 19, September 2019.

Schoeck ComBAR Brochure and Properties. August 2018. Accessed on 19, September 2019.

Schoeck ComBAR Technical Information. 2018. Accessed on 19, September 2019.

Soliman, Shehab M., El-Salakawy, Ehab and Benmokrane, Brahim. “Flexural behaviour of concrete beams strengthened with near surface mounted fibre reinforced polymer bars”. Canadian Journal for Civil Engineering Vol. 37. 2010. Accessed on 19, September 2019.

Soror, A. Y., et al. “State of the Art Review: Flexural Strengthening of Reinforced and Pre-Stressed Concrete Beams Using Fiber Reinforced Polymers.” Engineering Research Journal, vol. 42, no. 2, Apr. 2019. Accessed on 2, May 2021.

Szabó, Zsombor and Balázs, György. “Near surface mounted FRP reinforcement for strengthening of concrete structures”. Periodica Polytechnica-civil Engineering. 2007. Accessed on 19, September 2019.

Xing, Guohua, Chang, Zhaoqun and Ozbulut, Osman. “Behavior and failure modes of reinforced concrete beams strengthened with NSM GFRP or aluminum alloy bars”. 2018. Accessed on 19, September 2019.